Biomechanical Characerization and Evaluation of Conservative Clubfoot Correction

Tamara Loren Cohen
Marquette University

BIOMECHANICAL CHARACTERIZATION AND EVALUATION OF CONSERVATIVE CLUBFOOT CORRECTION

by

Tamara L. Cohen, B.S.

A Dissertation submitted to the Faculty of the Graduate School,

Marquette University,

in Partial Fulfillment of the Requirements for

the Degree of Doctor of Philosophy

Milwaukee, Wisconsin

December 2015

ABSTRACT
BIOMECHANICAL CHARACTERIZATION AND EVALUATION OF CONSERVATIVE CLUBFOOT CORRECTION

Tamara L. Cohen, B.S.

Marquette University, 2015

Congential talipes equinovarus, or clubfoot, affects approximately 200,000 newborns worldwide each year and presents with equinovarus of the hindfoot, as well as cavus and adduction of the midfoot. In addition to bone malformation and displacement, soft tissue contractures encapsulate the medial and posterior aspects of the affected foot. The Ponseti method is a conservative treatment that progressively repositions the clubfoot through weekly casting, followed by bracing. Concerns exist regarding the variability in outcomes, resistance to treatment, and risk of relapse, which occur in approximately 10% of the population. Potential factors contributing to variability and resistant clubfoot include cast material performance, as well as biomechanics of medial soft tissue of the clubfoot. There are no clinical guidelines for clubfoot correction based upon mechanical response of commonly used casting materials, nor the mechanics of the medial fibrotic clubfoot tissue. Untreated or under-corrected clubfoot can result in abnormal gait, pain, and further foot deformity.

The purpose of this research was to investigate the biomechanics of conservative clubfoot correction through: i) a kinematic assessment of the creep behavior of three common cast materials used during conservative correction, ii) development and validation of a benchtop system for the mechanical evaluation of miniature soft tissue specimens, and iii) performing a mechanical analysis to model the behavior of medial fibrotic mass tissue (MFMT) from children with clubfoot.

Utilizing a model to simulate clubfoot correction, creep rotation was found to be dependent on cast material with maximum values for plaster-of-Paris ($\theta \approx 2.1$ deg). Reducing cast creep may result in a more efficient correction. Utilizing nylon monofilament, the benchtop system was validated against a commercial system (MTS). Versatility was demonstrated with quasistatic and viscoelastic protocols performed on PTFE tape and rabbit ligament, respectively. Clubfoot MFMT underwent a quasistatic and viscoelastic protocol, including requisite preconditioning as well as stress relaxation. Major findings include high specimen variability, less relaxation than reported for normal deltoid ligaments, and estimated QLV model parameters with $R^2 > 0.8$ for 16 specimens. Results from this research provide mechanical insight into the correction process that may lead to individualized, evidence-based clubfoot care. Future directions include *in vivo* analysis of tissue properties and mechanical-genetic correlation.

ACKNOWLEDGEMENTS

Tamara L. Cohen, B.S.

The journey toward my PhD is Biomedical Engineering began my sophomore year of college. After watching a documentary about pediatric victims of war in need of prosthetics, I was inspired to direct my engineering education to understand and help the body. That said, I'd like to first and foremost, thank the patients whose donated tissue made this research possible. Further, I'd like to thank the children and adults who, in spite of injury or disability, strive for more and inspire me to do the same.

The completion of my dissertation would not have been made possible without the support and guidance of many people. I'd like to thank my dissertation advisor, Dr. Gerald Harris, who provided me with unfailing guidance, advice, and opportunities for growth. His expertise, enthusiasm for knowledge, and confidence in my abilities enabled me to be a better researcher and problem solver. I would like to thank my committee members, Dr. Lars Olson, Dr. Mei Wang, Dr. Stephen Heinrich, Dr. Peter Smith, Dr. Haluk Aliok for their guidance over the years. Special thanks are due to Dr. Smith, Dr. Altiok, and Dr. Luiz Caicedo for their collaborative and surgical efforts in the recruitment of patients, as well as harvest and transport of tissue for this research. Many thanks are due to Dr. Jeffrey Toth for his histological expertise and tissue preparation assistance, Dr. Scott Beardsley for his expertise and guidance in bioelectronics and controls, and Dr. Sergey Tarima for his expertise in statistics and R programming. In addition, I am grateful to Dr. Carolyne Albert for her impact on my research and life, providing both expertise in material and tissue mechanics as well as mentorship. My tissue mechanics education would not have been complete without the efforts and generosity of Dr. Stephen Abramowitch (University of Pittsburgh).

I am indebted to the many who remained during the long hours of experimentation and to those whose assistance made this research possible. First, I'd like to thank Jacob Rammer, my labmate, business partner, and friend, for being generous with his time, patient, a good listener, a great problem solver, and a supplier of caffeine. I'd also like to thank Ms. Emily Schaefer and Ms. Linda McGrady, both of whom made the experimentation phases of my research possible. Finally, I'd like to thank Dr. Joseph Krzak and Mr. Adam Graf for their continued support.

I'd also like to thank Marquette University, the Graduate School, and specifically those involved in the execution of Dissertation Boot Camp. My time spent at DBC propelled my writing (thanks to Dr. George Corliss), opened my eyes to other areas of research, and helped me look at my research in a different way (see Appendix G).

I could not have gotten through graduate school without the support from my friends, both in Milwaukee and on the east coast. In Milwaukee, I have people like Matt Friedel, whose laughter, kindness, honesty, and friendship gives my life balance and Kate Dechambre, whose kindness and generosity has no limit, not even at midnight. I'd like to

especially thank Brian Schlatter for being in my life, for his continued support and confidence in me, and for helping me finish my marathons. Special thanks go out to Ian Ziegler for always keeping my brain stimulated. My running and workout families in Milwaukee have kept me strong and healthy, both mentally and physically.

Most importantly, I would not be here at the finish line without my family. Though hundreds of miles away, their love and support were always felt. They are my role models, my pillars of strength, and my confidants. I owe the most to my parents, who instilled in me perseverance, a love a math and science, and the importance of education. My admiration of my brother stems from his thirst for knowledge and his strength in overcoming obstacles. Last but not least, I thank my twin sister for challenging me to do more, inspiring me to find my own path, and for always being my best friend.

Finally, I'd like to acknowledge my funding sources. The contents of this dissertation were developed under a grant from the National Institute on Disability, Independent Living, and Rehabilitation Research (NIDILRR 90RE5006-01-00). NIDILRR is a Center within the Administration for Community Living (ACL), Department of Health and Human Services (HHS). The contents of this dissertation do not necessarily represent the policy of NIDILRR, ACL, HHS, and you should not assume endorsement by the Federal Government.

TABLE OF CONTENTS

LIST OF TABLES

LIST OF FIGURES

CHAPTER 1: INTRODUCTION

1.1 Statement of Problem

Clubfoot is a congenital deformity of the lower extremity, occurring in approximately 1 in 1000 births (Dobbs et al., 2009; Parker et al., 2009; Roye, Hyman and Roye, 2004; Roye and Roye, 2002; Shabtai, Specht and Herzenberg, 2014; Wallander, 2010; Zhang et al., 2014). It presents with equinovarus of the hindfoot, as well as cavus and adduction of the midfoot, due to bone displacement and malformation, as well as soft tissue abnormalities (Dobbs et al., 2009; Morcuende, 2006; Roye, Hyman and Roye, 2004). Morphological studies remark on thickening of soft tissue and describe a fibrous mass encapsulating the medial and posterior side of the foot, resulting in reduction in movement and elasticity of the tissue (Aurell et al., 2002; Fukuhara, Schollmeier and Uhthoff, 1994; Hersh, 1967; Ippolito and Ponseti, 1980; Sano et al., 1998; Turco, 1971; Windisch et al., 2007). The Ponseti method is a widely accepted conservative treatment that uses weekly manipulation and castings to progressively elongate the soft tissue and correct the positions of the bones of the clubfoot (Dobbs et al., 2009; Morcuende et al., 2005; Ponseti, 2000; Ponseti and Morcuende, 2004). Although this technique is highly successful, there are still concerns in the variability in outcomes, resistance to treatment, and risk of relapse. This pathology has a strong tendency to relapse, possibly due to treatment incompliance and the nature of deformity (Ponseti, 2002). Although various casting materials have been qualitatively studied in conjunction with the Ponseti method, the mechanical performance of these materials during treatment has yet to be assessed (Brewster et al., 2008; Coss and Hennrikus, 1996; Ng, Lam and Cheng, 2010; Pittner et

al., 2008). In addition, little is known about the material properties and mechanical behavior of the soft tissue exposed to treatment.

The purpose of this research is to investigate the biomechanics of conservative clubfoot correction. This will be completed by: i) conducting a kinematic assessment of the creep behavior of three common cast materials used during conservative correction, ii) developing and validating a benchtop system for the mechanical evaluation of miniature soft tissue specimens, and iii) performing a mechanical analysis to model the behavior of medial fibrotic mass tissue (MFMT) from children with clubfoot. The results from this study will provide mechanical insight into the correction process that may lead to improved patient care.

1.2 Clubfoot Pathology and Morphology

Congenital talipes equinovarus, or clubfoot, affects 130,000 to 200,000 newborns every year worldwide (Owen et al., 2012). This deformity may present as secondary to other disorders, such as those neuromuscular in nature, or as idiopathic. The etiology of idiopathic clubfoot is not well understood and may have multiple factors (Dobbs et al., 2009; Roye, Hyman and Roye, 2004; Wallander, 2010; Zhang et al., 2014).

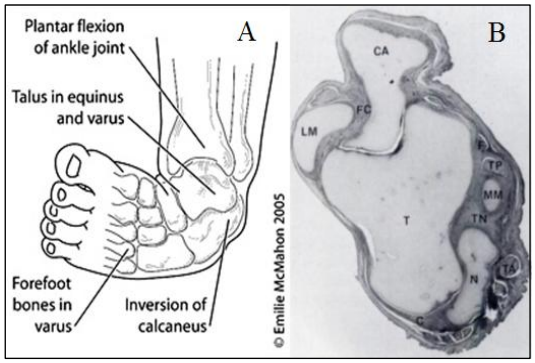

Figure 1-1: Clubfoot Deformity. A) Clubfoot presentation. ("Selected Pediatric Conditions," 2010) B) Transverse section of right clubfoot shows tibionavicular ligament (TN) to be very thick and short (Ippolito and Ponseti, 1980).

The condition varies in severity and is characterized by an equinovarus hindfoot deformity, as well as cavus and adduction of the midfoot (Figure 1-1 A) (Aurell et al.,

2002; Dobbs et al., 2009; Ippolito, 1995; Morcuende, 2006; Roye, Hyman and Roye, 2004; Roye and Roye, 2002). Not only are the bones displaced, but alterations in the soft tissue are observed (Figure 1-1 B). Histological studies have noted a thick, fibrotic mass encapsulating the medial and posterior side of the clubfoot, which may affect success of treatment (Aurell et al., 2002; Fukuhara, Schollmeier and Uhthoff, 1994; Hersh, 1967; Ippolito and Ponseti, 1980; Sano et al., 1998; Turco, 1971; Windisch et al., 2007). Hersh described a disc-like fibrous mass between the medial end of the navicular and the medial malleolus. Turco expressed that the pathological contractures of the deltoid and spring ligaments, talonavicular capsule, and posterior tibialis tendon bind the navicular, sustentaculum tali and medial malleolus. The effect of this abnormally occurring tissue, termed the medial fibrotic mass tissue (MFMT) by our group, on the success of conservative treatment is unknown.

1.3 Clubfoot Treatment and Relapse

Treatment typically is performed within the first month of birth and can include surgical or conservative interventions. Within the last few decades, the Ponseti method, developed by Dr. Ignacius Ponseti, has become the standard conservative clubfoot correction (Dobbs et al., 2009; Ponseti and

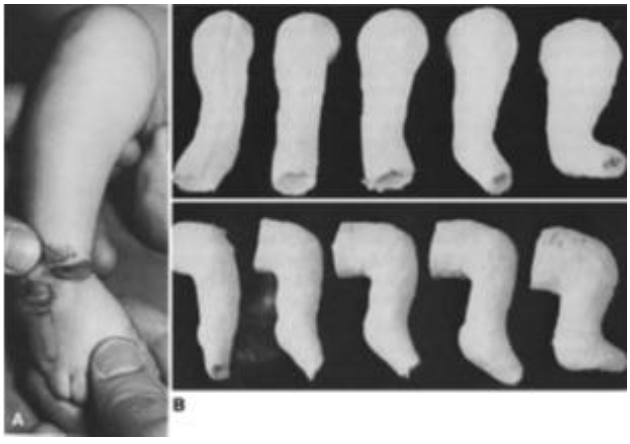

Figure 1-2: Phases of Ponseti Method, represented by casts of the left clubfoot (Ponseti and Campos, 1972)

Campos, 1972; Ponseti and Morcuende, 2004). This treatment involves weekly manipulation and plaster casting of the clubfoot to progressively re-position the foot towards normal form. Although this treatment is widely accepted and successful, relapses of the deformity do occur. In cases of resistance to conservative treatment, the clubfoot is corrected surgically. Results from previous studies have indicated the potential success of the Ponseti method with the use of cast materials other than plaster of Paris (Brewster et al., 2008; Coss and Hennrikus, 1996; Ng, Lam and Cheng, 2010; Pittner et al., 2008). Cast the comfort level of the patient, but also the efficacy of the technique. A biomechanical characterization of clinical casting materials when applied to correct pathological clubfoot has not been performed. There are no clinical guidelines for clubfoot correction based upon mechanical response of commonly used casting materials. Untreated or under-corrected clubfoot can result in abnormal gait, pain, and further foot deformity.

Clubfoot has a strong tendency to relapse, especially the hindfoot equinus and varus deformities, regardless of treatment method (Ponseti, 2002). Relapse is dependent on both treatment compliance as well as the nature of the clubfoot deformity. Contractures of the soft tissue, such as those comprising the MFMT, may hinder treatment. To date, research on clubfoot structure has focused on this tissue pathogenesis and morphology (Fukuhara, Schollmeier and Uhthoff, 1994; Ippolito, 1995; Ippolito and Ponseti, 1980; Ponseti and Campos, 1972; Sano et al., 1998). However, few studies have investigated the mechanics of these tissues, nor have longer term strategies for the treatment of severe clubfoot been based upon these principles (Hattori et al., 2007). Mechanical tests can provide information on material properties and time-dependent

(viscoelastic) behavior of the soft tissue as it responds to treatment. The ultrastructure and mechanical behavior of the fibrotic mass must be characterized in order to understand the deformation it undergoes during conservative correction.

1.4 Current Conservative Clubfoot Treatment

Early conservative strategies of clubfoot correction, such as forceful manipulations or manipulations that correct individual components of the deformity, have resulted in incomplete corrections or additional complications (Dobbs et al., 2009; Herzenberg, Radler and Bor, 2002; Ippolito et al., 2003; Richards et al., 2008). However, within the last half century, more successful, non-invasive treatments have been developed, such as the French Functional Method and the Ponseti method (Dobbs et al., 2009; Faulks and Richards, 2009; Ponseti, 2000; Richards et al., 2008).

The French Functional Method is a non-operative method of correction that requires daily manipulations of the clubfoot by a physiotherapist and immobilization with elastic and non-elastic adhesive tape. Success rate for this strategy is reported to be 74% (Cassis and Torres-Gomez, 2009; Dobbs et al., 2009; Richards et al., 2008), however, it is time consuming, as this treatment is performed daily by the physician and parents until the child is walking.

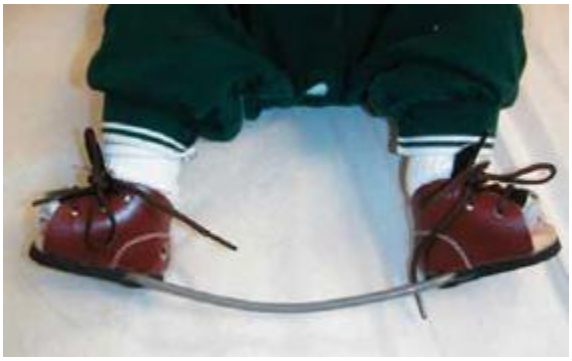

Figure 1-3: Denis-Browne brace. To be worn 23 hours per day for at least a year to prevent relapse.(Ponseti, 2000)

The Ponseti method involves a series of manipulations and castings followed by brace application, and often a percutaneous Achilles tenotomy, to

progressively obtain the correct position of the foot (Dobbs et al., 2009; Morcuende, 2006; Morcuende et al., 2005; Ponseti and Campos, 1972; Ponseti and Morcuende, 2004). Average treatment length is about five weeks, although, it varies depending on the severity of the deformity. Following casting, the patient is required to wear a foot abduction brace, such as the Denis-Browne brace, 23 hours a day for at least a year to prevent relapse. Investigators have reported high success rates, above 80%, using the Ponseti method as a treatment for clubfoot (Abdelgawad et al., 2007; Docker et al., 2007; Laaveg and Ponseti, 1980; Ponseti and Morcuende, 2004; Zionts et al., 2010). Treatment success is typically based on qualitative assessments using severity scores (Dimeglio et al., 1995; Dyer and Davis, 2006; Flynn, Donohoe and Mackenzie, 1998; Scher, 2004) and visual analysis of the affected foot (Cassis and Torres-Gomez, 2009; Graf et al., 2012; Smith et al., 2013). Although the Ponseti method is regarded as the standard of practice for clubfoot correction, not all clubfeet respond to this treatment. In addition, some patients experience relapse of the deformity. This is due to not only compliance issues, but the nature of the deformity as well. Unfortunately, it is still unclear as to how the etiology and nature of the abnormal tissues in the clubfoot affect the success of treatment.

The historical standard for clubfoot immobilization has been plaster of Paris (Dobbs et al., 2009). It has been praised for its moldability and patient comfort for serial casting purposes. However, it can be heavy, takes a long time to dry completely, and requires soaking for several hours or a cast saw to remove, risking skin injury. Alternative cast materials, such as fiberglass, used in conjunction with the Ponseti method have been proposed (Brewster et al., 2008; Coss and Hennrikus, 1996; Ng, Lam and Cheng, 2010; Pittner et al., 2008; Zmurko, Belkoff and Herzenberg, 1997). Recent

studies have examined the effect of using other orthopaedic cast materials on the efficacy of the Ponseti method, however, conclusions were unclear. Pittner et al. reported lower severity scores for patients treated using plaster of Paris than for those treated with semi-rigid fiberglass, however, satisfaction ratings favored the latter. Coss et al. found that parents preferred semi-rigid fiberglass over plaster of Paris, as well, due to its ease of removal, durability, and performance. In addition, results of using semi-rigid fiberglass from Brewster et al. were comparable to those of previous studies using plaster of Paris. Efficacy based on mechanical behavior of the cast materials has not been addressed. Material selection could affect not only the comfort level of the patient, but also treatment outcomes and duration.

1.5 Cast Materials in Orthopaedics

Three common cast materials utilized in orthopaedics are plaster of Paris, rigid fiberglass, and semi-rigid fiberglass. Although studies have qualitatively examined casts used in the Ponseti method, the appropriate casting material has not been identified based on mechanical properties. Over the last few decades, studies have been conducted to determine the mechanical properties and advantages of different cast materials, as well as to identify the advantages of using one material over another (Berman and Parks, 1990; Callahan et al., 1986; Davids et al., 1997; Deshpande and Deshpande, 2005; Martin et al., 1988; Mihalko, Beaudoin and Krause, 1989; Philbin and Gittins, 1999; Rowley et al., 1985; Schmidt, Somerset and Porter, 1973; Zmurko, Belkoff and Herzenberg, 1997). Several metrics have been investigated to define material properties, including stiffness, ultimate strength, and yield strength, based on tests applying short durations of compression, tension and bending. These metrics were examined after the recommended

curing time for weight bearing and at high loads. Several studies found plaster of Paris to be stiffer, yet less strong, than synthetic cast materials. Few studies have examined the time dependent behavior of these materials, however, it has not been modeled (Davids et al., 1997; Deshpande and Deshpande, 2005; Mihalko, Beaudoin and Krause, 1989). Mihalko et al. attributed different regions of elasticity to the individual materials in the plaster of Paris cast, hard plaster and elastic gauze. Investigations of pressure response on different cast materials concluded that these materials do exude a viscoelastic behavior (Davids et al., 1997; Deshpande and Deshpande, 2005). However, none of these tests were based on models that adequately represent clubfoot correction. Corrective casts used with the Ponseti method are applied across a joint and are subjected to complex loads for up to seven days. These previous models do not account for the permanent deformation that occurs under prolonged, low level loading conditions, or creep.

1.6 Characterization of Clubfoot Soft Tissue

Ligaments are connective tissue that link bones to bones, and act as passive joint stabilizers (Frank, 2004; Martin, Burr and Sharkey, 1998; Winkelstein, 2013). The mechanical behavior of ligaments is influenced by

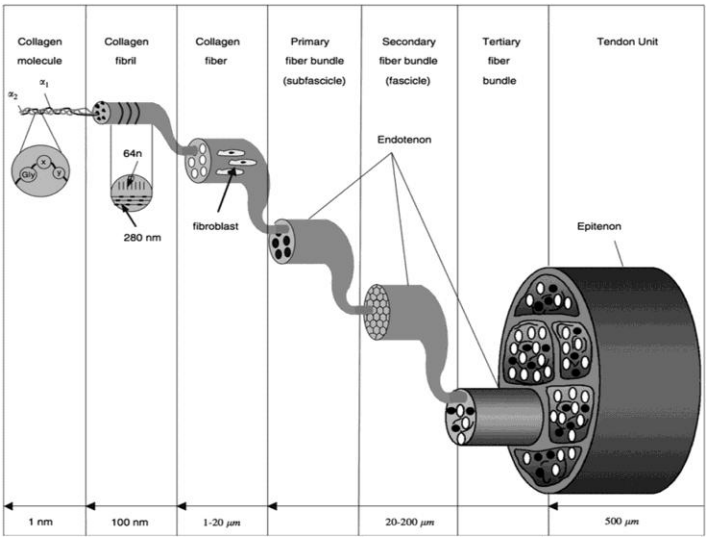

Figure 1-4: Ligament structure. (Galloway, Lalley and Shearn, 2013)

the tissue's composition and structure, which consists of densely packed aligned type I collagen fibers (70% of dry weight) in an amorphous extracellular matrix of proteoglycan, glycosaminoglycan (20%-30% dry weight), and water (Figure 1.4) (70% wet weight) (Elliott et al., 2003; Frank, 2004; Oza, Vanderby and Lakes, 2006; Wang, Guo and Li, 2012; Winkelstein, 2013). Orientation of the collagen fiber bundles in typically developing ligaments is along the principal axis of stress (Frank, 2004; Jung, Fisher and Woo, 2009; Martin, Burr and Sharkey, 1998; Nordin and Frankel, 2012; Winkelstein, 2013).

Studies describing the pathology have focused on morphology and pathogenesis (Aurell et al., 2002; Fukuhara, Schollmeier and Uhthoff, 1994; Ponseti and Campos, 1972; Sano et al., 1998), however, they have yet to give a quantifiable depiction of the clubfoot connective tissue. Ippolito and Ponseti showed shortened and thicker than normal medial ligaments. These findings were supported by those of Aurell, who used ultrasound to measure the increased thickness of the medial soft tissue. Histological and immunohistochemical studies have found medial soft tissue of clubfeet to have disorganized arrangement of collagen fibers (Fukuhara, Schollmeier and Uhthoff, 1994; Ippolito and Ponseti, 1980; Sano et al., 1998). An immunohistochemical study by Sano et al. found the ligamentous cells to be arranged haphazardly with varying nuclei shapes. Findings from Fukahara et al. included disruption of collagen fiber orientation, fragmented bundles, irregular fascicles, and densely packed collagen fibers.

Little is known about the material properties and mechanical behavior of the soft tissue in the clubfoot. Hattori in 2007 examined elasticity of medial, posterior and lateral

specimens of clubfoot hindfoot soft tissue (deltoid and calcaneofibular ligaments and capsular tissue) using scanning acoustic microscopy (Hattori et al., 2007). This technology measures the tissue sound speed at the microscopic level. A relationship exists between speed of sound and elastic modulus, density and Poisson's ratio. Medial tissue had reportedly lower sound speed, therefore, lower elastic modulus values than its lateral tissue counterparts. However, the Poisson's ratio of these tissues was unknown and the values of the modulus were not able to be calculated. In addition, no studies have investigated the viscoelastic behavior of clubfoot soft tissue and its effect on conservative treatment.

The lack of information regarding the time- and history- dependent behavior of cast materials and of the MFMT of the clubfoot necessitates the current study to biomechanically characterize clubfoot treatment.

1.7 Time-Dependent Mechanical Testing and Analysis

Viscoelasticity is the time-dependent stress and strain behavior of a material. When subjected to a low-level constant load or stress for a prolonged period of time, a material will experience a phenomenon called creep (Figure 1-5B). When elongated and held at a constant and small displacement or strain for a prolonged period of time, the material is said to undergo stress relaxation (Figure 1-5A), Another phenomena of viscoelasticity is called hysteresis, which occurs during the loading and unloading of a material, and represents the energy dissipated as heat during deformation and recovery phases (Figure 1-5C). For ligaments, it has been hypothesized that these phenomenon are due to molecular reorganization and interaction between collagen and proteoglycans

(Elliott et al., 2003; Frank, 2004; Purslow, Wess and Hukins, 1998; Woo, Johnson and Smith, 1993).

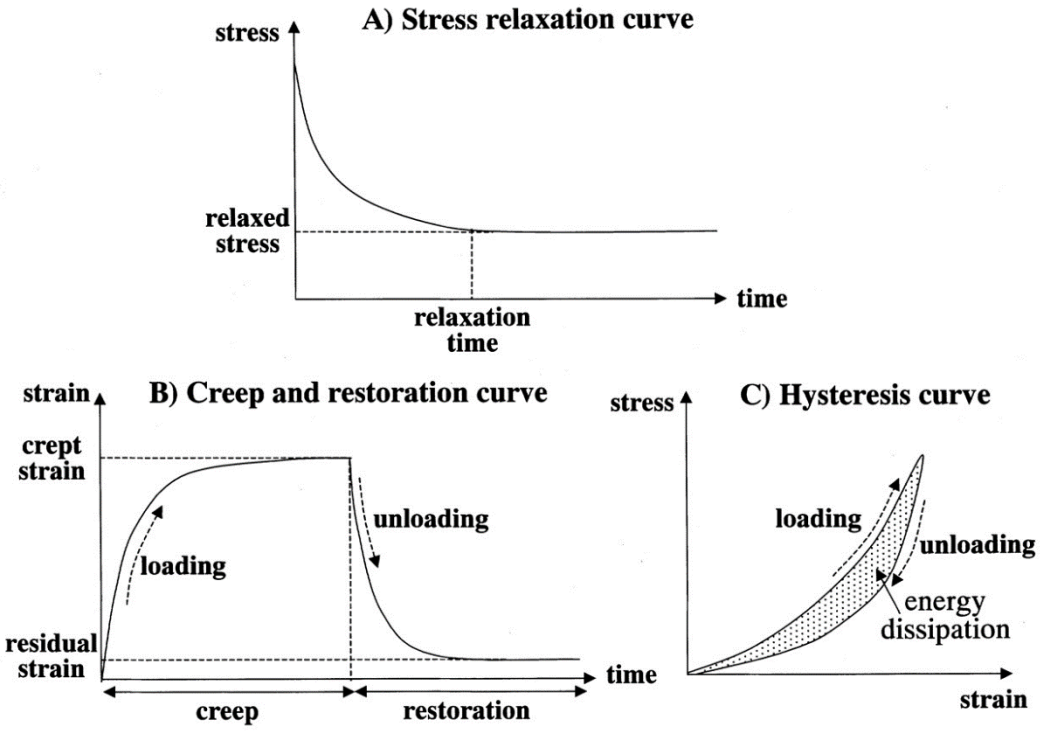

Figure 1-5: Phenomenon of viscoelasticity (Tanaka and van Eijden, 2003).

Viscoelasticity can be linear and dependent on time, or nonlinear and dependent on both time and stress or strain. For a linear viscoelastic material, strain is proportional to stress, e.g. at any given time during creep, the strain ε resulting from a stress $c\sigma$ equals the constant c times the strain resulting from σ [i.e., $\varepsilon(t_i, c\sigma) = c\varepsilon(t_i, \sigma)$]. Alternatively, the stress-strain relationship for nonlinear viscoelastic materials does not follow this trend. Linearity can be determined using an isochronous stress vs. strain plot, where stress and strain are plotted for a given time. Mathematical models have been developed to describe both types of behavior (Abramowitch and Woo, 2004; Oza, Vanderby and Lakes, 2006; Woo, Johnson and Smith, 1993; Woo, 2005).

The most common model used for ligament behavior characterization is the quasi-linear viscoelastic model presented by Fung and has been used by many investigators to model ligaments and tendons (Abramowitch and Woo, 2004; Abramowitch et al., 2003; Fung et al., 1972; Funk et al., 2000; Oza, Vanderby and Lakes, 2006; Woo, Johnson and Smith, 1993; Woo, 2005). Quasi-linear viscoelasticity (QLV) is a special type of nonlinear superposition for which time and stress dependence are separable (Fung et al., 1972). For this case, the creep compliance or relaxation modulus is a product of time dependent and stress or strain dependent functions. If $\varepsilon(t)$ is the time dependent strain, $\sigma(t)$ is the time dependent stress, $\bar{J}$(t) is the reduced creep function, and $\bar{G}(t)$ is the reduced relaxation function (Eqs. 1.1 and 1.2),

Creep: $$\varepsilon(t) = \bar{J}(t)\varepsilon^e(\sigma) \quad (1.1)$$

Stress Relaxation: $$\sigma(t) = \bar{G}(t)\sigma^e(\varepsilon). \quad (1.2)$$

The elastic responses, $\sigma^e(\varepsilon)$ and $\varepsilon^e(\sigma)$, represent the maximum stress and strain in response to an instantaneous step input of strain ε and stress σ, respectively. The reduced creep and relaxation functions represent the time-dependent stress and strain responses normalized by the stress and strain at the time of the step input, respectively [i.e., $\bar{J}(t) = \frac{\varepsilon(t)}{\varepsilon_o}$, $\bar{J}(0^+) = 1$; $\bar{G}(t) = \frac{\sigma(t)}{\sigma_o}$, $\bar{G}(0^+) = 1$.] Assuming the validity of the Boltzmann superposition principle, for a general strain history, the stress at time *t*, $\sigma(t)$, takes the form of the convolution integral:

$$\sigma(t) = \int_{-t}^{t} \bar{G}(t-\tau)\frac{\partial \sigma^e(\varepsilon)}{\partial \varepsilon}\frac{\partial \varepsilon}{\partial \tau}\partial\tau. \quad (1.3)$$

The overall height of the relaxation curve is representative of the purely strain dependent elastic nonlinearity, while time dependence manifests itself in the shape of the curve. Time dependent behavior is the same for creep curves regardless of stress level and

relaxation curves for any level of strain. For soft tissue whose stress-strain relationship is not very sensitive to strain rate, the relaxation function can be expressed by the equation proposed by Fung (Eq. 1.4) (Abramowitch and Woo, 2004; Fung et al., 1972) and used to define specific material coefficients:

$$\bar{G}(t) = \frac{1 + C\left(E_1\left(\frac{t}{\tau_2}\right) - E_1\left(\frac{t}{\tau_1}\right)\right]}{1 + Cln\left(\frac{\tau_2}{\tau_1}\right)}, \tag{1.4}$$

where $E_1(y) = \int_y^\infty \frac{e^{-z}}{z} dz$ is the exponential integral. Parameters $C, \tau_1,$ and τ_2 are material coefficients, where *C* determines the magnitude of viscous effects and is related to the percentage of relaxation, while $\tau_1,$ and τ_2 govern initial and late relaxation (Abramowitch et al., 2004). A more generalized function for relaxation is the decaying exponential function (Eq 1.5) (Funk et al., 2000; Thornton et al., 1997; Toms et al.; Wills, Picton and Davies, 1972):

$$\overline{G}(t) = G_1 e^{-\lambda_1 t} + G_2 e^{-\lambda_2 t} + G_5 e^{-\lambda_3 t}, \tag{1.5}$$

where $G_{1\text{-}3}$ are material coefficients, while $\lambda_{1\text{-}3}$ are rates representing exponential decay constants and related to exponential the time constant [$\lambda = 1/\tau$]. If *A* and *B* are material coefficients, the elastic response $\sigma^e(\varepsilon)$ can be described using the exponential approximation (Eq. 1.6),

$$\sigma^e(\varepsilon) = A(e^{B\varepsilon} - 1). \tag{1.6}$$

Physically, parameter *B* represents the rate of change of the slope of the stress-strain curve and the product *AB* represents the initial slope of the curve (Abramowitch et al., 2004). The effect of QLV and decaying exponential parameter variation can be seen the stress relaxation curves in Figure 1-6. Parameter *A* has a linear effect on the peak and equilibrium stresses, while parameter *B* affects these values nonlinearly (Winkelstein,

2013). Variations in G_1 and λ_1 have a linear and nonlinear effect on the relaxation rate, respectively. G_2 contributes linearly to the peak stress, while λ_2 influences the late

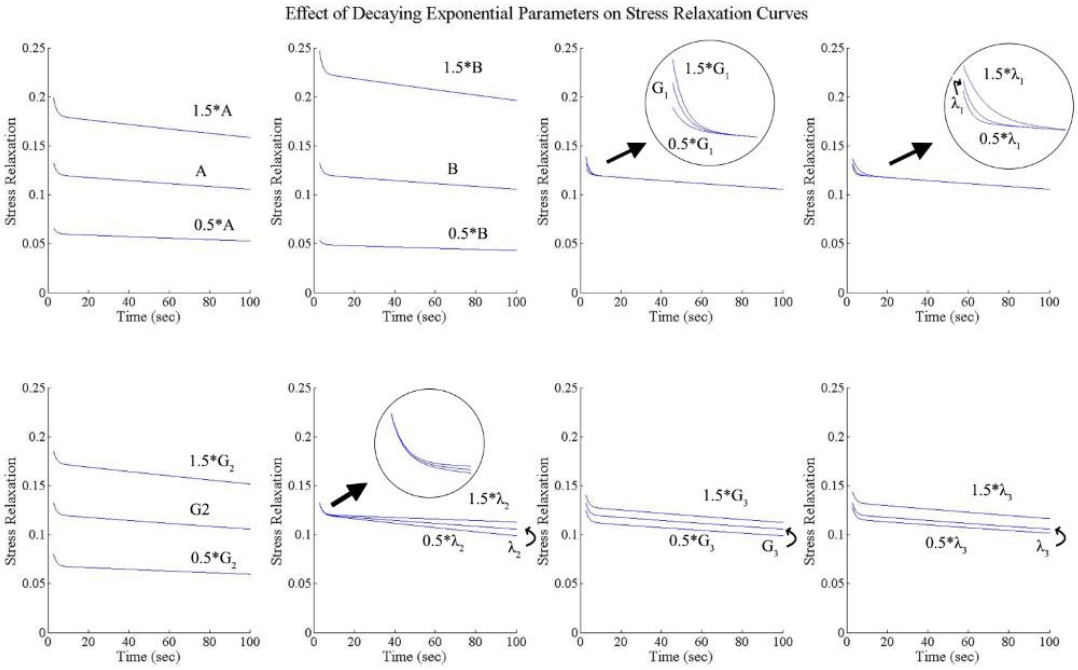

Figure 1-6: Effect of parameter variation on stress relaxation curves. Parameters include those from the decaying exponential function ($G_{1\text{-}3}$, $\lambda_{1\text{-}3}$**)** and elastic response *A, B).* For each subplot, all parameters except the parameter indicated on the plot are kept constant.

relaxation behavior. G_3 and λ_3 have minimal influence over the relaxation behavior, linearly and nonlinearly.

To determine these parameters from reduced relaxation function $\overline{G}(t)$ and elastic response, $\sigma^e(\varepsilon)$, curve-fitting is performed on the experimental data. Two methods are commonly utilized in literature: 1) instantaneous step assumption (Butler et al., 2004; Funk et al., 2000; Thornton et al., 1997) and 2) strain history approach (Abramowitch and Woo, 2004; Moon et al., 2006). The first assumes an instantaneous step input of the stress or load, therefore the initial rise is ignored and the relaxation function *G(t)* is calculated

defining the time of peak force response as $t = 0$. This requires higher strain rates to minimize the rise time. To find *A* and *B*, elastic response from the stress-strain response during the ramping portion or approximated with the stress-strain isochrones at peak stress values of various strain magnitudes can be fitted with Eq. 1.6 (Abramowitch and Woo, 2004; Funk et al., 2000). The strain history approach, developed by Abramowitch and Woo (Abramowitch and Woo, 2004), takes into account the ramping phase of testing and assumes a constant strain rate γ during that time from $0<t<t_0$. In this method, the equation for reduced relaxation function (Eqs. 1.4 or 1.5) and the equation for elastic response (Eq. 1.6) are substituted into Eq. 1.3. For the decaying exponential function of relaxation, this takes the form:

$$\sigma(0 \le t \le t_0) = AB\gamma \int_0^t \{G_1 e^{-\lambda_1 t} + G_2 e^{-\lambda_2 t} + G_3 e^{-\lambda_3 t}\} e^{B\gamma\tau}\, \partial\tau \qquad (1.7)$$

$$\sigma(t > t_0) = AB\gamma \int_0^{t_0} \{G_1 e^{-\lambda_1 t} + G_2 e^{-\lambda_2 t} + G_3 e^{-\lambda_3 t}\} e^{B\gamma\tau}\, \partial\tau. \qquad (1.8)$$

This method takes into account the relaxation that occurs during the ramping; therefore the estimates of the constants may be different between the two methods (Abramowitch and Woo, 2004; Dortmans, Sauren and Rousseau, 1984).

1.8 Hypotheses and Specific Aims

The goal of this study was to biomechanically characterize conservative clubfoot correction in order to aid in the development of improved treatment strategies for affected children. The objectives of this dissertation are to: i) evaluate creep behavior of three common cast materials occurring during simulated clubfoot correction based on the Ponseti Method and ii) characterize the mechanical behavior of medial fibrotic mass tissue from children with resistant or recurring clubfoot. The results of this study will be

useful in identifying a more appropriate material to be used in conservative treatment. Mechanical insight into the abnormal clubfoot tissue may assist in developing new corrective approaches. It is hypothesized that:

1. Creep responses of three cast materials undergoing simulated clubfoot correction for minimum and maximum joint stiffness are pairwise the same.
2. Tissue material properties and stress relaxation behavior of medial fibrotic mass tissue from clubfoot patients undergoing corrective surgery vary between specimens and differ from those of normal medial foot ligaments.

To achieve the study objectives, the following specific aims were accomplished:

1. Quantify and compare the creep response of the cast-foot system as a function of resistive joint stiffness.
    a. Develop a casting technique to be used in accordance with the Ponseti method.
    b. Design and build a mechanical test system to be used to simulate conservative clubfoot correction.
    c. Develop and employ a two segment, three-dimensional motion analysis protocol to calculate joint (Euler) angles.
    d. Statistically analyze and model kinematic data using a 2-way ANOVA, post-hoc pairwise comparison with Tukey adjustment, and curve fitting.
2. A) Develop and validate a soft tissue testing system for uniaxial material experimentation, and B) demonstrate system versatility via the testing of synthetic and biological specimens.

a. Develop structure and control program for a benchtop, portable mechanical system for the evaluation of miniature soft tissue specimens.
b. Calibrate the system via a voltage-to-force correlation.
c. Perform comparative uniaxial tensile tests on nylon monofilament using the custom-made machine and a commercially available material testing system.
d. Statistically analyze elastic modulus to address system and machine validity.
e. Conduct quasistatic and viscoelastic tests on PTFE tape and rabbit knee ligaments, respectively, to assess versatility.

3. Obtain material properties and model the behavior of the clubfoot MFMT in response to Ponseti method-based stress relaxation protocol.
    a. Perform a Ponseti method-based stress relaxation protocol on medial fibrotic mass tissue from pediatric clubfoot patients.
    b. Compute preconditioning hysteresis area, stiffness, elastic modulus, and reduced relaxation for each specimen.
    c. Assess the linearity of the stress relaxation behavior of the tissue via quasi-linear viscoelasticity.
    d. Statistically analyze the mechanical properties and stress relaxation model of the tissue between specimens and against reported values for normal medial ankle ligaments.

CHAPTER 2: CAST MATERIAL ASSESSMENT

This chapter details a quantitative evaluation of the response of three common cast materials during simulated conservative clubfoot correction. The creep rotation of three commonly used cast materials was monitored through the application of an experimental foot model simulating the second phase of clubfoot correction. Low and high constant torques were applied to the model to represent ankle joint stiffness severities. A version of this chapter was previously published in Journal of Engineering in Medicine (Cohen et al., 2013) and as an IEEE EMBS conference short paper (Cohen et al., 2012).

2.1 Introduction

Idiopathic clubfoot is a congenital deformity of the lower extremity, with a prevalence of one to six in 1000 births (Dobbs et al., 2009; Morcuende, 2006; Owen et al., 2012; Parker et al., 2009; Shabtai, Specht and Herzenberg, 2014; Terrazas-Lafargue et al., 2007). The Ponseti method is a mainstay conservative treatment technique that is widely accepted and practiced today (Dobbs et al., 2009; Morcuende, 2006; Ponseti and Campos, 1972; Richards et al., 2008; Roye, Hyman and Roye, 2004). It relies on manipulation and casting of the foot performed weekly for on average of five weeks, depending on deformity severity. Clubfoot correction by use of the Ponseti method has been shown to be successful in progressive correction of the foot (Abdelgawad et al., 2007; Brewster et al., 2008; Herzenberg, Radler and Bor, 2002; Laaveg and Ponseti, 1980; Morcuende, 2006; Radler et al., 2007; Zionts et al., 2010).

The historical standard for clubfoot immobilization has been plaster of Paris (POP) (Dobbs et al., 2009; Laaveg and Ponseti, 1980; Pittner et al., 2008; Ponseti and Campos, 1972). It has been praised for its moldability and patient comfort for serial casting purposes. However, it can be heavy, takes a long time to dry completely, and requires soaking for several hours or a cast saw to remove it, risking skin injury. Material selection could affect not only the comfort level of the patient, but also treatment outcomes and duration (Pittner et al., 2008). Alternative cast materials used in conjunction with the Ponseti method have been considered (Brewster et al., 2008; Coss and Hennrikus, 1996; Pittner et al., 2008; Zmurko, Belkoff and Herzenberg, 1997). Coss et al. found that parents preferred semi-rigid fiberglass (SRF) over POP due to its ease of removal, durability, and performance (Coss and Hennrikus, 1996).

Over the last few decades, studies have been conducted to determine the mechanical properties and advantages of different cast materials, as well as to identify the advantages of using one material over another (Berman and Parks, 1990; Callahan et al., 1986; Davids et al., 1997; Deshpande and Deshpande, 2005; Martin et al., 1988; Mihalko, Beaudoin and Krause, 1989; Philbin and Gittins, 1999; Rowley et al., 1985; Schmidt, Somerset and Porter, 1973; Zmurko, Belkoff and Herzenberg, 1997). Several metrics have been investigated to define material properties, including stiffness, ultimate strength, and yield strength, based on tests applying short durations of compression, tension, and bending. However, these tests were based on models that do not adequately represent the clinical application. Corrective casts used with the Ponseti method are applied across a joint and are subjected to complex load for up to seven days. These previous models do not account for the permanent cast deformation that occurs under

prolonged, low level loading conditions, or creep. In a recent study performed by our group, differences in performance were seen between SRF and rigid fiberglass (RF) casts that were monitored on a custom-made clubfoot correction model (Cohen et al., 2012). POP has yet to be examined in this manner, and models addressing the linearity of the viscoelastic behavior of these cast materials have not been investigated. Further insight regarding the biomechanics of Ponseti cast correction will require continued modeling efforts (Zmurko, Belkoff and Herzenberg, 1997). A better understanding of the cast creep behavior may influence the duration and efficacy of clubfoot treatment.

The purpose of this study was to assess the ability of three common cast materials to hold the foot in position. The objectives addressed in this study were 1) to quantify creep of POP during Ponseti correction under two different corrective joint load conditions, 2) to assess the viscoelastic linearity of the limb-cast composite, and 3) to compare the results of the POP behavior test to those of synthetic cast materials. Cast creep was evaluated through application of an experimental foot model with an articulation acting in the transverse plane. Low and high torques were applied through the transverse plane to the model during the setting process and beyond as measured using three-dimensional motion capture technology. Cast creep was monitored by tracking the motion of the internal "foot" structure of the model.

2.2 Materials and Methods

2.2.1 Device Design

A quasi-static cast testing device (QSCTD) was built to model pediatric clubfoot correction with long leg casting (Figure 2-1). Anatomic segments were constructed from

1-inch diameter PVC couplings (Dura Plastic Products, Beaumont, CA). A stainless steel hinge (¼-inch diameter pin, 3-11/32 inch leaf length) (McMaster-Carr, Illinois, USA) was cemented into the foot and shank segments. This hinge represented a single axis of correction about which the cast creep behavior was evaluated. Two joint stiffness conditions were simulated by the application of a constant torque through a weighted cable. These values represented the minimum and maximum corrective torques required to sufficiently abduct the foot of a Ponseti teaching model (MD Orthopaedics; Wayland, IA) to neutral position. Details of the torque acquisition protocol can be found in section 2.2.2.

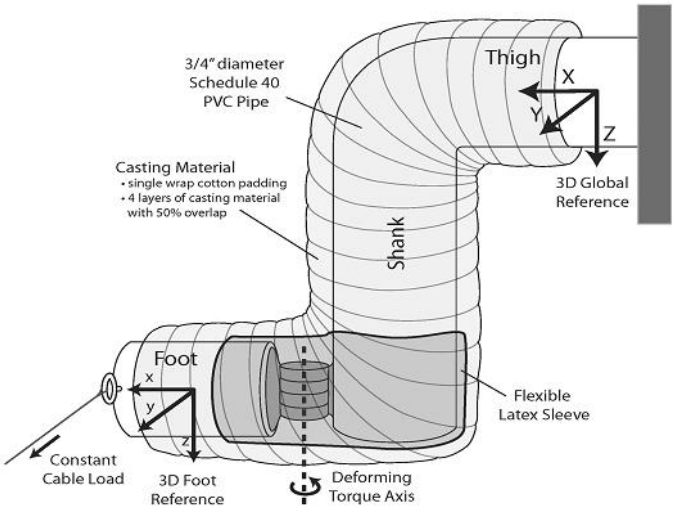

Figure 2-1: Representation of quasistatic cast testing device.

A triad of 7-mm diameter Infra-Red-light-Emitting-Diode (IRED) markers (Northern Digital Inc., Ontario Canada) was placed at each end of the device. The distal triad was situated at the same distance from the axis of rotation as the load application. It was secured in place with a metal rod through the shell of the PVC coupling with cyanoacrylate and bone cement. The proximal triad was formed by securing two markers at the ends of a thin metal rod that poked through the shell of the fixed PVC segment. The third marker was position with the same method, at an angle to the aforementioned rod. All markers faced an Optotrak Measurement System (0.01 mm resolution; 0.1 mm

3D accuracy) (Northern Digital Inc., Ontario Canada) in order to monitor three-dimensional motion during testing.

2.2.2 Torque Acquisition

The constant torque values used in this study were acquired through the use of a pre-treated pediatric clubfoot training model (MD Orthopaedics; Wayland, IA). Two experienced orthopaedic surgeons (HA and PAS, Shriners Hospitals for Children®, Chicago, IL) simulated the Ponseti method of correction on the training tool. A force scale and calipers were used to measure the force applied to the model and the lever arm, the distance from the head of the talus to the point of load application, respectively. Seven trials in total were recorded and the minimum and maximum torques equated to 0.45 Nm and 0.75 Nm respectively.

2.2.3 Cast Materials

The cast materials in this study included plaster of Paris (BSN Medical; Charlotte, NC), rigid fiberglass (3M™; Parsippany, NJ), and semi-rigid fiberglass (3M™; Parsippany, NJ) (Table 2-1). In accordance to standard casting practices, a single layer of cast padding (3M™; Parsippany, NJ) was wrapped around the device. Casting materials were supplied by the Orthopaedic Department at Shriners Hospitals for Children® in Chicago, IL.

Table 2-1: Casting materials and specifications.

Material	Brand Name	Manuf.	Size	Water Temp	Layers	Setting Time
Plaster of Paris	Extra Fast Setting Specialist® Plaster Bandage	BSN Medical	2 in x 3 yrds	75° F	4	2-4 min
Semi-Rigid Fiberglass	3M™ Scotchcast™ Soft Cast	3M™	2 in x 4 yrds	75° F	4	3-4 min
Rigid Fiberglass	3M™ Scotchcast™ Plus Enhancing Performance Casting Tape	3M™	2in x 4 yrds	75° F	4	3-4 min
Padding	3M™ Synthetic Cast Padding	3M™	2 in x 4 yrds	N/A	1	N/A

2.2.4 Cast Testing Protocol

Per vendor instructions, room temperature water was used for cast soaking. A latex sleeve, filled with two cotton balls, was placed loosely around the joint and secured to the two segments with rubber bands to protect the hinge from the padding and cast material. The device was held in static position with a stopper during the set-up and setting time. The torque (minimum or maximum value) was applied prior to application of padding and cast. A single layer of padding was wrapped, with 50% overlap, around the device, enveloping both segments, beginning at the point of load application on the distal segment.

Figure 2-2: Cast testing device set-up.

The device was casted by a trained

investigator with each material based on the Ponseti method (9), standard casting practices, and manufacturers' recommendations. The cast material was soaked in the room temperature water until all air bubbles escape from the roll. For plaster of Paris, the roll was lightly squeezed to remove excess water. For synthetic material, removal of excess water was not performed. Four layers of the cast were wound around the device, with 50% overlap and along the same length as the padding (Figure 2-2). Molding and contouring was performed to ensure a proper fit and adhesion. Timing began at the initiation of casting to monitor the setting time and data acquisition intervals.

The distal segment was unfixed at three minutes forty-five seconds after the start of cast application. Data acquisition began four minutes after the start of cast application, for a period of ten minutes at a sampling frequency of 1 Hz. Two more ten minute intervals were collected beginning at eighteen minutes and sixty minutes into the trial. Five trials were completed for each cast material per torque for a total of thirty trials in this study.

2.2.5 Coordinate System Set-up

The coordinate systems of the foot and the shank-thigh segments were oriented with the z-axis pointing up, the y-axis pointing to the subject's left, and the x-axis pointing forward (Figure 2-1). The origin of the distal segment was taken as the midpoint of the line between markers 1 and 2. The y-axis was defined as the vector from the origin pointing in the direction of marker 2. The z-axis was defined as the normal to the plane created by the vector from the origin in the direction of marker 3 and the y-axis. The x-axis was calculated as the normal to the plane created by the y-axis and the z-axis. The origin of the proximal segment was taken as the midpoint of the line between markers 4

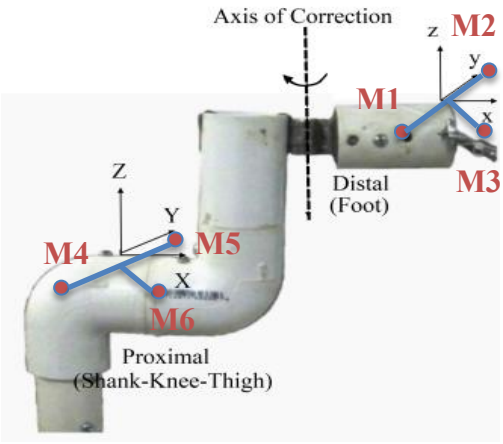

Distal Segment

$$D_o = \frac{M_1 + M_2}{2}$$

$$Y_D = \frac{M_2 - D_o}{|M_2 - D_o|}$$

$$Z_D = \frac{M_3 - D_o}{|M_3 - D_o|} \; x \; Y_D$$

$$X_D = Y_D \; x \; Z_D$$

Proximal Segment

$$P_o = \frac{M_4 + M_5}{2}$$

$$Y_P = \frac{M_5 - P_o}{|M_5 - P_o|}$$

$$Z_P = \frac{M_6 - P_o}{|M_6 - P_o|} \; x \; Y_P$$

$$X_P = Y_P \; x \; Z_P$$

Figure 2-3: Coordinate system set-up and equations.

and 5. The y-axis was the vector from the origin pointing in the direction of marker 5. The z-axis was defined as the normal to the plane created by the vector from the origin in the direction of marker 6 and the y-axis. The x-axis will be calculated as the normal to the plane created by the y-axis and the z-axis.

2.2.6 Analytical Methods

The motion data from each trial were analyzed in a custom-written program in Matlab (MathWorks, Natick, MA), and Euler angles and translation were computed throughout testing. The Euler angle sequence, Z-Y-X, were used to describe the joint movement of the distal (foot) segment with respect to the proximal (shank-thigh) segment. The z-axis was assumed to align with the axis of the hinge. Creep rotation about the z-axis was calculated as:

$$\Delta\theta(t) = \theta(t) - \theta_o, \qquad (2.1)$$

where $\theta(t)$ is the angle at time t, θ_o is the angle at time t_o, and t is the time interval in seconds starting at t_o(elapsed time = 66 min). Creep rotation values were compared at the end of each trial and at the end of each interval. The creep rotation versus time data was

curve-fitted using a nonlinear least squares formulation. Predicted values were calculated from the best-fit model at times of 20 minutes, 70 minutes, 72 hours, 5 days, and 7days.

To further explore the behavior of the limb-cast composite, the quasi-linear viscoelasticity model (QLV), proposed by Fung (Fung et al., 1972), was used to assess stress and time dependencies of the creep (Eq. 2.2).

$$\varepsilon(t,\sigma) = \bar{J}(t)\varepsilon^{e}(\sigma), \tag{2.2}$$

where $\varepsilon(t,\sigma)$ is the creep strain at time *t* under stress σ, $\varepsilon^{e}(\sigma)$ is the instantaneous elastic response and $\bar{J}(t)$ is the reduced creep compliance function representing the time-dependent strain response normalized by the strain at the time of the step input of stress.

From torsional deformation theory, shear strain (γ) is proportional to the radius (r) and length (L) of a circular rod, as in Eq. 2.3:

$$\gamma = \frac{r\theta}{L}, \tag{2.3}$$

where θ is the rotation angle. Assuming equal radii and lengths across trials, it was possible to relate shear strain across groups in the form of rotation. Substituting Eq. 2.3 into Eq. 2.2, the relationship between creep strain and creep compliance became:

$$\theta_{c}(t,\sigma) = \bar{J}(t) * \theta^{e}(\sigma), \tag{2.4}$$

where $\theta_{c}(t,\sigma)$ is the creep shear strain represented by the rotation at time *t* under shear stress condition σ, and $\theta^{e}(\sigma)$ is the elastic response at σ. The rotation data from each trial was normalized with the instantaneous elastic strain response to calculate the reduced creep function. Curve fitting was performed on the reduced creep function from trials of all three cast materials using nonlinear least squares formulation.

Statistical analysis was performed using R (www.r-project.org). The distribution of residuals of the creep rotation, creep compliance, and parameter data were tested using

the Shapiro-Wilk test. Cast material and torque were the factors explored via one- and two-way ANOVA models and Tukey Honest Significance Difference tests. A Kruskal-Wallis one-way ANOVA were performed on data not normally distributed. Significance level was defined as $p < 0.05$. This statistical approach was determined in conjunction with the project biostatistician.

2.3 Results

Translational and rotational kinematic data were computed from the recorded marker positions for all trials and used to determine creep. The resultant translational displacement between the segments was less than 0.05 mm for each of the cast materials under either torque. Creep rotation about the axis of the hinge (z-axis) of the POP, SRF, and RF trials corresponds with forefoot adduction (Figure 2-4). Figure 2-4 presents the mean and banded standard deviation of the experimental creep responses for the three cast materials tested during the three recorded time intervals.

The mean creep rotation was calculated for the total trial and per interval (Table 2-2). Comparing all three cast materials, the greatest amount of creep rotation was experienced by the POP. Within the first ten minutes of the hour long creep trial, all three cast materials underwent at least 65% of the total creep experienced. A two-way ANOVA found material type to significantly affect the total and interval creep rotation, while the effect of torque was negligible (Table 2-3).

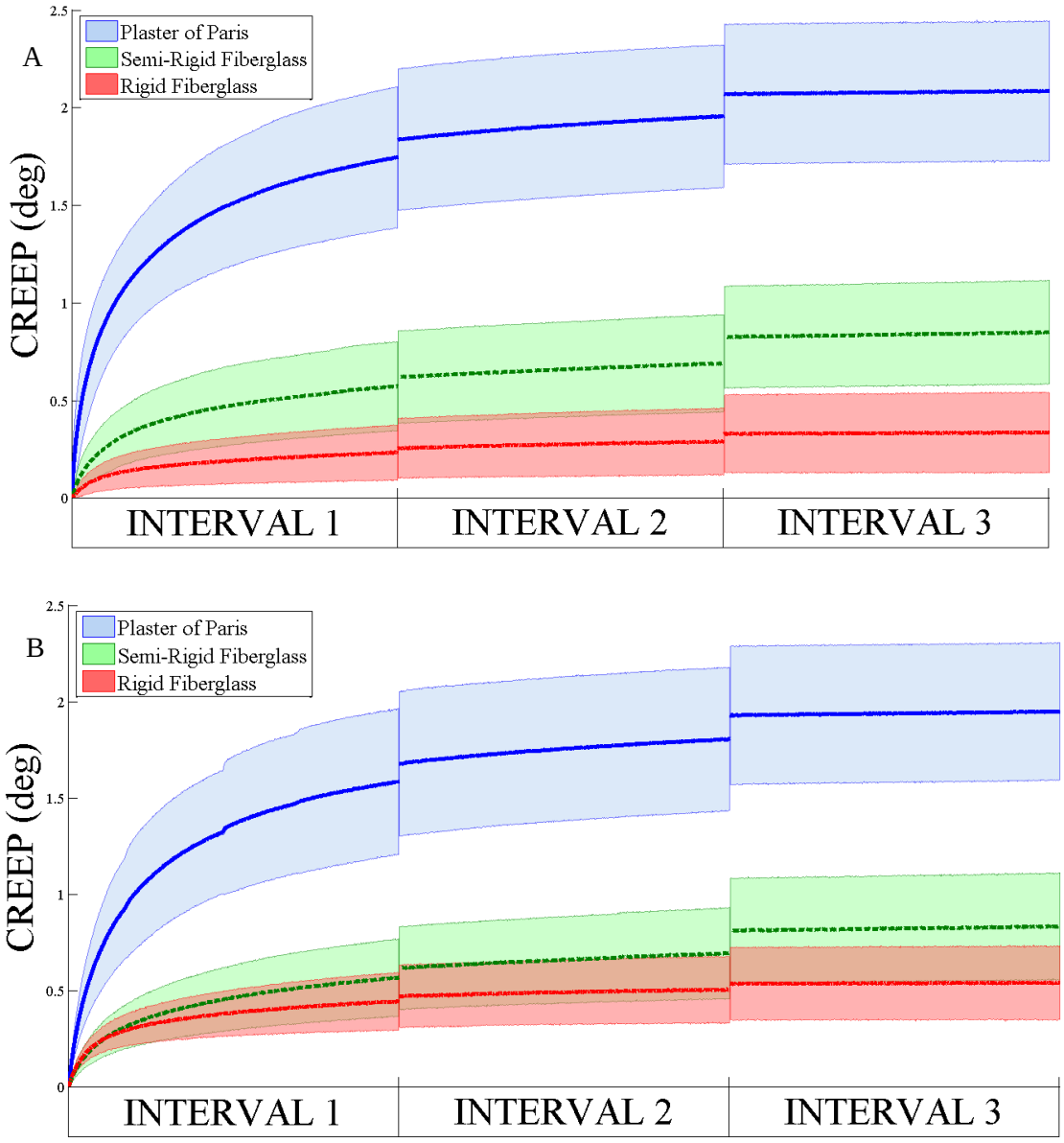

Figure 2-4: Mean and standard deviation of creep rotation for POP, SRF, and RF under A) low and B) high torques. Interval 1: 4 – 14 minutes; Interval 2: 18 – 28 minutes; Interval 3: 60 – 70 minutes.

Table 2-2: Creep rotation. Mean ± standard deviation creep rotation in each interval and total creep rotation about the axis of correction (z) of 3 cast materials under 2 torque conditions during simulated clubfoot correction. Interval 1: 4 – 14 minutes; Interval 2: 18 - 28 minutes; Interval 3: 60 – 70 minutes.

Cast Material	Plaster of Paris		Semi-rigid Fiberglass		Rigid Fiberglass	
Torque	**Low**	**High**	**Low**	**High**	**Low**	**High**
Interval 1 (deg)	1.7 ± 0.4	1.6 ± 0.4	0.6 ± 0.2	0.6 ± 0.2	0.2 ± 0.1	0.4 ± 0.2
Interval 2 (deg)	0.1 ± 0.03	0.1 ± 0.01	0.07 ± 0.02	0.08 ± 0.02	0.03 ± 0.02	0.3 ± 0.02
Interval 3 (deg)	0.01 ± 0.001	0.02 ± 0.01	0.02 ± 0.008	0.02 ± 0.01	0.008 ± 0.008	0.007 ± 0.007
Total (deg)	2.1 ± 0.4	2.0 ± 0.4	0.9 ± 0.3	0.8 ± 0.3	0.3 ± 0.2	0.5 ± 0.2

Table 2-3: Table of statistics. Significance *p*–values are from the 2-way ANOVA and Tukey tests performed on the overall creep model for the total trial and the creep rotation seen during each interval. Intervals: (1): 4–14 min; (2): 18–28 min; (3): 60–70 min. **p<0.05.*

		Material	Torque	Interaction
		p	***p***	***P***
Total		< 0.0001*	0.85	0.4
	POP – SRF	< 0.0001*		
	POP – RF	< 0.0001*		
	SRF – RF	0.01*		
Interval 1		< 0.0001*	0.87	0.3
	POP – SRF	< 0.0001*		
	POP – RF	<0.0001*		
	SRF – RF	0.13		
Interval 2		< 0.0001*	0.55	0.86
	POP – SRF	< 0.0001*		
	POP – RF	< 0.0001*		
	SRF – RF	< 0.0001*		
Interval 3		0.0005*	0.88	0.58
	POP – SRF	0.16		
	POP – RF	0.036*		
	SRF – RF	0.0003*		

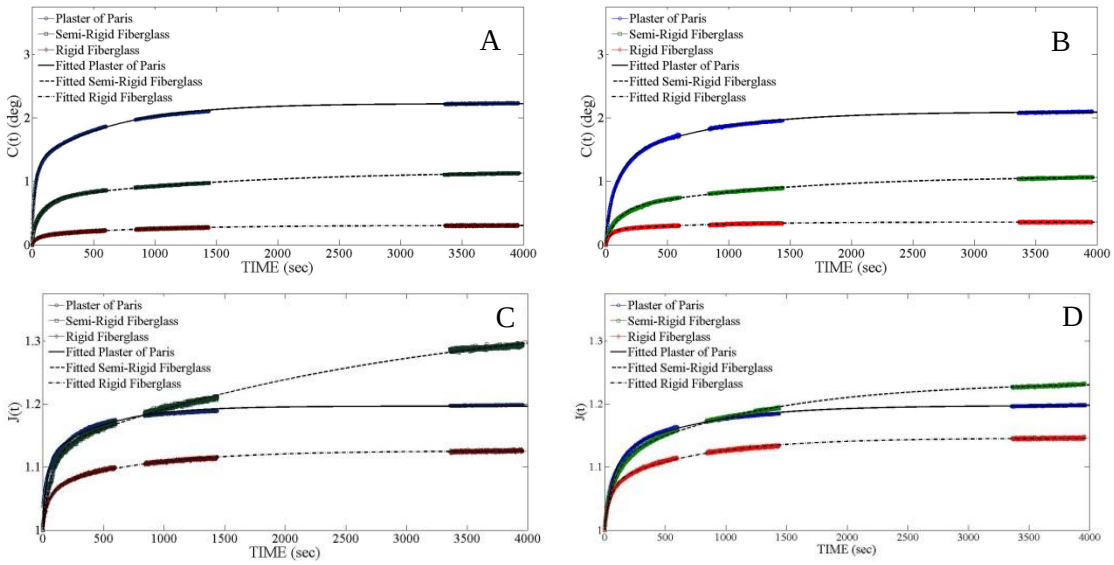

Figure 2-5: Mathematical models of creep. Experimental and model fit creep rotation curves (A, B) and creep compliance curves (C, D) of POP, SRF, and RF under A,C) low and B,D) high torques. ($C(t) = A_1e^{-b_1t} + C_1e^{-d_1t} + E_1$ and $J(t) = A_2e^{-b_2t} + C_2e^{-d_2t} + E_2$)

Mathematical models of the creep rotation behavior of each cast material are presented in Figure 2-5(A-B). The responses of the cast materials were best described using a decaying exponential equation,

$$C(t) = A_1e^{-b_1t} + C_1e^{-d_1t} + E_1 \quad (2.5)$$

where $C(t)$ is the creep rotation response, t is the time (in seconds), and A_1, b_1, C_1, d_1 and E_1 are parameters. Parameter values were significantly different between cast materials, however not across torque (Table 2-4). From these models, the mean amount of creep rotations was calculated for each material at 20 minutes, 70 minutes, 72 hours, five days, and seven days (Figure 2-6A). These predicted values were significantly different between cast materials. The percent of the seven day creep rotation at 70 minutes is 99% for the POP under both torques, 94% and 98% for the SRF under low and high torque, respectively, and 99% for the RF under both torques.

Trials curves of the creep function, $J(t)$, shown in Figure 2-5(C-D), were fit with a five parameter exponential equation:

$$J(t) = A_2 e^{-b_2 t} + C_2 e^{-d_2 t} + E_2 \quad (2.6)$$

where $J(t)$ is the reduced creep function, *t* is equal to time (in seconds), and A_2, b_2, C_2, d_2 and E_2 are parameters. Significant differences were not found across torque, however all parameters except A_2 showed differences between the synthetic casts (Table 2-5). For values of $J(t)$, differences between cast materials are not seen during the trial length, however, extended out, significant differences are seen between the synthetic materials (Figure 2-6B).

Table 2-4: Parameters and R2 values of creep rotation model $C(t) = A_1 e^{-b_1 t} + C_1 e^{-d_1 t} + E_1$. Significant p–values are from Tukey tests of normal parameter data and Kruskal-Wallis tests of non-normal parameter data across cast materials.

Material	Torque	A_1	b_1	C_1	d_1	E_1	R^2
POP	Low	-0.959	0.0113	-0.6233	0.001469	2.018	0.9954
		-1.094	0.03366	-0.9318	0.001532	2.225	0.9978
		-1.03	0.01186	-0.6737	0.001265	1.804	0.9983
		-0.7796	0.01357	-0.8761	0.001177	1.736	0.9993
		-1.608	0.009426	-0.8679	0.001406	2.613	0.9991
	High	-0.8816	0.009919	-0.7119	0.001138	1.691	0.9990
		-1.338	0.01267	-0.8969	0.001629	2.383	0.9968
		-1.191	0.01154	-0.7552	0.001162	2.057	0.9991
		-1.097	0.01169	-0.8478	0.001336	2.094	0.9986
		-0.6427	0.01138	-0.7964	0.001145	1.494	0.9997
SRF	Low	-0.5742	0.01165	-0.458	0.000648	1.161	0.9980
		-0.4523	0.009642	-0.5942	0.000724	1.107	0.9980
		-0.2903	0.009605	-0.5252	0.000769	0.8401	0.9994
		-0.1967	0.01183	-0.3908	0.000317	0.6032	0.9988
		-0.29	0.01177	-0.4204	0.000695	0.7449	0.9989
	High	-0.4843	0.01012	-0.6256	0.000772	1.18	0.9992
		-0.2945	0.01139	-0.4448	0.000762	0.7773	0.9988
		-0.4725	0.009771	-0.5495	0.000763	1.086	0.9986
		-0.1799	0.01026	-0.2916	0.000781	0.4907	0.9987
		-0.2835	0.01161	-0.3896	0.000904	0.7095	0.9988
RF	Low	-0.2071	0.01728	-0.4178	0.000867	0.6406	0.9992
		-0.2101	0.0154	-0.2005	0.001198	0.4385	0.9971
		-0.1076	0.02352	-0.07158	0.001189	0.1836	0.9878
		-0.1313	0.02053	-0.1636	0.001141	0.3065	0.9940
		0.01371	0.04286	-0.1268	0.000956	0.1252	0.9965
	High	-0.2753	0.01673	-0.2901	0.001285	0.5927	0.9982
		-0.4026	0.01759	-0.3352	0.001288	0.8036	0.9977
		-0.2207	0.02355	-0.1267	0.00135	0.3591	0.9955
		-0.2068	0.02314	-0.1203	0.001367	0.3515	0.9942
		-0.261	0.02465	-0.3151	0.002165	0.5948	0.9979
p – values							
Tukey Test	POP - SRF	< 0.0001*	-	< 0.0001*	-	< 0.0001*	
	POP - RF	< 0.0001*	-	< 0.0001*	-	< 0.0001*	
	SRF - RF	0.21	-	0.0001*	-	0.0056*	
Kruskal - Wallis	POP - SRF	-	0.56	-	< 0.0001*	-	
	POP - RF	-	0.012*	-	0.88	-	
	SRF - RF	-	0.001*	-	< 0.0001*	-	

Table 2-5: Parameters and R^2 values of reduced creep function $J(t) = A_2 e^{-b_2 t} + C_2 e^{-d_2 t} + E_2$. Significant *p*-values are from non-parametric Kruskal-Wallis tests across cast materials. * $p < 0.05$.

Material	Torque	A_2	b_2	C_2	d_2	E_2	R^2
POP	**Low**	-0.1122	0.03014	-0.08489	0.002098	1.196	.9948
		-0.2651	0.0448	-0.1925	0.001584	1.448	.9987
		-0.04441	0.01404	-0.02898	0.001341	1.073	.9988
		-0.05534	0.01597	-0.0591	0.001211	1.114	.9994
		-0.1814	0.0111	-0.1048	0.001522	1.287	.9992
	High	-0.04861	0.01193	-0.03925	0.001208	1.088	.9990
		-0.4475	0.0159	-0.3122	0.001772	1.758	.9982
		-0.04179	0.01345	-0.02627	0.001228	1.068	.9991
		-0.1117	0.01468	-0.08551	0.001427	1.197	.9987
		-0.1265	0.01303	-0.1516	0.001174	1.278	.9996
SRF	**Low**	-0.3039	0.0162	-0.2184	0.000745	1.525	.9975
		-0.3573	0.01224	-0.4521	0.00078	1.811	.9984
		-0.05489	0.01114	-0.0962	0.000793	1.151	.9995
		-0.126	0.01324	-0.2317	0.000333	1.358	.9990
		-0.05661	0.01412	-0.07666	0.000725	1.133	.9990
	High	-0.1054	0.01272	-0.129	0.00082	1.235	.9990
		-0.08494	0.01397	-0.1207	0.000795	1.205	.9989
		-0.2128	0.01233	-0.2384	0.000822	1.452	.9987
		-0.05965	0.01228	-0.09249	0.000811	1.152	.9990
		-0.1306	0.01428	-0.1695	0.000942	1.3	.9990
RF	**Low**	-0.1367	0.01956	-0.2581	0.000877	1.393	.9994
		-0.0667	0.01886	-0.05934	0.001245	1.126	.9982
		-0.1079	0.02541	-0.06857	0.001204	1.174	.9951
		-0.00261	0.003875	-0.04319	0.000894	1.045	.9941
		-0.02629	0.02348	-0.03035	0.001158	1.056	.9981
	High	-0.07369	0.01954	-0.07295	0.001316	1.146	.9989
		-0.05222	0.02089	-0.04296	0.001328	1.095	.9986
		-0.05302	0.02585	-0.02898	0.001375	1.081	.9983
		-0.1624	0.02785	-0.08719	0.001424	1.247	.9975
		-0.05347	0.02802	-0.06088	0.0022	1.113	.9990
p – values							
Kruskal - Wallis	**POP – SRF**	0.55	0.23	0.06	0.0002*	0.17	
	POP – RF	0.26	0.10	0.47	0.20	0.23	
	SRF – RF	0.06	0.002*	0.002*	0.0003*	0.01*	

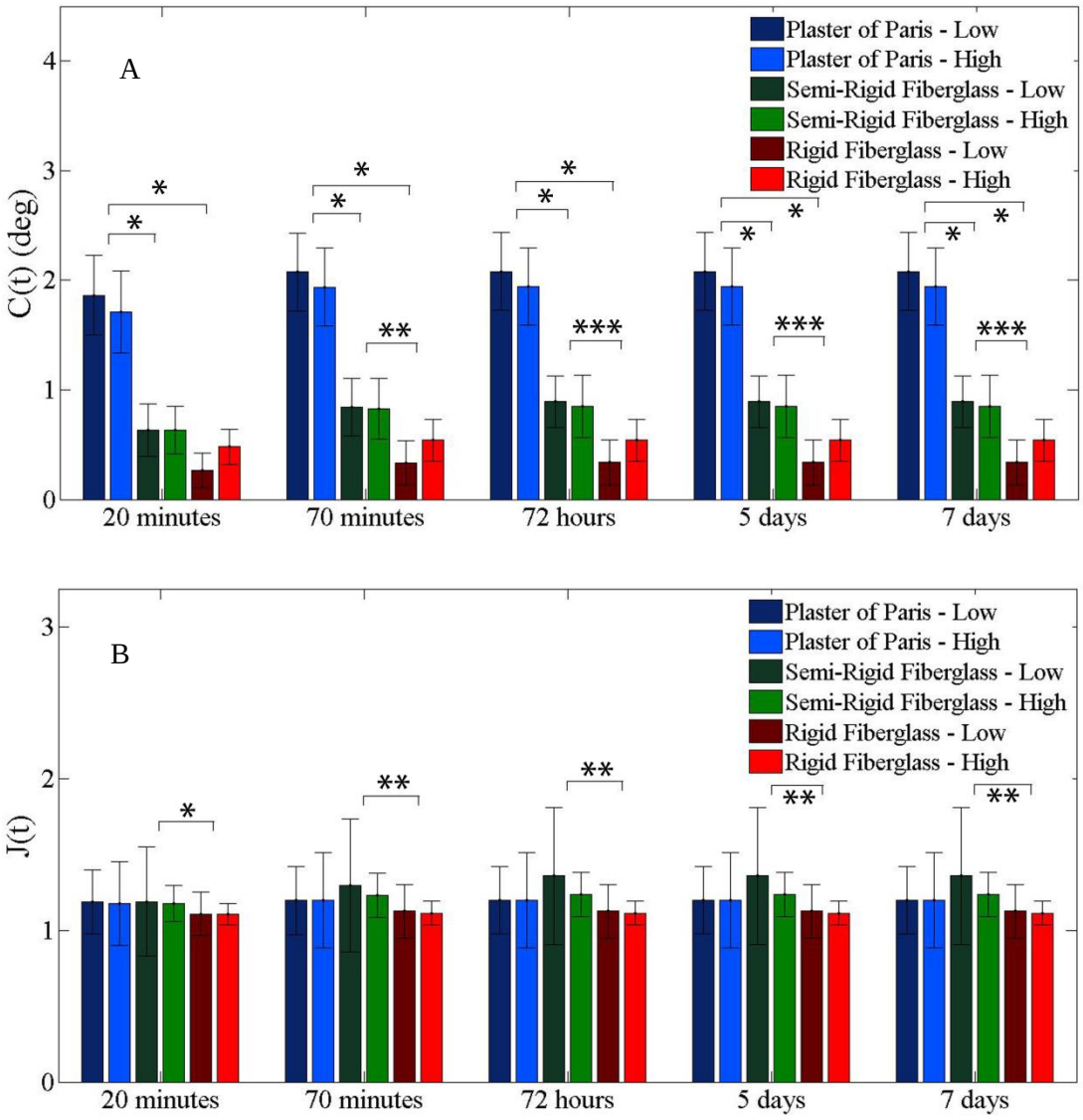

Figure 2-6: Parameterics of predicted model parameters. A) Mean and standard deviation of predicted values of creep rotation, *C(t)*, of Pop, SRF, RF, under low and high torque conditions at 20 min, 70 min, 72 h, 5 days, and 7 days. *$p < 0.0001$, **$p < 0.01$, ***$p = 0.006$. B) Median and interquartile range of predicted values of reduced creep compliance, *J(t)*, of Pop, SRF, RF, under low and high torque conditions at 20 min, 70 min, 72 h, 5 days, and 7 days. *$p = 0.04$, **$p = 0.01$.

2.4 Discussion

The current work presents the evaluation of creep response of POP and two synthetic cast materials using a novel experimental set-up to simulate conservative

clubfoot correction under a constant torque (Cohen et al., 2012). The study resulted in creep rotation responses of less than 2 degrees for all cast materials, and was considered minimal by surgical co-authors (PAS, HA). The findings indicated that the most creep occurs in the POP, then the SRF, and then the RF, regardless of the torque level. In addition, the effect of the two torque levels on creep compliance curves was negligible, suggesting quasi-linear viscoelastic material behavior. Outcomes of this experiment include the creep dependence on cast material and independence on torque at low levels. Clinically, this could indicate that severity of deformity may not affect the performance of the cast material.

The current study shows the behavior of the material under low loads while it is curing (hardening), however, many earlier studies examining mechanical properties of these cast materials looked at the material properties after the recommended curing time for weight bearing and at higher loads (Callahan et al., 1986; Martin et al., 1988; Mihalko, Beaudoin and Krause, 1989; Rowley et al., 1985). As a result, their conclusions were of the ultimate and yield behaviors of the materials, and may differ from the findings of this investigation. Several of these studies have found POP to be stiffer, yet less strong, than synthetic cast materials. In Mihalko et al., two regions of linear elasticity were seen, the first attributed to the hard plaster and the second attributed to the elastic gauze. In this study, creep rate was highest in the beginning of the trial, and then plateaued within the last time interval, indicating that the behavior of the gauze was seen initially, and the stiffness of the plaster became more dominant over time. This could indicate that a portion of the creep rotation seen is related to the material setting properties. Schmidt et al. and Berman et al. analyzed optimal mechanical properties of

POP and synthetic casts, respectively, with respect to time and water content (Berman and Parks, 1990; Schmidt, Somerset and Porter, 1973). Schmidt et al. found that 72 hours of drying and 21% water content produced the optimal mechanical properties of POP, while Berman et al. found that synthetic cast material had reached 75% of its 5 day strength within an hour of drying. In this study, it is predicted with an exponential model that at 72 hours, creep rotation response of the POP plateaus and by the end of the trial, at least 70% of the creep rotation response is reached by the synthetic casts.

The results of this study differ slightly from the pressure-volume study conducted by Deshpande et al., as that study showed the SRF to be most compliant (Deshpande and Deshpande, 2005). However, the findings do correspond with those of both Deshpande et al. and Davids et al., in that RF was the most rigid of all the cast materials tested and that all the cast materials exhibited viscoelastic behavior (Davids et al., 1997; Deshpande and Deshpande, 2005). Results in these studies were determined by gauging the pressure change when infusing measured volumes of fluid into bladders that are surrounded by cast material. The current study modeled a different clinical application. These discrepancies can be attributed to not only dryness of the material, but also the complex combination of motion, padding, and/or multilayering effect that were based on the standard clinical procedure (Ponseti method) that was applied.

Studies examining the use of different orthopaedic casting materials have resulted in unclear conclusions as to which material is best for clubfoot treatment based on patient satisfaction and efficacy (Pittner et al., 2008; Zmurko, Belkoff and Herzenberg, 1997). Zmurko et al. found that although his tests showed that SRF was best used with non-rigid immobilization, one of the authors found it to be sufficiently rigid in the correction of

clubfoot and metatarsus adductus. Pittner et al. found that in clinical trials, the clubfeet corrected with either POP or SRF both resulted in a 95% overall correction rate with the addition of percutaneous tendoachilles lengthening. Those feet treated with SRF casts had statistically significant lower Dimeglio-Bensahel scores at the completion of non-operative manipulation, however, patient satisfaction in terms of convenience, cast weight, and cast durability was higher for this material. In a study comparing parent satisfaction with POP and SRF used during serial casting, Coss et al. found that parents preferred the SRF based on its ease of removal, durability, and performance (Coss and Hennrikus, 1996). In their study though, the authors did not correlate each cast material in regard to their efficacy. Similarly, Brewster et al., using SRF, and Kin-Wah Ng et al., using fiberglass material, published their favorable clinical results (Brewster et al., 2008; Ng, Lam and Cheng, 2010).

In the current study, an internal torque, representative of joint stiffness, supplied the driving force on the cast after the recommended setting time, which is clinically relevant to the conservative clubfoot treatment procedure. The forces being applied to the cast during treatment were significantly lower than those seen at yield, meeting the constraints of the creep phenomena. At the initial application of the cast material, the force on the cast is at its greatest. Over time, the force imposed by the clubfoot on the cast would decrease due to stress relaxation of the soft tissue in the foot and ankle. In addition, after 20 minutes, creep values surpassed 88%, 70%, and 77% of the predicted seven day creep experienced by the POP, SRF, and RF, respectively. Therefore, the decaying exponential function is an adequate model of the creep rotation curve. The results of the statistics on the parameters of this function indicated that the response was

different between cast materials. Further analysis into the parameters showed that parameters *b* and *d* affect the rate of change in displacement, especially seen in the initial slope during interval 1.

Just as with the creep rotation curves, the reduced creep function was fitted with an exponential function. The materials were modeled as quasi-linear viscoelastic, meaning that the ratio of creep to elastic response is the same under different loads. To further verify this behavior, additional tests at a range of load levels would need to be performed. The reduced creep function J(t) was found to be different between SRF and RF, which could support the differences found in the displacement data. Parameter d_2 of the SRF proved to be different from that of the other casts, which may explain the difference in curvature. Furthermore, when reviewing J(t) at different time points, it was seen that within the trial time frame, the values for the three materials did not differ significantly. However, over time, the values diverged.

Some limitations are present in this examination. This study models rigid bodies that are connected by a single, revolute hinge joint. While the ankle-subtalar complex is not a simple revolute joint, the model does best represent the second, most prominent phase of clubfoot correction by addressing the transverse plane adduction. In addition, the cast materials' responses to the simulated joint stiffness may be a function of the number of layers used in the construction of the cast. The effect of the number of layers of cast material was not addressed in this study; however, this protocol was consistent with clinical standards and the Ponseti protocol. It was assumed in this study that the radii and lengths were the same across trials and materials, however, only the number of layers of material were monitored. If these measurements were inconsistent, they would have to be

factored into the shear strain equation. Error may also be attributed to bending in the PVC tubing of the model, as it was the motion of the tubing that was tracked. However, experimental bending tests and theoretical analysis indicated that the amount of angular deflection would be less than 1% of the total creep experienced by any of the cast materials. The effectiveness of the cast material also depends on the surgeon`s skill at molding. The moldability of the cast material and its significance on the ability to apply the cast material and its influence on the efficacy of clubfoot treatment is not addressed in this model. To date, there have been no studies that specifically address moldability.

The three cast materials selected for this study are all used clinically. Clinical selection includes a number of considerations, including availability of the material, cost effectiveness, patient comfort and physician preference. POP is currently the material of choice in developing countries due to cost and availability advantages. Further understanding of the mechanics of cast behavior, as defined in this study, may improve future strategies for clubfoot care and correction.

CHAPTER 3: DESIGN AND VALIDATION OF A BENCHTOP TESTING SYSTEM FOR MINATURE SOFT TISSUE SPECIMENS

This chapter details the design and validation of a benchtop testing system for the evaluation of miniature soft tissue specimens. To validate the constructed system and control program, nylon monofilament material properties were obtained and compared with results from a commercially available system and reported values. Results of the study indicated that the system accurately measures force and displacement of miniature samples. Versatility was demonstrated via the quasistatic testing of PTFE tape, as well as the viscoelastic testing of rabbit knee ligament. A version of this chapter has been submitted for publication in the Journal of Engineering in Medicine.

3.1 Introduction

The tissue mechanics of ligaments obtained during pediatric orthopaedic procedures may be analyzed to advance biomechanical understanding of tissue behavior to improve clinical strategies and treatment approaches. Pediatric soft tissues are small, which may affect the ease of testing when using mechanical techniques (Woo, Ohland and Weiss, 1990; Woo et al., 1986). The purpose of this research was to develop and validate a new mechanical testing device to resolve deficiencies in current technologies while seeking to improve clinical insight into pediatric orthopaedic disabilities.

Mechanical methods of obtaining properties and behavior of materials involve the monitoring of forces and displacements during the application of loading conditions. Traditionally, machine hardware consists of force transducers, actuators, gripping mechanisms, and software to control the synchronization of monitoring devices and storage of the key outputs. The machines may be capable of performing quasistatic or

dynamic tests, such as cyclic loading, ultimate strength, and time-dependent stress and strain tests. These evaluations support characterization of material properties and behaviors, including, but not limited to, elastic modulus, ultimate strength, and viscoelastic behavior. Such parameters provide mechanical insight used to predict material behavior, and are particularly valuable in engineering design.

An important application of mechanical materials testing is the characterization of biological tissue. Extensive research has been conducted on the relationships between the biomechanical function and mechanical properties of hard and soft tissue, including bone, cartilage, tendons, and ligaments, from cadaveric, adult, and animal donors (Albert et al., 2013; Albert, Jameson and Harris, 2013; Currey, 2012; Johnson et al., 1994; Jung, Fisher and Woo, 2009; Moon et al., 2006; Smith, Livesay and Woo, 1993; Woo, Johnson and Smith, 1993; Woo et al., 1986). Investigations characterizing ligaments have been largely performed on adult animal and human specimens, and only limited information is available on pediatric ligaments (Abramowitch et al., 2004; Butler et al., 2004; Oza, Vanderby and Lakes, 2006; Woo et al., 1987; Woo et al., 1986; Woo et al., 1990). Ligament specimens obtained from pediatric patients undergoing routine orthopaedic surgeries can be used for material characterization. The disparities between normal and pathological specimens can be quantified to gain clinical insight into the mechanisms and progression of orthopaedic disorders. Results of material characterization could be applied to injury analysis, prediction and prevention, treatment strategies for pediatric orthopaedic deformities and disorders, as well as evaluation of physiologic changes during growth and development.

To evaluate tissue, special considerations need to be made to accommodate the physical properties of the specimen. Pediatric surgical specimens are inherently small in size, resulting in a smaller grip area, lower aspect ratio, possible slippage, malalignment, and stress concentrations. Animal studies assessing the effect of age on the mechanical properties of ligaments found smaller cross-sectional areas in immature animals as compared to that of mature animals (Woo, Ohland and Weiss, 1990; Woo et al., 1986). Proper protocol includes maintaining physiologically representative conditions, e.g., temperature and hydration, during testing and ensuring that the attachment mechanisms are compatible with the viscous nature of the biological material (Jung, Fisher and Woo, 2009; Weiss and Paulos, 1999; Woo, Johnson and Smith, 1993; Woo et al., 1987).

Commercially available machines capable of miniature specimen testing in a laboratory environment tend to be relatively expensive. Such systems are typically more complex than required by the application, and may require substantial preparation and configuration time. The size and weight of these devices may preclude installation in more convenient clinical settings, where portability is desired. Key specifications, such as stroke length, sampling frequency, and test space adjustability are often not designed for pediatric specimens (Bose Corporation; Illinois Tool Works Inc.; MTS). Additional accessories, such as specialty grips and strain measurement configurations, may also be required to test biological specimens, adding to the overall cost of the system.

This study was done to design, develop, and validate a portable, benchtop Pediatric Tissue Evaluation System (PedsTES). The versatile, low cost system was designed to accommodate a range of pediatric specimen shapes and sizes, while providing simplified operation, and alterable programmed loading conditions. The

objective was to provide clinicians and researchers with the capability to obtain accurate, quantitative assessments of tissues extracted during surgical procedures. This paper: 1) describes the electromechanical design process and development of a testing protocol for the unique requirements of pediatric ligaments, 2) evaluates the accuracy of the system against a validated mechanical test machine commonly used in biological materials testing through nylon monofilament characterization, and 3) demonstrates the versatility of the system by characterizing exemplar synthetic and biological materials.

3.2 Materials and Method

The testing apparatus was designed to perform uniaxial tensile tests, including those with quasistatic and viscoelastic conditions, on miniature soft tissue specimens of an approximate length and width of 1 cm and 2 mm, respectively. Setup and validation of the machine included calibrating the voltage/force relationship and validating load and displacement measurement.

3.2.1 Design of Soft Tissue Uniaxial Testing Machine

PedsTES was designed to perform uniaxial tensile tests, including quasistatic and viscoelastic simulations, on a variety of materials including miniature soft tissue specimens. Setup and validation of the machine included calibration of the voltage/force relationship and validation of the load and displacement measurement. The system, controlled by a custom-written NI LabView VI (National Instruments, Austin, TX) (Figure A-2), was configured to synchronize the acquisition of motion data, video, and force data under a variety of load, position, and time constructs (Figure 3-1). Motion data was derived from the position of a high-precision linear actuator (M230.25, Physik

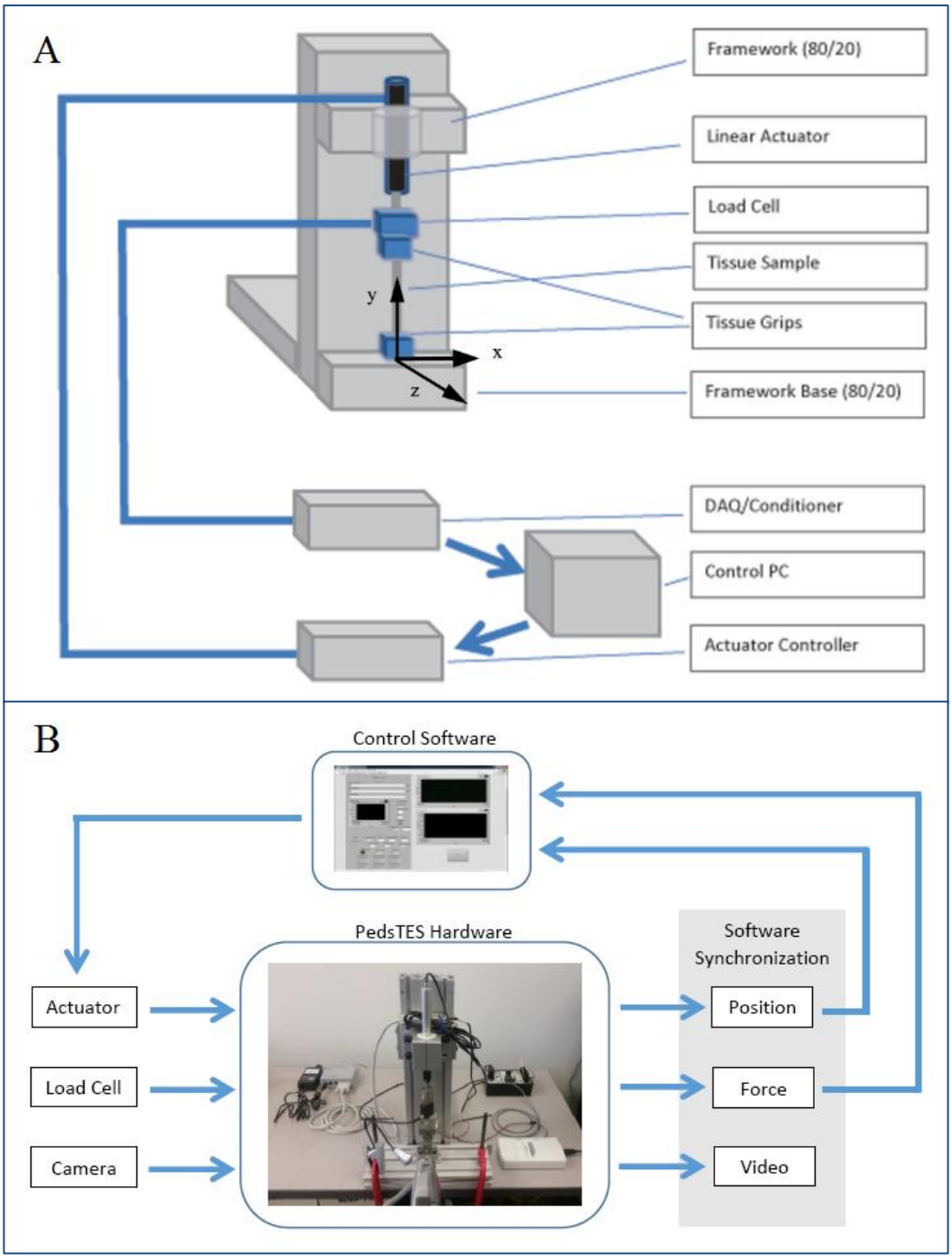

Figure 3-1: A) Mechanical schematic of the PedsTES design and B) flowchart of the control system. The actuator, load cell, and camera are synchronized to acquire position, force, and video during programmable loading conditions to simulate *in vivo* mechanics.

Instrumente, Karlsruhe, Germany) at a sampling rate of 100 Hz. The actuator, powered

by a DC gear motor and controlled by a PI Mercury controller (C-863.10, Physik Instrumente, Karlsruhe, Germany) and PIMotionMove2.8.0.3 software (Physik Instrumente, Karlsruhe, Germany), consists of an integrated rotary encoder with a resolution of 0.05 microns and has a travel range of 25 mm. Force data was derived from voltage output from a 111.2 N capacity load cell (MDB – 25, Ultra Precision Load Cell, Transducer Techniques, Temecula, CA) at a sampling rate of 1000 Hz. A differential amplifier/signal conditioner module (TMO-2, Transducer Techniques, Temecula, CA) provided balance and gain controls, as well as a bridge to a USB Multifunctional Data Acquisition Board (USB-6211, National Instruments, Austin, TX). Video was recorded using a DV camcorder (Z60, Canon, Tokyo, Japan) at a rate of 30 frames per second. A Light-Emitting-Diode (LED) circuit, in the view of the camcorder and wired to the DAQ board, will act as an event indicator. The entire construct was supported by a structure of T-slotted aluminum beams (1545 series, 80/20® Inc., Colombia City, IN). The platform provided rigid support while allowing for adjustability in three directions. The line of action was positioned in the vertical direction, with the actuator placed superior to the load cell and the grips. Vibration was also monitored using a Modified Mercalli Intensity Scale (Vibration Meter v1.4.5, Smart Tools Co, 2014) to minimize extraneous input. The load capacity of the system was limited to 70 N by the linear actuator.

In order to improve the versatility of the system, interchangeable grips were developed in two different designs to allow both filament and tissue material to be attached (Figure 3-2). The filament grips were constructed from steel components in a hook design that attached to the load cell and platform. The design allows filament samples to be attached by cyanoacrylate adhesive. The second grip design consists of two

stainless-steel jaws, furrowed to provide increased friction to prevent sample slippage. Grip design was based upon a previously validated design for larger soft tissue specimens (Feola et al., 2011; Moalli et al., 2005) scaled appropriately to account for the expected pediatric soft tissue specimen size (10 mm x 1.5 mm x 1.5 mm). A combination of compression of the jaws and cyanoacrylate adhesive allows the assembly to adequately

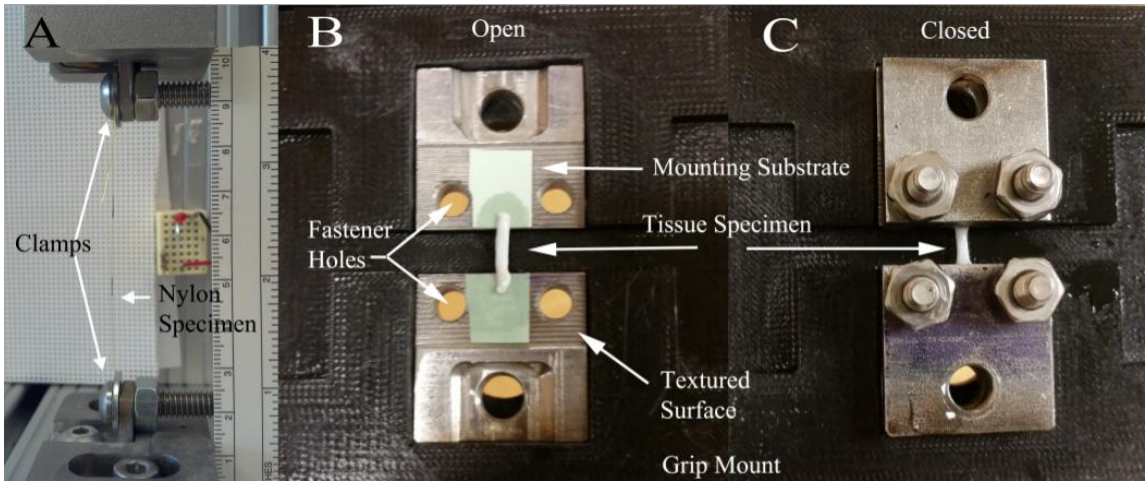

Figure 3-2: Grip designs. A) Grips for monofilament testing. Grips for testing of miniature soft tissue specimens in B) open position and C) closed position.

hold the samples in place during testing (Figure 3-2).

The cost of the hardware, including the grips, was approximately $6,000. This does not include the cost of NI LabVIEW software.

3.2.2 Instrument Calibration Protocol

Calibration focused on acquiring voltage to mass and force relationships. Manufacturer recommended calibration was performed prior to the following protocol (appendix). The machine was progressively loaded then unloaded with weights, from unloaded grips (0 g) to 1250 g at 50 g increments. Under no load, the voltage of the amplifier/conditioner, outputted by a connected multimeter, was zeroed by adjusting the

balance potentiometer. For each following increment, the weight was applied and allowed to stabilize. The resulting voltage from the load cell was read at a sampling frequency of 100 Hz and then averaged over five seconds using a LabView VI. This protocol was performed twice. The voltage-to-force relationship was determined using a linear regression model relating the mean voltage for each trial to its corresponding mass and force. In operation, the system was calibrated prior to each test and allowed force outputs to be obtained from the load cell. Total time for pre-testing calibration was approximately 5 minutes.

3.2.3 Instrument Validation

Nylon monofilament was used for the instrumentation validation portion of this study. Polymers and ligaments both exhibit viscoelastic behavior, which can be readily characterized using mechanical testing methods. Thirty specimens of nylon monofilament were obtained from a single roll of line (Sufix® Elite™ Hi-Vis Yellow Monofilament, Rapala VMC Corporation, Helsinki, Finland). The specimens were rated for a minimum tensile strength of 6 lbs. (26.7N) by the manufacturer, which exceeded the expected load range for low load soft tissue testing.

A uniaxial tensile test-to-failure protocol, based on ASTM D638 ("Astm D638-14, Standard Test Method for Tensile Properties of Plastics," 2014), was performed on each specimen using the PedsTES and an MTS Criterion™ (C43.104, MTS System Corporation, Eden Prairie, MN, USA) system. The monofilament attachment was used for this protocol on both machines. Each specimen was secured with compression and cyanoacrylate, which was allowed to dry for at least 5 minutes. After zeroing the load cell, each specimen was loaded to a gauge length load of 0.5 N. The gauge length and

diameter of the specimen were measured using digital calipers. Load-to-failure tests were conducted at a constant elongation rate of 10 mm/min, corresponding to a mean strain rate of 0.25 %/s for both systems. Force, position, and video were recorded during each PedsTES trial at sampling frequencies of 1000 Hz, 100 Hz, and 30 fps, respectively, with force and position recorded at 50 Hz during each MTS trial. Strain was calculated using the position data (*d)* of the actuator and gauge length (l_o) of the specimen [i.e., $\Delta d/l_o$]. Engineering stress was calculated using the force transducer output (*P*) and circular cross-sectional area (CSA) of the specimen [i.e., *P/CSA; CSA* = πr^2]. Computed values of the elastic modulus were compared across machines using a Mann-Whitney *U* test with a significance level of 0.05. A nonparametric method was chosen due to the rejection of the normality assumption based on the Wilks-Shapiro test. Descriptive statistics, including median and range, were reported.

3.2.4 Demonstration of Versatility

PedsTES was designed to adapt to a variety of constraints and conditions, depending on the material characteristics and protocol requirements. Versatility was demonstrated through a series of tests on different materials, including those of a synthetic and biological composition.

3.2.4.1 Load-to-Failure Test of Polytetrafluoroethylene (PTFE) tape

Uniaxial tensile loading was performed on specimens of PTFE tape (CSA =12.7 mm x 0.089 mm, length = 71.3 ± 1.9 mm) using the PedsTES and MTS machines and following a protocol similar to that used on the nylon monofilament. A threaded design was utilized to connect the ends of the specimen to the grips of the machines.

3.2.4.2 Testing of biological tissue

Medial collateral ligament (MCL) (n = 3) and lateral collateral ligament (LCL) (n = 4) from four fresh-frozen, farm-raised, food-grade rabbits (lapine) (Krinkeys Farms) specimens underwent preconditioning, stress relaxation, and load-to-failure protocols (Duenwald, Vanderby and Lakes, 2010; Moon et al., 2006). The CSA of each ligament was reshaped using a custom-made tissue slicer, created from two 0.009 inch single edge razor blades and a metal spacer of approximately 1.5 mm thickness, to represent the dimensions of pediatric ligamentous tissue (CSA = 1.5 mm x 1.5 mm). Specimens were refrozen in saline at a temperature of -29^{o}C until testing.

To prepare for testing, specimens were thawed and hydrated in phosphate-buffered saline (PBS) solution at 37^{o}C for 30 minutes in a custom-fabricated environmental chamber. After such time, the width and thickness were measured using digital calipers at each end and midsubstance, as well as the length. Each specimen was secured between stainless-steel jaws through compression and cyanoacrylate adhesive (Figure 3-2B) and adjusted along x-, y-, and z-axes (Figure 3-1A) to ensure alignment. The tissue was marked with skin marker ink at the grips and at mid-substance for reference.

Each specimen underwent preloading, preconditioning, stress relaxation, and load-to-failure protocols. Dimensions were measured at a preload of 0.5 N, the preload position. During preconditioning, loading was cycled between 0.5 N and 2.5 N for 20 cycles. Under the stress relaxation protocol, each specimen was: 1) elongated to lengths corresponding to forces between 2 N and 10 N at 2 N increments, 2) held at the length for 100 seconds, 3) unloaded to the preload position, and 4) allowed to recover for 3 minutes.

A load-to-failure was then performed. The specimen was hydrated with PBS solution between test phases. Loading and unloading occurred at a constant rate of 10 mm/min.

Force, position, and time data were used to quantify the tissue response to each protocol. To describe stress relaxation behavior of ligament specimens, the Quasi-Linear Viscoelastic (QLV) theory (Eqs. 1 and 2) (Abramowitch and Woo, 2004; Fung, 1993) was applied to the stress relaxation test output.

$$\sigma(t,\varepsilon) = \bar{G}(t)\sigma^{e}(\varepsilon) \tag{3.1}$$

where $\sigma(t,\varepsilon)$ is the stress relaxation at time *t* under strain ε, $\sigma^{e}(\varepsilon)$ is the instantaneous elastic response, and $\bar{G}(t)$ is the reduced stress relaxation function representing the time-dependent stress response normalized by the stress at the time of the step input of strain [i.e., $\bar{G}(t) = \frac{\sigma(t)}{\sigma_o},\ \bar{G}(0^{+}) = 1$].

3.3 Results

3.3.1 Calibration

Calibration results, shown in Figure 3-3, indicated a linear relationship between the force and voltage output with a slope of 10.9 N/V.

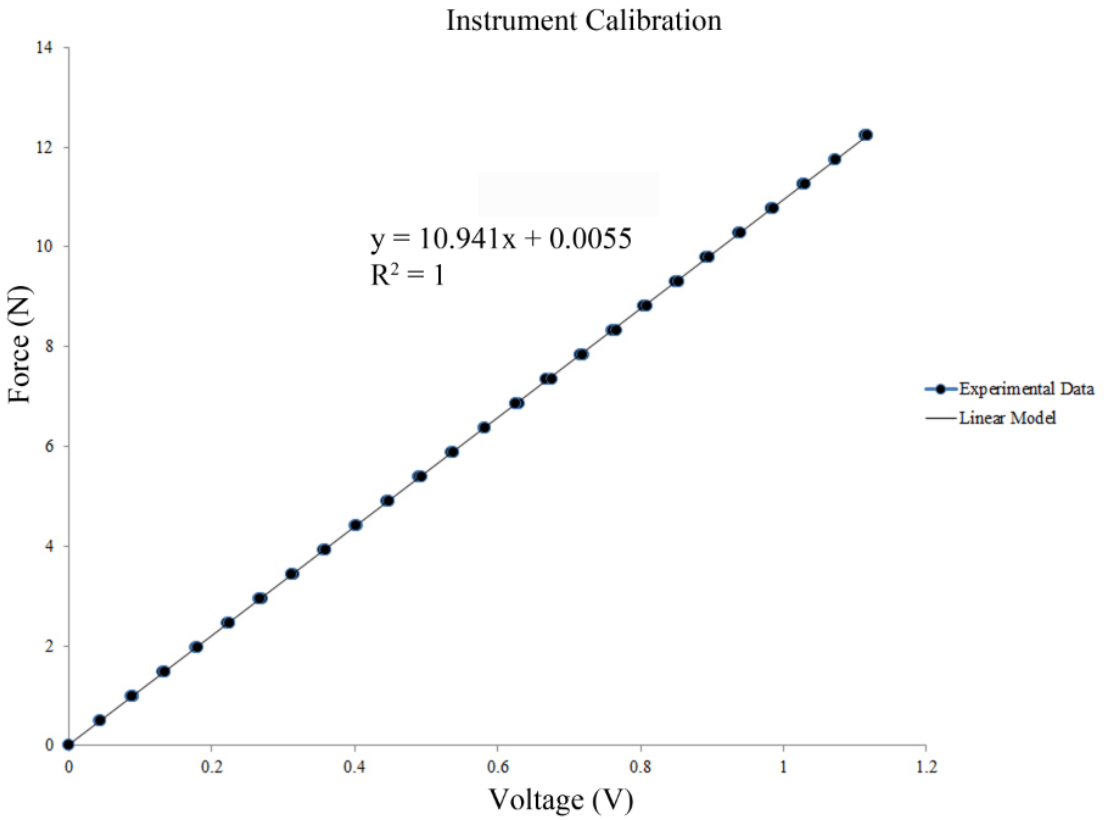

Figure 3-3: Instrument calibration. Force (N) versus voltage (V) calibration curve, displaying experimental data and linear model.

3.3.2 Validation

Pilot testing of multiple nylon samples revealed repeatable stiffness measurements within samples obtained from the same batch of material. Based on these results, this material was found to be suitable for the validation protocol. Stress versus strain data for the monofilament specimens are presented in Figure 4. Results indicated that the elastic modulus values between the machines were not significantly different and fell within the reported ranges for the material (Box; Gere and Timoshenko, 1997) (Table 3-1).

Table 3-1: Instrument validation results. Median (range) of elastic modulus values of nylon monofilament loaded using the PedsTES and MTS devices. $\alpha = 0.05$

Machine	Elastic Modulus (GPa) Median (range)
PedsTES	3.36 (1.35 - 3.79)
MTS	3.53 (2.52 - 4.03)
p	**0.1465**
Typical values for nylon	**2 – 4(Box; Gere and Timoshenko, 1997)**

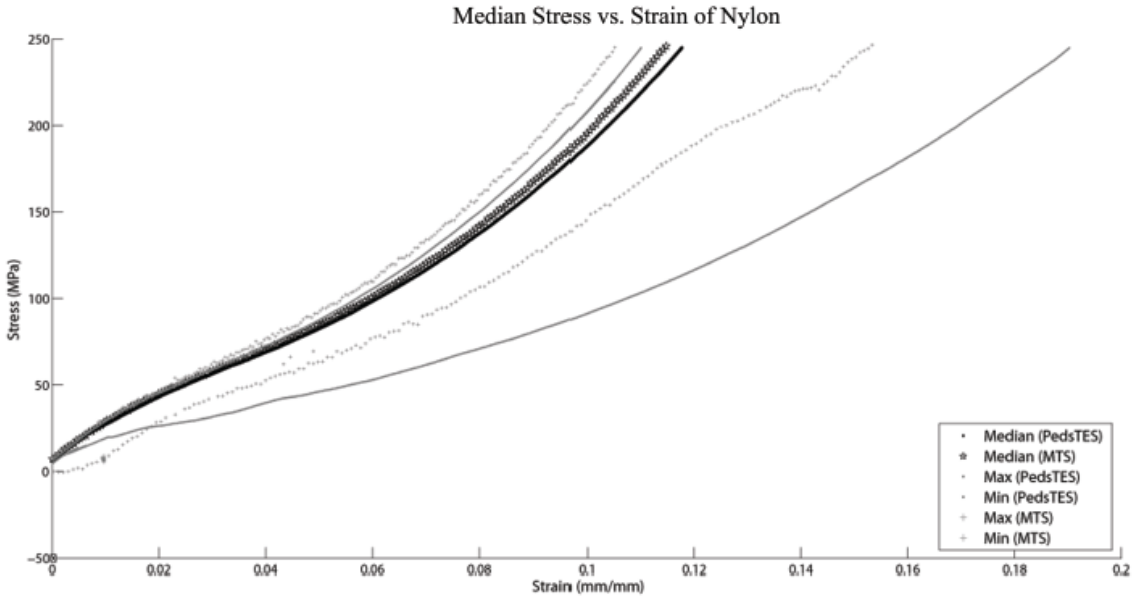

Figure 3-4: Instrument validation curves. Median, maximum, and minimum stress versus strain curves of nylon monofilament obtained with the PedsTES and MTS machines.

3.3.3 Demonstration of Versatility

3.3.3.1 Load-to-Failure Test of Polytetrafluoroethylene (PTFE) tape.

A representation of the force and displacement results of this test on PTFE specimens is presented in Figure 3-5.

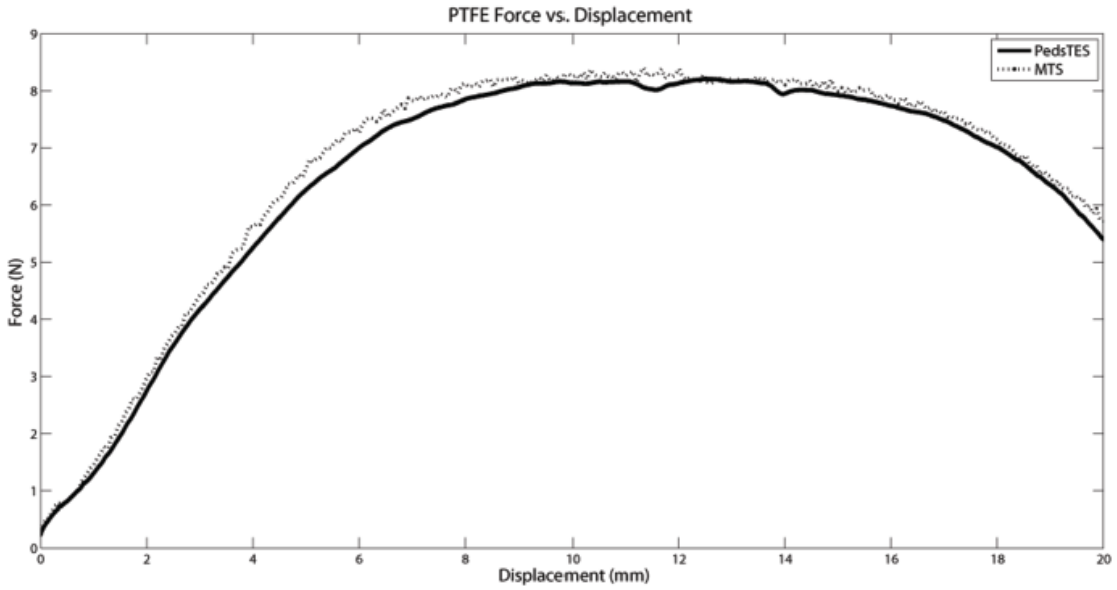

Figure 3-5: PTFE force vs displacement. Representative results of force versus displacement for the PTFE specimens undergoing a load-to-failure test using the PedsTES and MTS machines.

3.3.3.2 Testing of biological tissue.

Results from a representative MCL are illustrated in Figure 3-6. Preconditioning cycles converged after 20 cycles. Figure 3-6A illustrates the force versus displacement data obtained during the load-to-failure protocol.

A representative specimen response to the stress relaxation protocol is presented in Figure 3-6B. A generalized decaying exponential function was fitted to each curve in the following form:

$$\bar{G}(t) = A_1 e^{-A_2 t} + A_3 e^{-A_4 t} + A_5 \quad (3.2)$$

where *t* is time in seconds and $A_1 \ldots \ldots A_5$ are constant coefficients.

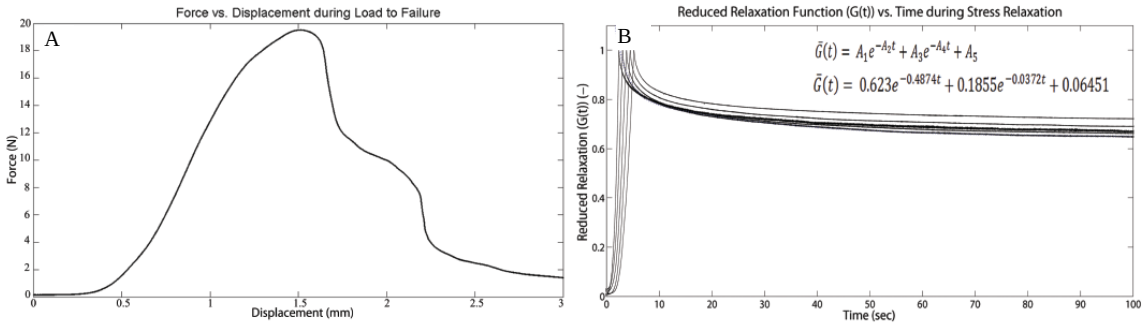

Figure 3-6: Results from representative rabbit MCL. For a representative MCL specimen: A) Force versus displacement during load to failure. B) Multiple reduced relaxation functions, G(t), versus time for a single specimen undergoing the stress relaxation protocol are depicted. A fitted generalized decaying exponential function is represented.

3.4 Discussion

The purpose of this study was to: 1) describe the design and development of the PedsTES, a benchtop evaluation system for pediatric tissue specimens, 2) validate the mechanical testing capability of the system, and 3) illustrate the versatility of the system through the characterization of synthetic and biological tissue. Validation results of this study provide evidence to support the use of this machine for material characterization, including that of miniature pediatric soft tissue. This system resolves the key deficiencies of previous commercial devices by simplifying the protocol, reducing device cost, and enhancing the versatility.

Mechanical systems and test methods are typically used to characterize material properties and behaviors through the measurement of force, displacement, and other parameters while exposed to standardized loading conditions (Jung, Fisher and Woo, 2009; Weiss and Paulos, 1999). The PedsTES accomplishes this through a mechanical framework, which supports a linear actuator, a load cell, and a gripping mechanism. The control system synchronizes the acquisition of force, position, and video data from these components. In addition, it provides a means to program multiple test protocols by controlling position and monitoring force output, using either forward- or feedback-based control. The adaptability of the machine to accept different grip designs has been demonstrated. The design supports a variety of materials of different physical characteristics and composition, including those of synthetic and biological makeups. The overall system provides a compact, versatile, and cost-effective alternative to commercially available products.

Currently available material test machines typically are designed to accommodate a wide variety of materials and thus are less adept at testing miniature tissue samples in a cost-conscious environment. A sample of available devices with relevant specifications is provided in Table 3-2. The cost of these machines can range from $30,000 to more than $100,000 depending on capabilities, as well as additionally purchased accessories (Bose Corporation; Illinois Toll Works Inc.; MTS). Many of these systems also have size and

Table 3-2: Comparison of features of PedsTES to those of applicable commercially available mechanical test machines.

	Mass (kg)	Dimensions (mm x mm x mm)	Force Sampling Frequency (Hz)	Vertical Test Space (mm)	Dynamic Stoke (mm)	Max Force (N)
PedsTES	11	470 x 305 x 432	1000	380	25	111
MTS Acumen™	159	1511 x 679 x 485	>100	26 – 603	70	850
Bose ElectroForce® 3100	18	500 x 300 x 178	100	178	5	22
Instron 3342	38	900 x 382 x 500	NA	651	482	500

weight specifications, reducing or even eliminating portability and versatility. The PedsTES uses similar components to these systems and compares favorably in specifications most relevant to small specimen testing (Table 3-2).

Calibration and validation of the system provided quantitative evidence of its accuracy. Monofilament validation showed no significant difference between the detection capabilities of the PedsTES and exemplar machine. Values of elastic modulus from both machines were within range of the reported nylon material properties (Box; Gere and Timoshenko, 1997). Pilot testing of nylon monofilament from multiple batches produced varying results, which may account for variations in inter-sample performance. To reduce this effect on the validation analysis, a single batch was used, with the samples being selected randomly.

The testing protocol developed for the PedsTES takes into account typical strategies used to secure materials to mechanical testing machines in industrial and

biomedical applications, with additional consideration paid to the unique aspects of miniature ligamentous tissue. The system can accept various attachment methods for monofilament and tissue, including specialized grip designs. To provide a physiologically accurate environment for maintenance of tissue properties, tissue was equilibrated to 37°C and hydrated regularly (Jung, Fisher and Woo, 2009). The system does not fully incorporate an environmental chamber, although one could be added to the existing design. Additional aspects of the mechanical testing of biological tissue testing include the prerequisite preconditioning of the specimen, performed via cyclic loading. In the current system, a delay artifact of 500 ms exists between loading and unloading, which may produce an error in hysteresis area calculation. Future work will focus on enhancing this algorithm.

This study of the PedsTES demonstrated its capabilities as a portable and cost-effective alternative to commercial machines. The lack of statistically significant differences between the force reporting of the PedsTES and MTS validates the use of the new system as an accurate tool for small specimen material testing. This validation did not address grip design performance with respect to tissue specimens. Future work will explore grip design alternatives for specific tissue applications, which can range from cryogenic fixtures to the use of adhesives and grip face sculpting.

3.5 Conclusion

The PedsTES, a small benchtop test system, was designed and validated for the mechanical characterization of materials, including miniature pediatric tissue specimens. This study demonstrated the versatility of the system through pilot testing of synthetic and biological materials under quasistatic and viscoelastic loading conditions. The system

design compared favorably to commercial alternatives, particularly with respect to the ability to support miniature specimens. Analysis of nylon monofilament revealed no statistical difference in the resulting elastic modulus measures when compared to a standard system. Pilot testing revealed that the PedsTES is capable of accommodating a range of materials.

CHAPTER 4: BIOMECHANICAL MODELING OF MEDIAL FIBROTIC TISSUE OF THE CLUBFOOT

This chapter details the biomechanical analysis of clubfoot soft tissue, with the intention of obtaining insight into the mechanical properties and viscoelastic nature of this tissue. This research utilized the PedsTES to evaluate 16 surgically obtained medial fibrotic mass tissue samples from assenting pediatric patients undergoing routine clubfoot corrective surgery. Quasistatic and viscoelastic protocols, based on clinical conditions of conservative treatment, were performed to obtain structural (stiffness) and material (tangent modulus) properties, as well as preconditioning convergence and stress relaxation behavior.

4.1 Introduction

Clubfoot is a congenital deformity of the lower extremity, characterized by bone malformation and displacement, as well as alteration in the connective tissue of the foot. The condition varies in severity (Dimeglio et al., 1995; Dyer and Davis, 2006) and is characterized by an equinovarus hindfoot deformity, as well as cavus and adduction of the midfoot (Dobbs et al., 2009; Morcuende, 2006; Roye, Hyman and Roye, 2004). Histological studies have noted a thick, fibrotic mass encapsulating the medial and posterior side of the clubfoot, which may affect treatment outcomes (Aurell et al., 2002; Fukuhara, Schollmeier and Uhthoff, 1994; Hersh, 1967; Ippolito and Ponseti, 1980; Sano et al., 1998; Turco, 1971; Windisch et al., 2007). Equinus, restraint of the foot in plantarflexion, and adduction and inversion of the navicular and calcaneus are commonly seen in clubfoot. This results from the tautness and increased cross-sectional dimensions

of the medial and posterior ankle. Conservative treatment promotes eventual return of the navicular, calcaneus and cuboid to normal position through lengthening of the ligaments.

Conservative treatment, such as the Ponseti method, consists of weekly manipulation and casting, followed by bracing, in order to reposition the affected foot. Throughout each phase of the Ponseti method, the foot is manipulated and then held at a constant position for up to 7 days (Cohen et al., 2013; Dobbs et al., 2009; Ponseti, 2000; Ponseti, 2002; Ponseti and Campos, 1972; Terrazas-Lafargue et al., 2007) translating to a constant elongation (stress relaxation) of the soft tissue of the medial and posterior aspects of the clubfoot. Manipulation, or cyclic loading, is performed to precondition the tissues for correction.

Few studies have investigated the mechanics of these tissues, nor have longer term strategies for the treatment of severe clubfoot been based upon these principles (Hattori et al., 2007). Hattori in 2007 examined the relative elasticity of medial, posterior and lateral specimens of clubfoot hindfoot soft tissue (deltoid ligament, calcaneofibular ligament, and capsular tissue) using scanning acoustic microscopy. Mechanical tests can provide information on structural and material properties, as well as time-dependent (viscoelastic) behavior of the soft tissue as it responds to treatment.

The purpose of this study was to examine the mechanical properties and viscoelastic behavior of the clubfoot medial fibrotic mass tissue (MFMT). Miniature samples of tissue underwent preconditioning and stress relaxation protocols based on conservative clubfoot treatment conditions. Insight into the mechanical nature of this soft tissue may aid in improvement of conservative treatment strategies as well as prescription of treatment and prediction of outcomes.

4.2 Materials and Methods

4.2.1 Specimen Selection

Twenty-six medial fibrotic mass tissue (MFMT) specimens were collected in total. Seven specimens were harvested at Shriners Hospitals for Children® in Chicago (SHC), IL from 6 IRB approved assenting pediatric clubfoot patients undergoing routine surgical correction for resistant or recurring clubfoot. The origin of the MFMT was marked by surgical ink and/or suture. Specimens were placed in 0.9% saline solution filled specimen containers and fresh frozen at a temperature of -85^{o}C. Nineteen specimens of MFMT were also be obtained from 15 assenting surgical clubfoot patients, with the same age and pathology requirements as above, from Ortopedia Infantil at Fundación Clínica Infantil Club Noel in Cali, Colombia (CC), care of Dr. Luis Fernando Caicedo. The origin of these specimens were marked with surgical ink and/or suture, fresh frozen, and shipped from Cali, Colombia to Marquette University in dry ice via DHL. All specimens were stored at Marquette University at a temperature of -29^{o}C until testing. For the samples originating from Shriners Hospitals for Children – Chicago, this study was approved by the Institutional Review Boards of Rush University Medical Center and Marquette University (#10101309 Rush University Medical Center; #HR-2167 Marquette University). Tissue samples originating from Fundación Clínica Infantil Club Noel (Cali, Colombia) were de-identified and did not meet the regulatory definition of "human subject."

For mechanical testing, specimens were included if they met a length requirement of at least 7 mm. Two specimens from the SHC sample and 6 specimens from CC were

excluded from mechanical testing, but saved for histological analysis (not included in this study). Thus, a total of 19 specimens underwent mechanical testing.

4.2.2 MFMT Preparation

The MFMT specimens were prepared similarly to the tissue preparation protocol described in section 3.2.4.2. Each specimen was inspected and qualitatively assessed to ascertain a ligamentous area of interest. A tissue cutter was used to section each specimen longitudinally into 3 segments, the middle ligamentous segment having a width of approximately 1.5 mm (Figure 4-1). The two lateral sections were marked with histopath marking dye, secured in mesh inserts and cassettes, and placed in formalin to be saved for histologic analysis (not part of this study). The middle section was designated for mechanical testing.

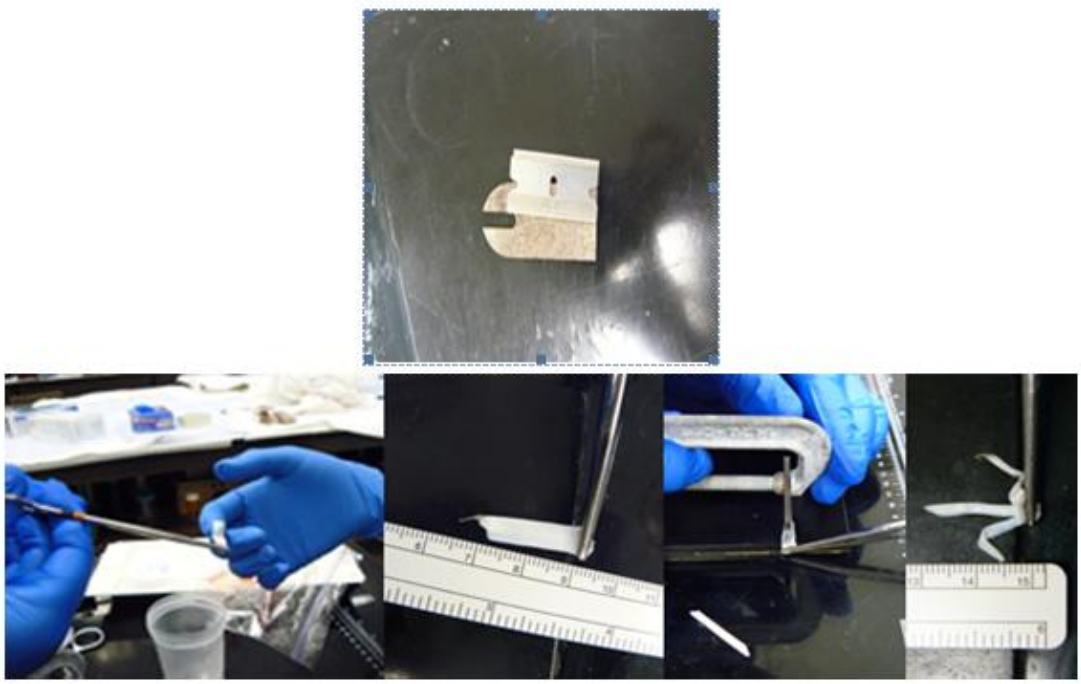

Figure 4-1: Specimen Preparation. Tissue cutter consisting of 2 razor blades and spacer, used to section the tissue into 3 segments.

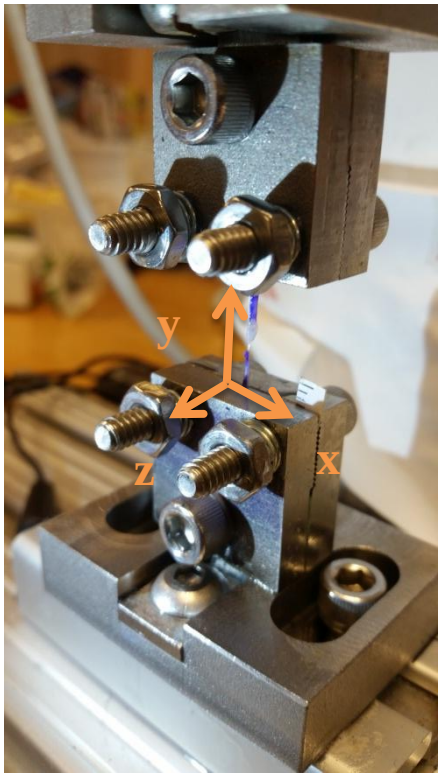

Figure 4-2: Tissue attachment grips. Grips use friction, compression, and cyanoacrylate to secure the tissue in place. Adjustments can be made along the x-, y-, and z-axes, as well as about the y-axis.

Prior to mechanical testing, each specimen was placed in a specimen container filled with PBS solution, then placed in a water bath heated to 37^{o}C for at least 30 minutes. After such time, the width and thickness were measured using digital calipers at each end and midsubstance, as well as the length, of the ungripped specimen.

Each specimen was placed and secured between the custom-made stainless steel grips with compression and cyanoacrylate (Figure 4-2). The assembly was then anchored to the test machine. Adjustments along the x- and z-axes and about the y-axis were made to ensure proper alignment. The tissue was marked with skin marker ink at the grips and at midsubtance for optical monitoring.

4.2.3 Mechanical Testing Protocol

The PedsTES, previously described in chapter 3, was used in the mechanical testing of the MFMT specimens. The system calibration was checked prior to testing each specimen, as described in section 3.2.2. The voltage-to-force relationship was implemented in the control program.

The following protocol is based on the methods described previously in section 3.2.4.2. Each specimen underwent preloading, preconditioning, stress relaxation, and load-to-failure phases of testing, during which time force, position, and video data were

acquired. The tissue was subjected to a preload of 0.5 N and the position of the actuator was recorded as the preload position. Following measurement of the dimensions, the specimen was preconditioned between 0.5 N and 2 N for 20 cycles. Stress relaxation was performed to strain levels corresponding to loads between 2 N and 5 N at 0.5N increments, followed by loads between 6 N and 10 N at 2 N increments, or until tissue failure. The constant strain was applied for 100 seconds. The strain was removed at a constant rate by sending the actuator to the preload position. The specimen was allowed to recover for 3 minutes between each stress relaxation trial. A load-to-failure test was performed following the stress relaxation protocol. The specimen was sprayed with heated PBS solution between test phases and during the recovery period to keep the tissue hydrated.

All loading and unloading occurred at a constant rate of 10 mm/min. Force, position, and video data were recorded at sampling frequencies of 1000 Hz, 100 Hz, and 30 frames per second, respectively. Following the load-to-failure phase, the specimen was removed from the grips, secured in a cassette, and placed in formalin to histological analysis (not part of this study).

4.2.4 Analytical Methods

4.2.4.1 Structural and Material Properties

Structural and material properties, including stiffness and tangent modulus, were calculated for each specimen. Tissue stiffness was estimated from the slope of the linear region of the load-to-failure force versus displacement data. Stress and strain were computed using the values of CSA and length of the preloaded specimen. The slope of

the linear region of the stress versus strain curve was used to determine the tangent modulus. The stiffness and tangent modulus were compared across specimens as well as compared to those values of normal cadaveric adult ankle ligaments (deltoid ligament) reported in literature (Butler et al., 2004; Funk et al., 2000). Median and ranges were reported for both properties.

4.2.4.2 Viscoelastic Behavior

The viscoelastic behavior of the ligaments was evaluated during the preconditioning and stress relaxation phases of testing. The stored energy (i.e., area between the loading and unloading curves) of each preconditioning loop was calculated to assess the decrease in hysteretic effect. A Shapiro-Wilks test was performed to determine normality ($\alpha = 0.05$). Lack of normality in several of the cycles necessitated the use of a Friedman non-parametric test of significance ($\alpha = 0.05$) and post-hoc analysis to identify differences between cycles.

The QLV model(Abramowitch and Woo, 2004; Fung, 1993; Fung et al., 1972; Funk et al., 2000; Toms et al., 2002), as described in section 1.7, was utilized to characterize the stress relaxation behavior exhibited by the MFMT specimens (Eqs. 4.1 – 4.7). Briefly, this theory assumes that the stress relaxation behavior of soft tissue can be expressed by the convolution integral:

$$\sigma(t, \varepsilon) = \bar{G}(t)\sigma^e(\varepsilon) \tag{4.1}$$

where $\sigma(t, \varepsilon)$ is the stress at time *t* under strain ε, $\sigma^e(\varepsilon)$ is the instantaneous elastic response, and $\bar{G}(t)$ is the reduced relaxation function representing the time-dependent stress response normalized by the stress at the time of the step input of strain [i.e., $\bar{G}(t) =$

$\frac{\sigma(t)}{\sigma_o}$, $\bar{G}(0^+) = 1$]. Assuming the Boltzmann superposition principle is valid, for a general strain history, the stress at time *t* takes the form:

$$\sigma(t) = \int_{-t}^{t} \bar{G}(t-\tau)\frac{\partial \sigma^e(\varepsilon)}{\partial \varepsilon}\frac{\partial \varepsilon}{\partial \tau}\partial\tau. \quad (4.2)$$

Two approaches were used in the determination the coefficients of the reduced relaxation function $\bar{G}(t)$ and the elastic response $\sigma^e(\varepsilon)$. To assess the linearity of the stress relaxation behavior exhibited by each specimen, the reduced relaxation curves were modeled with a decaying exponential function (Toms et al., 2002; Wills, Picton and Davies, 1972) consisting of 2 exponential terms and 6 coefficients (Eq. 4.3) using a nonlinear least squares algorithm. Goodness-of-fit was assessed via adjusted R^2. In addition, $\bar{G}(t)$ data were averaged for each specimen across trials, and then fitted with Eq. 4.3 to acquire parameter values of the averaged curves. A goodness-of-fit test was performed between the averaged fit model and each trial.

$$\overline{G}(t) = G_1 e^{-\lambda_1 t} + G_2 e^{-\lambda_2 t} + G_5 e^{-\lambda_3 t} \quad (4.3)$$

The elastic response $\sigma^e(\varepsilon)$ was approximated by curve-fitting the stress versus strain isochrones at $t = 0$ from the stress relaxation curves to Eq. 4.4. Adjusted coefficient of determination, adjusted R^2, was used to measure goodness-of-fit. The slope of the initial elastic response, AB, was calculated for each specimen and trial.

$$\sigma^e(\varepsilon) = A(e^{B\varepsilon} - 1) \quad (4.4)$$

The strain history approach (Abramowitch and Woo, 2004) accommodates for a ramp load with a constant, finite strain rate γ to strain level ε at time t_0, where t_0 is the time at peak load. By substituting Eqs. 4.3 and 4.4 into Eq. 4.2, the corresponding stress rise from $0<t<t_0$ can be written as:

$$\sigma(0 \le t \le t_0) = AB\gamma \int_0^t \{G_1 e^{-\lambda_1 t} + G_2 e^{-\lambda_2 t} + G_3 e^{-\lambda_3 t}\} e^{B\gamma\tau}\, \partial\tau \qquad (4.5)$$

while the subsequent stress relaxation $\sigma(t)$ from t_0 to t_∞ can be written as:

$$\sigma(t > t_0) = AB\gamma \int_0^{t_0} \{G_1 e^{-\lambda_1 t} + G_2 e^{-\lambda_2 t} + G_3 e^{-\lambda_3 t}\} e^{B\gamma\tau}\, \partial\tau. \qquad (4.6)$$

(See appendix B for analytical integration.) To determine the coefficients *A, B, $G_{1\text{-}3}$*, and $\lambda_{1\text{-}3}$, a nonlinear optimization algorithm of the sum of squares difference was performed on the experimental stress relaxation data for each curve of each specimen (Eq. 4.7) (Abramowitch and Woo, 2004).

$$\min_{A,B,G_{1-3}\lambda_{1-3},} \sum_{t_i=0}^{t_0} \left[\sigma_i^{exp}(t_i) - \sigma_i^{model}(t_i)\right]^2 + \sum_{t_j=t_0}^{t^\infty} \left[\sigma_j^{exp}(t_j) - \sigma_j^{model}(t_j)\right]^2. \quad (4.7)$$

For both techniques, the goodness of fit for each curve was measured by adjusted R^2. A Lilliefors test was utilized to assess normality of the parameters. Failing normality, a nonparametric Wilcoxon rank sum test was performed to assess the difference in parameter values between approaches. An exploratory analysis was performed on strain history approach parameters A and B. Linear mixed regression modeling was utilized.

Percent relaxation and the time to reach that value was calculated from the reduced relaxation data. To gain additional insight into the initial relaxation behavior, 80% of these values were computed for each specimen. Mean and standard deviation were computed for the sample population.

4.3 Results

4.3.1 Specimen Demographics

Nineteen MFMT specimens harvested from assenting clubfoot patients undergoing routine corrective surgery underwent mechanical testing, of which, 19 were

pre-loaded, 13 underwent preconditioning, 16 underwent the stress relaxation protocol, and 18 were loaded to failure. Of the 16 stress relaxed specimens, 3 were unable to be preconditioned to the 2 N prescribed level in the protocol and underwent stress relaxation trials at loads lower than 2 N. An additional 5 specimens completed a portion of the prescribed relaxation protocol, while 8 specimens completed the entire protocol.

Demographics were collected for patient medical records by the collaborating hospitals and de-identified information was provided. This information included age, gender, affected extremity(s), height, weight, idiopathic or secondary, treatment history, Diméglio severity (summary in Table 4-1, full demographics in appendix Table A-1).

Table 4-1: Patient demographics. Demographics of patients whose specimens underwent mechanical testing. *Height was only obtained from SHC patients. **Treatment history: none indicates no previous casting or surgical treatment; casting represents serial casting with no percutaneous Achilles tenotomy; Ponseti indicates full Ponseti method used, including casting and tenotomy; surgery indicates that surgical procedures (posterior release, Achilles lengthening, comprehensive release, etc), prior to the excise surgery, were performed on the patient. A complete list is included in the demographic table in appendix Table A-1.

Demographic	Mean ± SD
Age (months)	41.1 ± 25.3
Gender (M/F)	12/3
Height (mm)*	1173.1 ± 132.1
Weight (kg)	14.4 ± 6.2
Bilateral/Unilateral	10/5
Affected Side (L/R)	9/6
Idiopathic/Secondary	8/7
Diméglio Severity	3.3 ± 0.72
Treatment history (None/Casting/Ponseti/Prior Surgery)**	1/5/9/5

Specimen gross appearance ranged from white to pink, with areas of dense connective tissue as well as friable sections. Mean dimensions of the specimens are reported in Table 4-2. These values correspond to those measured at the pre-load of 0.5N.

Table 4-2: Specimen dimensions. Table of specimen dimensions measured at pre-load of 0.5N.

	Length (mm)	Width (mm)	Thickness (mm)	Aspect Ratio (mm/mm)	Cross-Sectional Area (mm x mm)
C1	9.01	1.65	1.51	5.46	2.49
C11	9.31	1.27	2.15	7.33	2.73
C12	7.72	1.42	2.06	5.44	2.93
C13	12.38	1.25	2.96	9.90	3.70
C15	7.56	3.64	1.50	2.08	5.46
C2B	8.30	1.87	2.66	4.44	4.97
C3	6.82	2.18	3.28	3.13	7.15
C4.1	9.73	2.48	2.15	3.92	5.32
C4.2	9.05	2.93	1.75	3.09	5.10
C6	9.37	2.65	2.57	3.53	6.82
C7.2	8.65	1.69	2.02	5.12	3.41
C8R	8.07	1.42	2.88	5.70	4.07
C9	5.47	1.78	2.26	3.07	4.02
SC1	7.06	2.37	1.41	2.97	3.34
SC3	7.99	2.73	1.81	2.93	4.94
SC6	11.14	1.85	0.79	6.02	1.46
SC7	5.79	1.47	1.45	3.94	2.13
SC8	9.53	2.37	1.82	4.02	4.31
Mean ± std	8.4 ± 2.1	2.05 ±0.6	2.0 ± 0.7	4.4 ± 1.9	4.0 ± 1.4

4.3.2 Structural and Material Properties

Data from a representative MFMT specimen loaded to failure is illustrated in Figure 4-3 (For figures of all specimen data, see appendix Figure A-1). A high degree of variability in the stress-strain response was observed among the samples. Strain rates for all samples undergoing load-to failure are presented in Table 4-3. Strain energy values for all load-to-failure specimens are presented in Table 4-4.

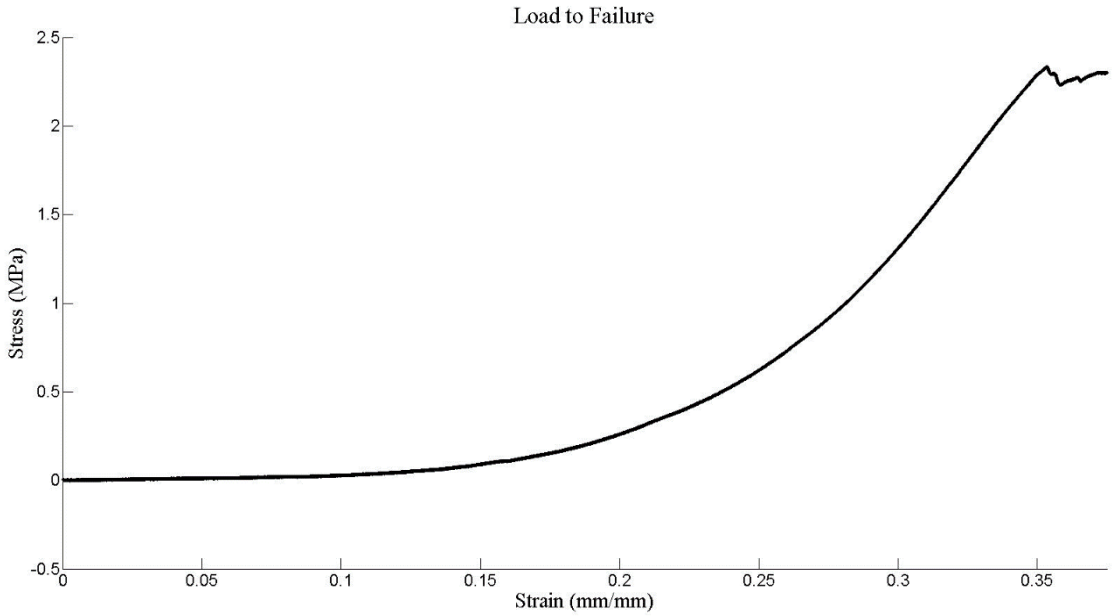

Figure 4-3: Representative MFMT specimen loaded to failure.

Table 4-3: Load-to-failure outcomes. Median load-to-failure strain rates for each specimen (%/s). Area under load-to-failure curves to peak load (energy absorbed (Nmm) and strain energy density (MPa)), stiffness (N/mm), tangent modulus (MPa), peak force (N) and stress (MPa) with corresponding displacement (mm) and strain (mm/mm) values. Sp.: specimen id

Sp.	Strain Rate (%/s)	Energy Absorbed (Nmm)	Strain Energy Density (MPa)	Stiff. (N/mm)	Mod. (MPa)	Disp. (mm)	Strain (mm/mm)	Force (N)	Stress (MPa)
C1	1.84	407.83	64.75	0.99	3.55	8.27	0.92	1.46	0.58
C11	1.78	1420.33	80.38	3.34	11.40	3.95	0.42	4.28	1.57
C12	2.15	424.65	197.65	11.93	31.49	3.49	0.45	11.90	4.07
C13	1.34	695.39	55.98	0.73	2.46	9.87	0.80	1.12	0.30
C15	2.20	1298.76	484.61	13.63	18.97	4.37	0.58	29.19	5.36
C2B	4.65	853.15	27.12	8.90	6.37	1.02	0.29	7.82	1.57
C3	2.44	1235.35	282.33	7.80	7.43	5.10	0.75	11.00	1.54
C4.1	1.71	308.43	20.87	2.74	5.00	1.77	0.18	2.94	0.55
C4.2	1.84	562.79	16.84	0.72	1.27	5.00	0.55	0.86	0.17
C6	1.75	68.88	56.66	6.52	10.48	2.61	0.28	4.97	0.85
C7.2	1.93	1021.70	199.57	6.56	16.59	2.78	0.32	26.82	7.86
C8R	2.06	437.11	120.01	11.75	23.28	2.89	0.36	9.99	2.45
C9	3.02	936.55	22.04	6.40	8.71	1.45	0.27	3.97	0.99
S1	2.36	943.52	235.42	20.99	43.02	3.38	0.48	16.59	4.82
S3	2.08	897.43	153.45	11.64	18.82	2.82	0.35	11.53	2.33
S6	1.49	229.54	29.93	1.00	7.77	5.21	0.47	1.12	0.76
S7	2.84	985.77	70.47	6.56	18.12	2.30	0.39	7.25	3.41
S8	1.74	848.25	74.61	2.50	5.53	4.84	0.51	3.13	0.73
Median	**2.06**	**850.70**	**72.54**	**6.54**	**9.60**	**3.43**	**0.44**	**6.11**	**1.55**
Min	**1.34**	**68.88**	**16.84**	**0.72**	**1.27**	**1.02**	**0.18**	**0.86**	**0.17**
Max	**4.65**	**1420.36**	**484.61**	**20.99**	**43.02**	**9.87**	**0.92**	**29.19**	**7.86**

4.3.3 Viscoelastic Response

Preconditioning results of a representative MFMT specimen are shown in Figure 4-4. Strain rates for all samples undergoing preconditioning were found to have a median

value of 2.02 %/s (1.67 - 2.89 %/s) (Full results in appendix Tables A-2, A-3). Analysis of the preconditioning loops revealed a decreasing trend in hysteresis area from the force-displacement data and stress-strain data for all specimens, with significant difference between cycles 2 and 20 ($p<<0.0001$). Post-hoc analysis indicated that convergence was reached at cycle 8 ($p = 0.55$).

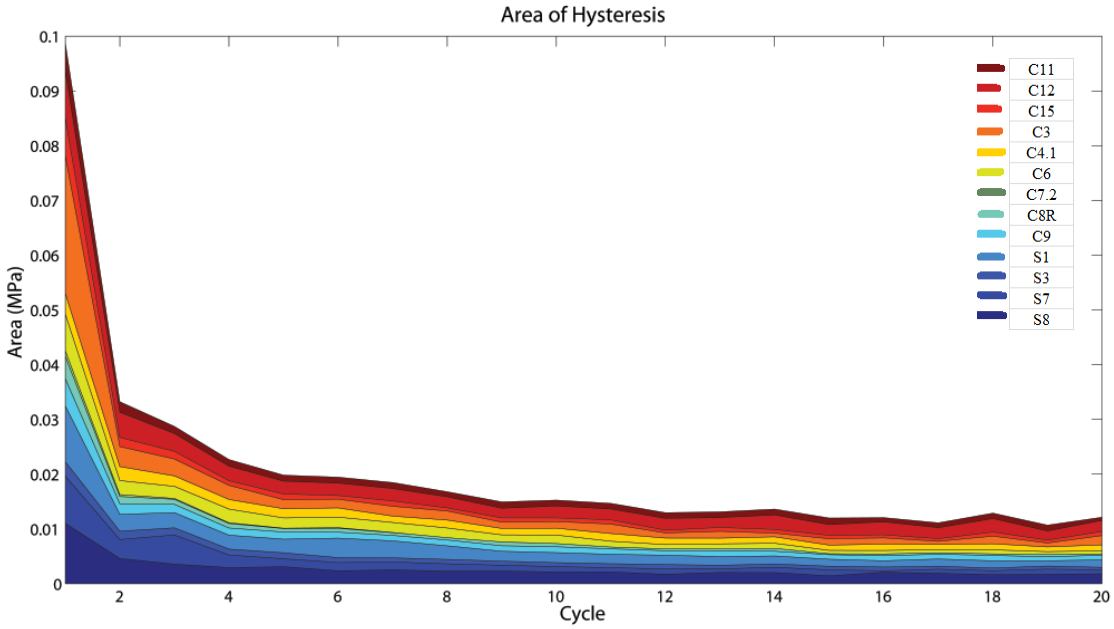

Figure 4-4: Preconditioning outcomes. Plot of area of hysteresis vs. cycle number for each specimen.

Stress relaxation results of a representative MFMT specimen are shown in Figure 4-5. Strain rates for all samples undergoing stress relaxation were found to have a median value of 1.99 %/s (1.48- 3.00 %/s) (Table 4-4, Full results in appendix Table A-4). Stress relaxation hold time was approximately 100s, during which time, the mean percent of relaxation equated to 71% (Table 4-5, Full results in appendix Table A-5). Relaxation reached 80% of the total relaxation by 31 seconds on average.

Table 4-4: Stress relaxation strain rates. Median (min/max) and per specimen stress-relaxation strain rate (%/s) undergoing stress-relaxation.

Specimen	% Strain Rate (%/s)
C1	1.84
C11	1.78
C12	2.15
C15	2.20
C3	2.44
C4.1	1.70
C4.2	1.84
C6	1.77
C7.2	1.93
C8R	2.06
C9	3.01
S1	2.35
S3	2.08
S6	1.48
S7	2.82
S8	1.74
Median	**1.99**
Min	**1.48**
Max	**3.01**

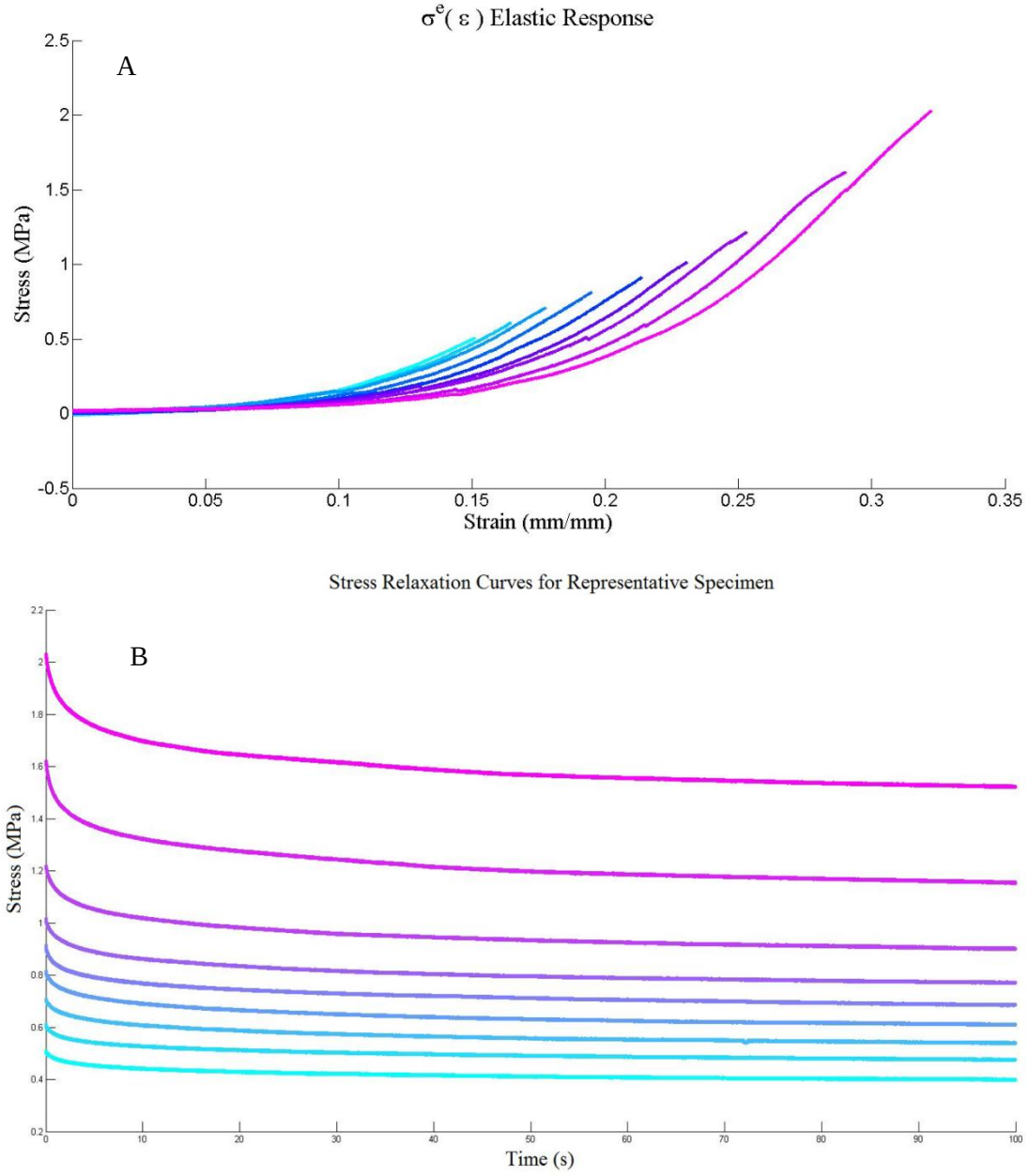

Figure 4-5: Representative MFMT specimen stress relaxation curves. A) Stress vs. strain curves from $0<t<t_0$ of the stress relaxation data (elastic response) for each trial. B) Stress vs. time curves from $t>t_0$ of the stress relaxation data for each trial during the stress relaxation protocol. Each trial represents a different load condition and corresponding strain level. Color gradient signifies individual trials, paired across plots A and B.

Table 4-5: Reduced relaxation outcomes. Columns 1-2: Mean and standard deviation of stress relaxation duration and percent total relaxation. Columns 3-4: Mean and standard deviation of time to reach 80% of the total percent of relaxation experienced by specimens. ATTL refers to the anterior tibiotalar ligament. Values of % relaxation were reported by Butler et al.(Butler et al., 2004).

	Time (s)	% Relaxation	Time (s) to 80% of Relaxation	80% of Relaxation
Mean	100.27	70.96	31.61	76.75
Std	3.25	7.25	7.04	5.79
ATTL(Butler et al., 2004)	180	66	N/A	N/A

Figure 4 -6 illustrates the reduced relaxation results of a representative specimen while utilizing the instantaneous step assumption method to determine model parameters ($R^2 > 0.90$). Comparison of mean parameter models to experimental data produced goodness-of-fit values greater than 0.90, though for specimen S8, $R^2 = 0.8043$ (Figure 4-7 and 4-8, Table4-6).

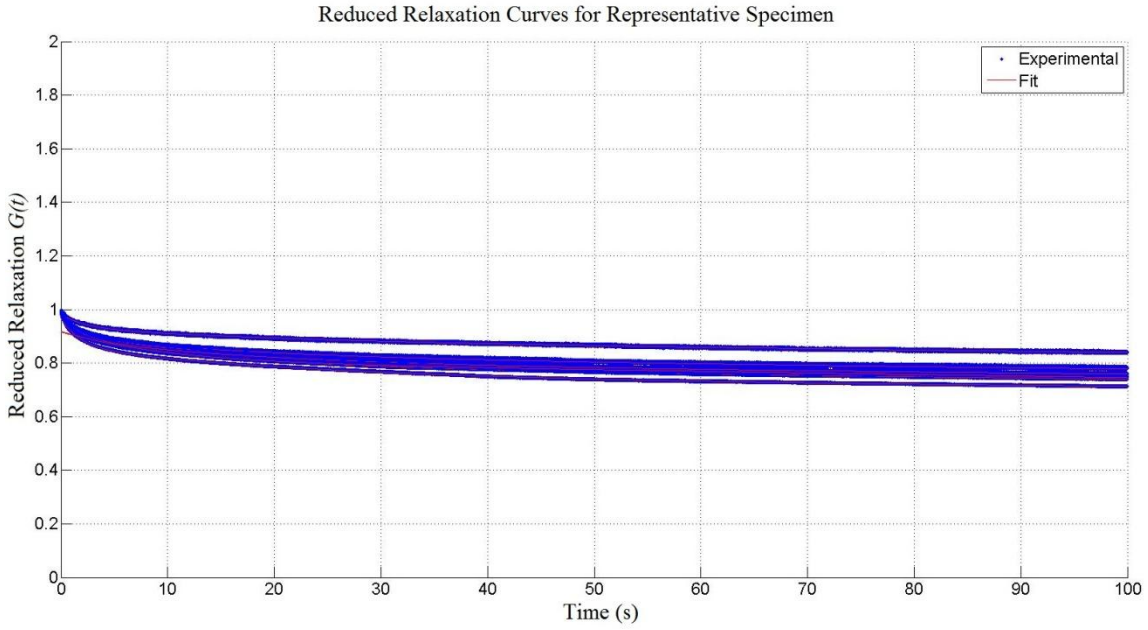

Figure 4-6: Reduced relaxation curves for each stress relaxation from a representative MFMT specimen. Experimental reduced relaxation curves regressed to $t = 0$ and predicted models for each curve fitting equation $\overline{G}(t) = G_1 e^{-\lambda_1 t} + G_2 e^{-\lambda_2 t} + G_5 e^{-\lambda_3 t}$.

Table 4-6: Parameters of averaged reduced relaxation curves for each specimen. Averaged trials were fitted with a 3-term, 6-parameter decaying exponential function. R^2 values > 0.90 for each specimen, except for 1 specimen (R^2 = 0.8043).

Specimen ID	G_1	λ_1	G_2	λ_2	G_3	λ_3	R^2
C1	0.1554	0.0650	0.6835	0.00104	0.1353	0.4628	**0.9871**
C11	0.2510	0.1163	0.6904	0.00104	0.0586	31771.5	**0.9159**
C12	0.1182	0.0608	0.7254	0.00081	0.1208	0.5529	**0.9892**
C15	0.0850	0.0559	0.8205	0.00063	0.0699	0.4505	**0.9943**
C3	0.1203	0.0905	0.8105	0.00098	0.0692	24985	**0.9720**
C4.2	0.1675	0.0755	0.5787	0.00147	0.2069	0.5673	**0.9945**
C6	0.1295	0.1153	0.7982	0.0015	0.0723	17022.2	**0.9055**
C7.2	0.0829	0.0566	0.8045	0.00059	0.0772	0.4716	**0.9950**
C8R	0.1096	0.0681	0.7646	0.00082	0.0886	0.6382	**0.9941**
C9	0.1044	0.0719	0.7622	0.00096	0.0970	0.6277	**0.9947**
S1	0.1364	0.0504	0.7045	0.00055	0.1104	0.5620	**0.9467**
S3	0.0913	0.0477	0.7983	0.00047	0.0806	0.4652	**0.9856**
S7	0.0935	0.0540	0.8078	0.00054	0.0725	0.4603	**0.9931**
S8	0.1790	0.0851	0.7045	0.00096	0.1423	2.0035	**0.8043**

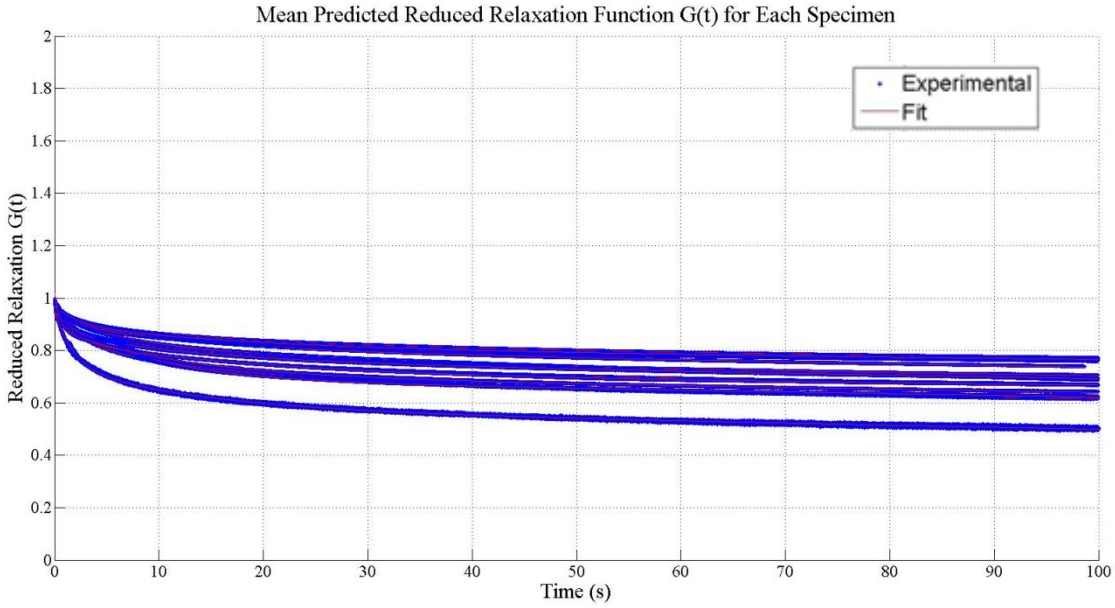

Figure 4-7: Average predicted reduced relaxation function *G(t)* for each specimen.

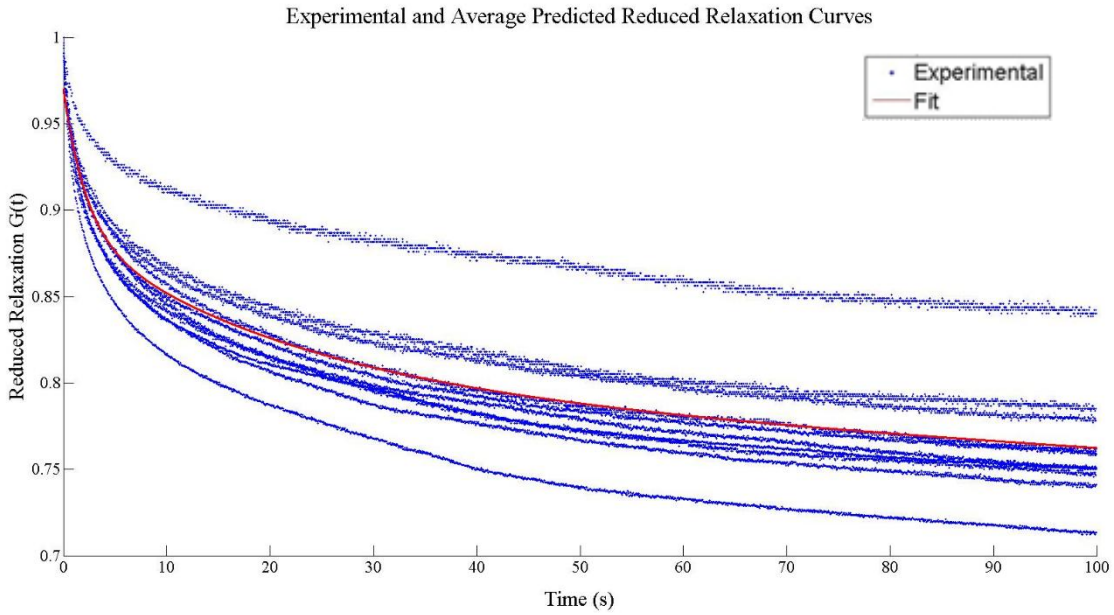

Figure 4-8: Experimental and average predicted reduced relaxation curves. Red curve represents average model fit. Blue curves correspond to experimental data for a representative specimen.

Elastic response isochronal plots of 10 specimens, which had 4 or more stress relaxation trials, are presented in Figure 4-9. Fitted curves illustrate a nonlinear elastic response with corresponding adjusted R^2 values greater than 0.82.

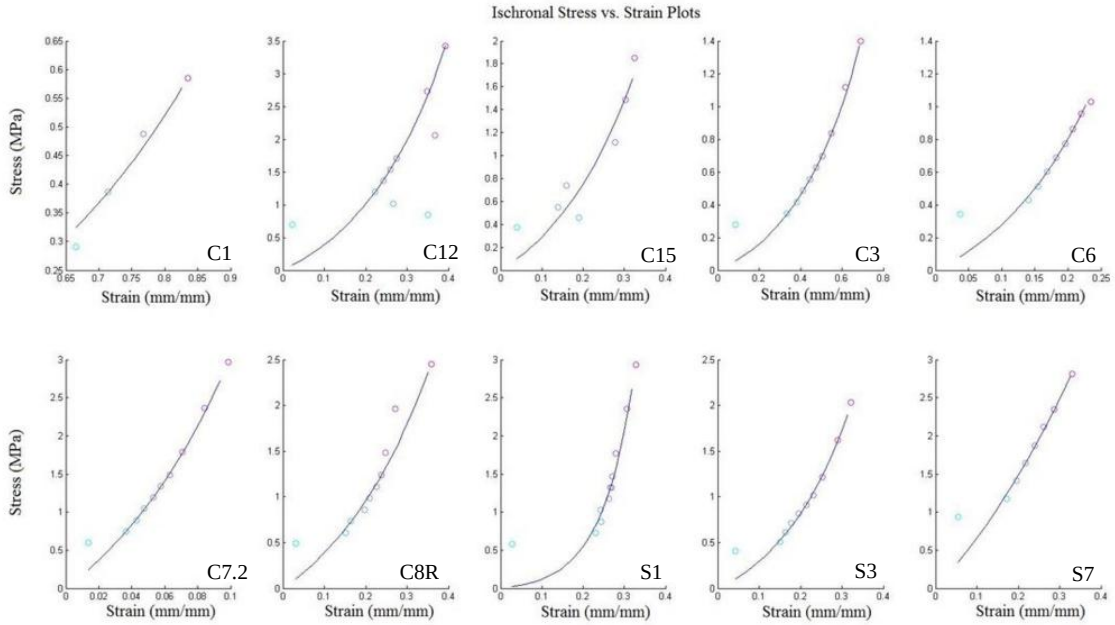

Figure 4-9: Isochronal stress vs. strain plots. Data points represent stress vs. strain data at peak stress for each trial for 10 specimens. A nonlinear exponential regression model characterizes the elastic response. $\sigma^e(\varepsilon)=A(e^{B\varepsilon}-1)$.

Table 4-7: Estimated parameters for isochronal data. Parameters *A* and *B* from the elastic response function (Eq. 4.6), as well as the slope *AB*. Values of goodness of fit, adjusted R^2 , were determined to be greater than 0.80. ATTL refers to anterior tibiotalar ligament. Values were obtained from Funk et al. (Funk et al., 2000). *AB calculated from presented A and B values; R^2 presented not adjusted.

Specimen ID	A	B	AB	adj R^2
C1	0.0457	3.1445	0.1438	0.9493
C12	0.6645	4.6191	3.0693	0.8380
C15	0.5057	4.5597	2.3059	0.8244
C3	0.1919	3.0557	0.5862	0.9858
C6	0.3226	6.2445	2.0142	0.9490
C7.2	1.4793	11.1529	16.4984	0.9918
C8R	0.8314	3.8321	3.1859	0.9679
S1	0.0480	12.6008	0.6052	0.9068
S3	0.388	5.6657	2.1983	0.9875
S7	2.8251	2.1074	5.9536	0.9527
ATTL(Funk et al., 2000)	2.06	20.11	*41.42	*0.989

Models produced using the strain history approach, illustrated in Figure 4-10, resulted in quality fit with median R^2 values falling above 0.80 (Table 4-8).

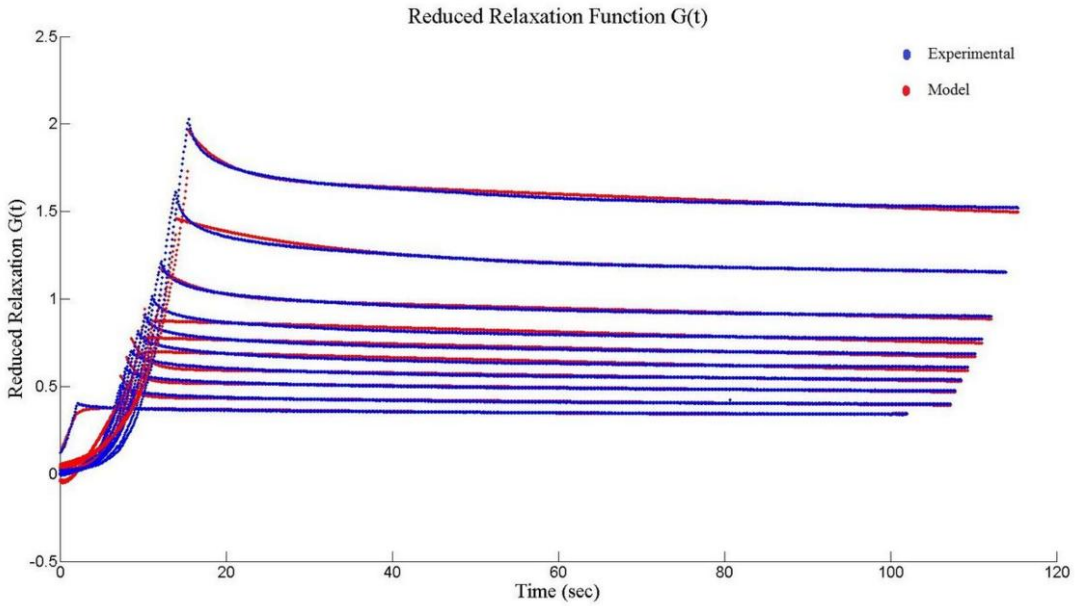

Figure 4-10: Experimental stress relaxation curves and predicted models using the strain history approach (Eqs. 4.5 and 4.6).

A Wilcoxon rank sum test comparing the parameters describing the relaxation behavior from the instantaneous step assumption and strain history approaches found that no significant difference existed between the two methods (p = 0.72, 0.41,0.43, 0.99, 0.67, 0.18).

Table 4-8: Non-parametric statics of parameters predicted using the strain history approach. Median, minimum and maximum (median (min-max)) values of parameters from Eq.s 5 and 6, and corresponding goodness of fit measure R^2.

Sample	A	B	G_1	λ_1	G_2	λ_2	G_3	λ_3	R^2
C1	0.00012 (0.00004-0.00063)	10.26406 (7.45999-12.10726)	1.48039 (1.32743-1.73851)	0.00196 (0.00095-0.00293)	2.02331 (1.34622-2.16485)	0.35633 (0.18594-0.47022)	-0.76452 (-1.10933--0.56988)	8.74859 (7.82714-10.36393)	0.9819 (0.9484-0.9855)
C11	0.00670 (0.00460-12.67741)	9.67274 (0.19776-12.59581)	0.48887 (-5.57273-10.16717)	0.05164 (-0.01859-11.10217)	2.49491 (0.10873-6.22109)	0.00317 (0.00074-0.06441)	7.54646 (-4.36512-27.54591)	1.15821 (0.13481-1.45005)	0.9382 (0.7874-0.9879)
C12	0.00065 (0.00005-2.82093)	17.17159 (4.71880-32.02773)	0.51791 (-25.22275-15.00623)	1.14505 (0.00156-59.51847)	3.67431 (-1.24707-78.74783)	0.00202 (0.00089-0.74382)	-2.28127 (-20.59833-1.01740)	4.51574 (0.11061-12.86800)	0.9827 (0.9580-0.9968)
C15	0.00736 (0.00033-25.48234)	14.09487 (0.07188-18.48531)	1.31838 (-19.00813-9.94075)	0.22478 (-0.00929-15.03544)	1.57155 (-0.03031-54.87198)	0.00156 (0.00121-0.09792)	3.33675 (-3.25674-48.77389)	6.38628 (0.61377-20.30042)	0.9853 (0.6810-0.9950)
C3	0.00473 (0.00022-1.37778)	8.16576 (3.13020-10.65132)	2.25642 (0.07684-4.90289)	0.00151 (-0.01101-0.11184)	0.92361 (0.02862-27.97244)	0.03696 (-0.01254-0.72423)	-0.00285 (-74.30358-2.41342)	6.16877 (1.35636-8.88007)	0.9920 (0.9787-0.9973)
C4.1	5.61663 (0.00051-11.81644)	0.54965 (0.09748-19.67305)	6.56468 (0.03341-17.90498)	0.41895 (-0.02080-3.66913)	0.05687 (-0.00473-4.96817)	0.00147 (-0.00134-0.00223)	7.80686 (-68.00355-17.68369)	1.27800 (1.25123-19.62453)	0.9831 (0.9759-0.9935)
C4.2	0.00232 (0.00052-0.00412)	9.92858 (6.88333-12.97383)	2.60210 (0.33482-4.86938)	0.08863 (0.00238-0.17489)	-1.09822 (-3.08727-0.89084)	0.50051 (0.00207-0.99896)	-5.65545 (-15.55563-4.24473)	4.17405 (-0.00297-8.35106)	0.8667 (0.7644-0.9690)
C6	11.00379 (0.00023-33.13981)	0.10925 (0.03328-18.53473)	2.54033 (-9.06343-18.04605)	0.46881 (-0.00185-14.15344)	-0.01512 (-0.78618-82.02436)	0.00176 (0.00160-0.44680)	23.82321 (-4.57728-64.13155)	2.06399 (1.46789-15.10165)	0.9744 (0.9004-0.9918)
C7.2	15.88557 (1.77203-41.24520)	0.11754) (0.01720-90.84832)	6.48861 (0.01384-109.46703)	0.30029 (0.04747-0.98784)	-0.04160 (-5.38639-0.08726)	0.00109 (0.00086-0.00201)	15.82172 (4.29057-41.09350)	0.79623 (0.03759-793.82618)	0.9825 (0.9796-0.9924)
C8R	0.00138 (0.00025-45.10097)	14.19210 (0.05577-20.46950)	0.24239 (-24.33013-6.44998)	0.63611 (-0.01288-96.66530)	10.20853) (-0.01696-47.53381)	0.00195 (0.00105-0.12396)	1.82258 (-4.52711-18.58009)	4.01226 (0.76330-13.86490)	0.9591 (0.4118-0.9881)
C9	0.90196 (0.01449-1.78943)	5.73858 (2.71860-8.75856)	1.79160 (1.70264-1.88056)	0.13741 (0.07646-0.19835)	1.35665 (-0.49228-3.20559)	0.00049 (-0.00014-0.00111)	1.40850 (0.93343-1.88357)	0.09759 (-0.01146-0.20664)	0.9431 (0.8931-0.9932)
S1	0.00018 (0.00010-75.39844)	22.11762 (0.00882-24.85561)	0.00053 (-13.24591-3.19079)	3.05274 (-0.02942-34.60109)	18.40242 (0.00032-31.97089)	0.00213 (0.00183-0.00401)	-0.00110 (-13.78532-57.16292)	5.44140 (1.71092-16.54156)	0.9753 (0.8476-0.9934)
S3	0.02184 (0.00067-35.59262)	11.68310 (0.10374-16.90056)	1.10098 (-25.19651-8.01172)	0.67589 (-0.04409-67.34742)	4.70712 (-0.00996-44.03848)	0.00135 (0.00057-0.20353)	3.04349 (-15.49962-14.90118)	1.87613 (0.04423-8.86973)	0.9791 (0.9370-0.9915)
S6	0.00165 (0.00002-1.78208)	15.81671 (0.05163-19.16061)	2.64993 (2.05771-7.00937)	-0.00168 (-0.00457-0.00103)	2.53171 (0.64105-2.85752)	0.05971 (-0.00043-6.66243)	-0.82959 (-3.86496-2.90092)	15.08064 (0.12688-38.52563)	0.9820 (0.7570-0.9974)
S7	27.95603 (0.02312-45.97881)	0.12527 (0.07581-12.34290)	1.94910 (0.00497-3.29368)	0.60398 (0.05689-0.67212)	-0.01823 (-0.09801-5.74752)	0.00118 (0.00056-0.00135)	16.93758 (-1.71371-35.25312)	1.79412 (0.47687-17.77365)	0.9801 (0.9766-0.9962)
S8	0.00634 (0.00083-48.20424)	12.09807 (0.04585-15.34396)	0.83659 (0.15206-19.40831)	0.17619 (-0.00222-0.81634)	1.10911 (-0.01600-38.65181)	0.00097 (-0.00019-0.00169)	-0.54483 (-25.88837-17.83617)	1.32515 (1.08680-10.74736)	0.9653 (0.8641-0.9939)

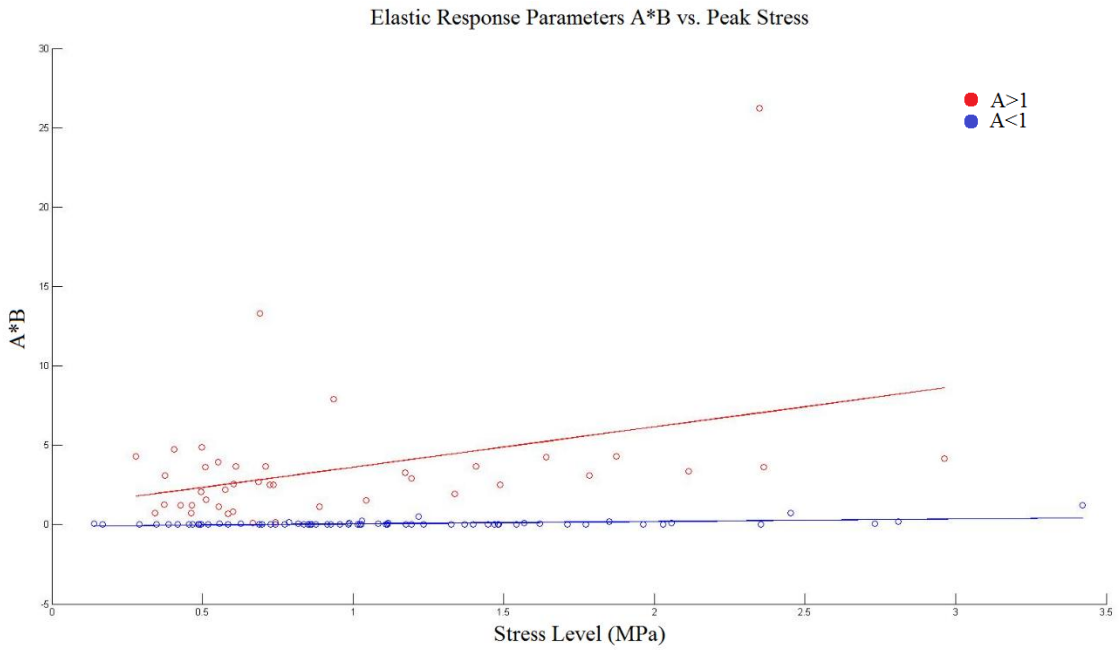

Figure 4-11: Exploratory analysis of AB vs. peak stress. Elastic response parameters AB values plotted against peak stress level. Linear model fit for two groups. Red group: A values >1, Blue group: A values <1.

Exploratory analysis of the parameters estimated by the strain history approach focused on the relationship between the slope AB and load conditions (Additional analysis in Appendix B). For example, Figure 4-11 contains the elastic response parameters AB vs. stress level. The plot shows two distinct groups in the data with different regression models. Further analysis of A and B revealed a nonlinear relationship between ln(A) and ln(B) (Figure 4-12). Linear regression analysis indicates that ln(B) is a significant predictor of ln(A) (p <<0.0001).

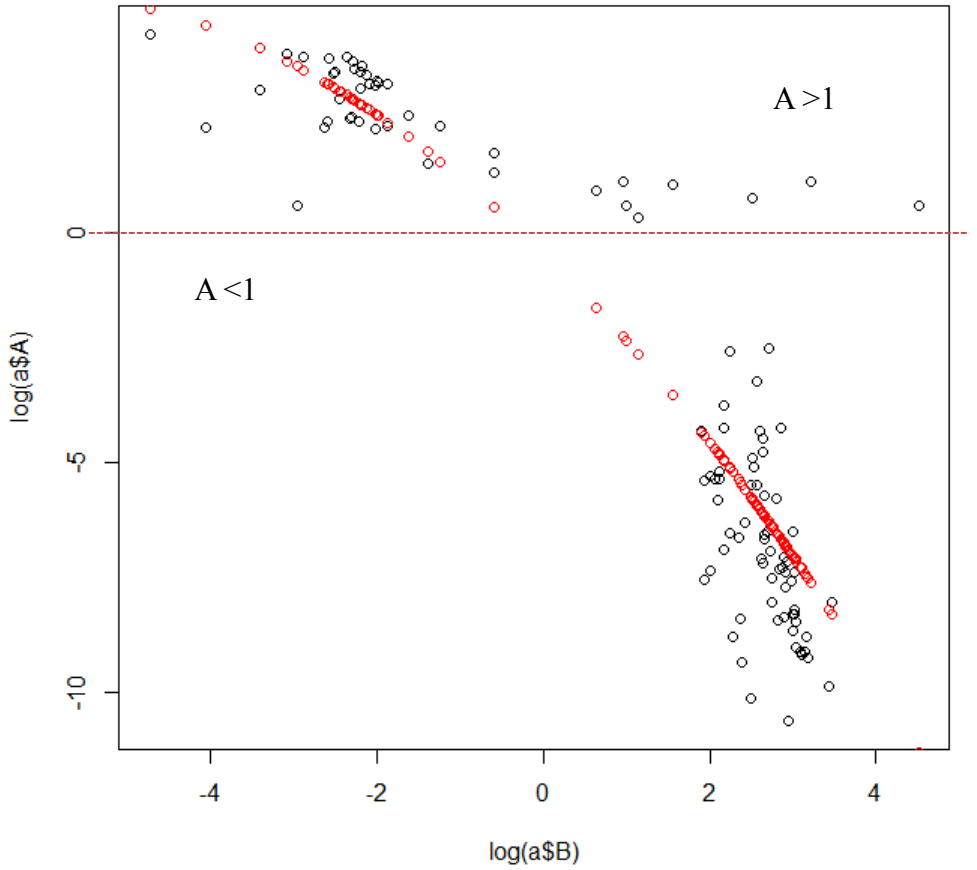


```
lm(formula = log(a$A) ~ log(a$B) + I(log(a$B) * log(a$B)))

Residuals:
    Min      1Q  Median      3Q     Max
-4.3851 -1.1185 -0.3355  0.7304 11.8599

Coefficients:
                          Estimate Std. Error t value Pr(>|t|)
(Intercept)               -0.44538    0.47281  -0.942   0.3483
log(a$B)                  -1.77856    0.09129 -19.482   <2e-16 ***
I(log(a$B) * log(a$B)) -0.13882    0.06423  -2.161   0.0329 *
---
Signif. codes:  0 '***' 0.001 '**' 0.01 '*' 0.05 '.' 0.1 ' ' 1

Residual standard error: 2.235 on 107 degrees of freedom
Multiple R-squared:  0.7928,    Adjusted R-squared:  0.789
F-statistic: 204.8 on 2 and 107 DF,  p-value: < 2.2e-16
```

Figure 4-12: Plot of ln(A) vs. ln (B). Parameters A and B computed from strain history approach. Linear model regression fit and analysis output.

4.4 Discussion

The current work presents an initial investigation of the mechanical behavior of the medial fibrotic mass tissue from pediatric clubfoot patients. Results from this study indicate that the structural and material properties vary between specimens. Findings from the instantaneous step assumption analysis of stress relaxation suggest a quasi-linear viscoelastic tissue behavior. Specimens saw preconditioning convergence begin after 8 cycles. Through isochronal assessment, elastic response of the tissue was found to be nonlinear in nature. In addition, specimens relaxed by approximately 30% during after 100s of hold. Findings from this research may aid in the improvement of conservative corrective strategies, such as accelerated protocols, as well as provide insight for the prediction of treatment outcomes.

Specimens were harvested from pediatric clubfoot patients undergoing corrective surgery for resistant or recurring deformity. A limited number of specimens were able to be obtained as the Ponseti method has become the gold standard of care for clubfoot correction(Zionts et al., 2010). Patients' demographics showed that 80% were male, which highlights the 3:1 male:female gender trend for clubfoot(Roye, Hyman and Roye, 2004). The mean Diméglio severity score was 3.3, indicating a relatively high degree of clubfoot severity in the sample population. This suggests that higher severity scores may be correlated with surgical necessity for better treatment outcomes or improved intensive non-invasive protocols. There was substantial variability in the age and prior treatment history. Age of the patient may have an effect on the variability in mechanical test results (Woo, Ohland and Weiss, 1990; Woo et al., 1986). Results from these studies on mechanical properties of rabbit ligament as a function of age found that hysteresis area,

tensile strength and energy absorption increase with maturation. In addition, it was noted that stiffness and elastic modulus were significantly lower for ligaments from immature donors as compared to those of matured specimens(Haut, 1983; Woo, Ohland and Weiss, 1990; Woo et al., 1986). Future analysis will address age as a factor of mechanical response variability.

A total of 26 specimens from two clinical institutions were recruited for this study. From this group, 10 specimens were unable to be mechanically tested due to length limitations. Guidelines for material testing suggest samples to have an aspect ratio (length divided by width) of at least 10, though for biological tissue, an aspect ratio of 4 is acceptable (Haut, 1986; Jung, Fisher and Woo, 2009; Schechtman and Bader, 1997). Studies investigating the effect of aspect ratio on mechanical testing responses of material found that increasing the aspect ratio increased specimen stiffness, while decreasing elongation(Carew et al., 2003; Haut, 1986; Schechtman and Bader, 1997). The mean aspect ratio of the MFMT specimens was 4.4 ± 1.9 mm/mm, though consideration and care was taken when segmenting and preparing the specimens for testing. Length was especially important with regard to gripping to ensure enough surface area was clamped and slippage was minimized. Slippage was also monitored via video capture during the trials.

Testing was performed at a displacement rate of 0.1667 mm/s (10mm/min) for all trials. However, due to variability in length, strain rates varied between specimens, as reported in the section 4.3 (Table 4-4). Strain rates were consistent across trials for each specimen, and ranged between 1.34 %/s and 4.65 %/s during load-to-failure testing. Studies investigating the effect of strain rate on the mechanical properties of tendons and

ligaments have reported that increasing strain rate increased elastic modulus slightly, as well as increased failure loads and strains, though bone is more susceptible to this relationship (Woo et al., 1990). Preliminary analysis of the effect of strain rate on the material properties (modulus, strain energy density) obtained from the quasistatic protocol showed an increasing trend. Further analysis and testing of a larger sample size is needed to assess this effect.

Following pre-loading of the tissue, specimens were exposed to 20 preconditioning loading and unloading cycles. Preconditioning is typically performed during the testing of soft tissue to bring the tissue sample to a steady state, where mechanical response will be more repeatable. This occurs due to changes in the structure of the tissue, including collagen fiber alignment and rearrangement, as well as microstructural alterations (Elliott et al., 2003; Frank, 2004; Miller et al., 2012; Purslow, Wess and Hukins, 1998; Woo, Johnson and Smith, 1993). Hysteresis represents the dissipation of energy stored in the material during preconditioning cycles and can be calculated from the area between the loading and unloading components in the preconditioning stress-strain curve. Analysis of hysteresis response indicated convergence began at 8 cycles for the MFMT specimens, and therefore, the tissue had reached steady state. Additionally, this illustrates the need to adequately manipulate or "prep" the clubfoot prior to casting the foot in order to stretch the medial soft tissue. Artifact was present in this phase of testing, as the test protocol included a 500 ms delay between loading and unloading. Further research is needed to study the effects of cycles and duration of preconditioning on the outcome of clubfoot treatment.

The stress relaxation protocol was utilized in this study in an effort to simulate conditions of the Ponseti Method (Section 2). To model stress relaxation, two equations were implemented. From $t = 0$ sec to t_i, where t_i is the time at which the prescribed load level for the trial was reached, Eq. 3 was used to model the elastic response of the curve. Reduced relaxation data, the normalized stress relaxation behavior, was taken from t_i to the end of the trial. The specimens were held at a constant elongation for approximately 100s. In a research study investigating the required duration for assessing ligament viscoelasticity, Manley, Jr. et al. found that viscoelasticity tests performed for at least 100 s produced similar accuracy in the viscoelastic behavior to those performed for at least 1000 s (Manley et al.). At this length of trial, the proportional relaxation reached a mean value of 71% ± 7.25 %, which was less relaxation than what was reported by Butler et al. for normal cadaveric medial ankle ligaments (66%, 64%, and 69%) and for lateral ankle ligaments (65%, 67%, 57%, 56%, 65%) (Butler et al., 2004). This may relate to changes the mechanisms that govern viscoelastic behavior in the clubfoot tissue, e.g. molecular structure and collagen and proteoglycan interaction in the MFMT tissue. Further analysis into the relationship between the tissue microstructure and mechanical behavior is necessary.

Stress relaxation parameters were derived via two optimization methods, the instantaneous step assumption method and the strain history approach, as described by Abramowitch and Woo (Abramowitch and Woo, 2004). No significant difference was found between the parameter values of each technique. Results from Abramowitch suggested that the difference in parameter values between the two methods could be due

to the absence of the relaxation occurring during ramping. Therefore, depending on the method used, the function predicted may result in greater relaxation (strain history).

Preliminary exploratory analysis of the parameters of the elastic response, as computed with the strain history approach, revealed two trends. First, two groups of values were found among parameter *A*, estimates above and below 1. This may be due to variability between specimens and/or potential microdamage in the specimen during the protocol. It was found that this trend affected most specimens. Also, as seen in Figure 4-12, the slopes of the two models for these groups are different. For trials where $A < 1$, the slope is approximately zero with respect to stress. Therefore, for those values of *AB* of the same specimen where $A < 1$, the slope, *AB,* is independent of stress level. However, for the second cluster of trials, $A > 1$ and the model fit has an increasing slope with respect to stress level. This could indicate stiffening with respect to stress. The second trend shows a decreasing nonlinear relationship between the natural log of *A* and natural log of *B*, where when $A > 1$, $B < 1$ and when $A < 1$, $B > 1$. Therefore, trials fitted with values of $A > 1$ have a more linear elastic response, while trials with parameter $A < 1$ have a more nonlinear elastic response (Abramowitch and Woo, 2004). Initial parameter estimates during the parameter optimization process may have reached a local minimum instead of a global minimum. To clear this as a potential error, multiple optimization iterations were performed with different starting values, producing the same parameters.

Quasistatic tests were performed on each specimen in order to investigate structural and material properties following stress relaxation. Analysis of this data revealed a high degree of variability between subjects in terms of the strain energy of the load-to-failure curves, as well as the peak load conditions. This may be due to fatigue or

yielding occurring from the previous stress relaxation tests, dimensional differences, or structural differences in the tissue. Median strain energy equated to 850.7 Nmm, and is comparable to earlier studies investigating medial ankle ligament properties. Butler et al. investigated the mechanical response of 8 ligaments from 8 fresh-frozen, geriatric cadaveric ankle specimens at low loads (Butler et al., 2004). The medial ligaments, including the deltoid ligaments, were found to be thicker than those of the lateral aspect of the ankle. Future quasistatic research on clubfoot could include higher load testing for the identification of yield stresses and permanent deformation.

Test conditions and external factors may have impacted the outcomes from this study. Mechanical properties of ligaments are sensitive to temperature and hydration. Studies have shown that major alterations in water content can alter viscoelastic behavior, such as in cyclic relaxation tests (Haut and Haut, 1997; Thornton, Shrive and Frank, 2001) Atkinson et al. found that high water content in human patella tendon resulted in faster and more relaxation (Atkinson, Ewers and Haut, 1999). For this study, the protocol called for hydrating the tissue throughout testing via a PBS solution spray. Any reduction in water content through evaporation could have decreased the amount of relaxation. Studies have investigated the effect of temperature on viscoelastic properties (Woo et al., 1987). Woo et al. found that temperature had an inverse relationship with area of hysteresis, i.e. higher temperatures resulted in smaller areas of hysteresis. In addition, lower temperatures resulted in less relaxation. Temperature was monitored throughout testing for the current study and air temperature averaged around 25^{o}C. Consequently, the amount of relaxation experienced by the MFMT specimens may have been less than what would have occurred at a higher physiologic temperature. The aforementioned

complications and limitations give rise to the need for an *in vivo* investigation of the mechanobiological response of the clubfoot tissue.

4.5 Conclusion

The purpose of this study was to mechanically characterize medial fibrotic mass tissue of the resistant and relapsing clubfoot in order to ascertain its behavior in response to conservative correction conditions. Limited information is available regarding the mechanical properties and viscoelastic behavior of the abnormal tissue. The mechanical nature of the soft tissue of the clubfoot may be a factor affecting the success of conservative treatment. Preliminary findings showed that MFMT specimens experienced less relaxation than that of normal deltoid ligaments of an older demographic in a given time period. Future work will assess the relationship between clubfoot tissue ultrastructure and mechanical behavior. MFMT specimens used in the current study are undergoing histological analysis to address fiber orientation and ultrastructure organization. As the Ponseti method of casting is theoretically a long-term stress relaxation protocol, assessing the tissue within physiologic conditions may provide a more accurate representation of the changes to the tissue over a longer period of time. An *in vivo* investigation of the medial ligaments of the clubfoot would yield not only the mechanical response of the tissue, but also an interaction with the biological response of adaptation.

CHAPTER 5: CONCLUSION

Improved knowledge of clubfoot and clubfoot treatment has the potential to affect and improve the lives of over 200,000 children worldwide each year. As technology improves, researchers have the tools to investigate the disorder in further detail and advance the state of clinical care. Global awareness and outreach for communities lacking the resources for proper treatment can extend the clinical impact of this research to those who truly need it most. With the advent of conservative treatment, specifically the Ponseti Method, surgical interventions have been limited to those who have the most severe deformity or recurrence. However, due to the time, logistics, and follow-up, conservative treatment can be a cumbersome and long term strategy. This effect is compounded for global communities where there may be more geographical limitations to care. In order to improve the efficacy and time efficiency of conservative treatment, a series of research studies was conducted to gain more insight into the biomechanical effects of the treatments, clubfoot soft tissue, and casting methodology.

The purpose of this dissertation was to investigate the biomechanics of conservative clubfoot treatment. The first research study (Chapter 2) executed a comprehensive analysis of the kinematic behavior of three common casting materials used in the progressive casting protocol of the Ponseti Method. The second research study (Chapter 3) developed and validated a benchtop material test system for the evaluation of miniature soft tissue specimens. The third research study (Chapter 4) utilized the material test system in order to perform quasistatic and viscoelastic protocols on medial fibrotic mass tissue obtained during surgery from pediatric clubfoot patients. The outputs of this investigation led to the mathematical modeling of the stress relaxation

behavior of this tissue. This research provides insight into the mechanical response of the deformity to conservative treatment. This may lead to innovative approaches focused on improved treatment efficacy and efficiency.

5.1 Summary of Findings

The hypotheses outlined in section 1.5 were verified via the specific aims of each research study. Through the use of a clubfoot correction model and motion analysis, the creep behavior of several casting materials was quantified. This analysis revealed minimal overall creep rotation for the three cast materials (< 2.0 deg), yet identified semi-rigid fiberglass to be a suitable alternative to plaster-of-Paris, as it resisted deformation earlier in the drying process. In addition, tests at different levels of torque failed to have significantly different results; therefore, the inherent nature of the material may not be susceptible to deformity stiffness and severity levels. Modeling of the viscoelastic nature of the cast material provided boundary conditions caused by the treatment. This could potentially be useful in simulation of *in vivo* tissue behavior based on external motion and musculoskeletal models. In addition, the behavior may provide a model or guideline for future devices or apparatuses used during conservative clubfoot treatment.

The investigation into the mechanical behavior required the development and validation of a benchtop and portable mechanical test system capable of handling miniature material specimens, including but not limited to those of a biological nature. Requirements for the system included an adjustable mechanical framework, grips for miniature specimens, electromechanical control, as well as software programmed interface. A comprehensive analysis of the system with synthetic and biological materials

validated the system's ability to detect force and position and demonstrated its versatility, respectively.

Finally, medial fibrotic mass tissue specimens from pediatric patients undergoing routine surgical clubfoot correction were characterized utilizing quasistatic and viscoelastic protocols. Results of this study allowed for the parameterization of a model of stress relaxation that can be used to describe tissue response to conditions of conservative correction. Interspecimen variability was found to be present and it is suggested that this may contribute to difficulties in evaluating this tissue *in vitro*. The preconditioning phase of the viscoelastic protocol allowed the tissue to reach a hysteretic equilibrium beginning at 8 cycles ($p > 0.05$). This finding may establish a minimum threshold for pre-casting manipulation. The stress relaxation protocol performed at several load levels on the MFMT permitted analysis of the linearity of the tissue behavior. As the standard model for ligament behavior, the quasi-linear viscoelastic model was implemented. Utilizing two different approaches, parameters quantifying the reduced relaxation behavior and elastic response were determined. Based on the instantaneous step assumption approach, the reduced relaxation function $G(t)$ was found to be independent of strain level with R^2 values greater than 0.90, when comparing the averaged model with individual strain levels. The elastic response parameters A and B were determined via a nonlinear regression of the isochronous stress-strain curve for each specimen (adjusted $R^2 > 0.82$). The strain history approach, developed by Abramowitch and Woo (Abramowitch and Woo, 2004), was used simultaneously calculate the parameters of the reduced relaxation function and elastic response. The parameters determined by the two approaches were not significantly different, though the strain

history approach takes into account the relaxation due to the ramping phase. While this is the first attempt at mechanically characterizing the MFMT, findings showed similar but less relaxation than did normal deltoid ligaments (Butler et al., 2004). In regards to elastic response, the influence of stress level on the slope *AB,* as determined via the strain history approach, depended on the value of A. Finally, the nonlinear relationship of *ln(A)* and *ln(B)* revealed a significant correlation and inverse relationship.

This research is the first step in understanding how and why the clubfoot responds to conservative correction. Findings from this analysis of tissue behavior may provide clinicians and researchers with a mechanical starting point for the future of clubfoot treatment.

5.2 Limitations and Future Directions

The research presented in this dissertation represents a novel introduction into the material mechanics of clubfoot soft tissue and conservative correction. The analysis of miniature soft tissue samples surgically extracted during routine corrective procedures may supply the clinical and therapeutic community with underlying mechanical insight for the future improvement of clubfoot correction. With a quantitative assessment of clubfoot correction via creep analysis, it may be possible to combine these findings to model patient specific responses to treatment. With the understanding of these conditions, new methods and materials could be utilized to more effectively and efficiently treat clubfoot.

The next focus beyond the mechanical aspects of the clubfoot tissue is to ascertain the biological correlation with the tissue mechanics. The initial step is to assess the statistical correlation of tissue ultrastructure with the findings of the present study, and

then evaluate connections to genetics. With the advent of fluoroscopy, ultrasound, and elastography, future directions could potentially address limitations brought on by the simulation set-up of the casting study, and the *in vitro* conditions of the clubfoot tissue mechanical evaluation. Fluoroscopy would allow for the merging of these two research topics by providing an internal view of the musculoskeletal system *in vivo* and allow correlation of mechanical tissue properties with functional behavior. Ultrasound and elastography are safe and non-invasive means to detect tissue structure, as well as material properties and behavior. The outcomes of the mechano-ultrastructure correlation could allow for clinical determination of treatment response at the tissue level. Both these techniques could provide a mechanobiological analysis of the tissue in response to conservative treatment, which would include: 1) casting during the Ponseti method; 2) immobilization in the Denis-Browne brace; and 3) pre-casting manipulation (cyclic loading). This assessment could pilot future correction strategies, devices, and therapy.

BIBLIOGRAPHY

Abdelgawad, A.A., et al. "Treatment of Idiopathic Clubfoot Using the Ponseti Method: Minimum 2-Year Follow-Up." *Journal of Pediatric Orthopaedics B* 16.2 (2007): 98-105. Print.

Abramowitch, S.D., and S.L. Woo. "An Improved Method to Analyze the Stress Relaxation of Ligaments Following a Finite Ramp Time Based on the Quasi-Linear Viscoelastic Theory." *Journal of Biomechanical Engineering* 126.1 (2004): 92-7. Print.

Abramowitch, S.D., et al. "An Evaluation of the Quasi-Linear Viscoelastic Properties of the Healing Medial Collateral Ligament in a Goat Model." *Annals of Biomedical Engineering* 32.3 (2004): 329-35. Print.

Abramowitch, S.D., et al. "*The Healing Medial Collateral Ligament Following a Combined Anterior Cruciate and Medial Collateral Ligament Injury—a Biomechanical Study in a Goat Model*." *Journal of Orthopaedic Research 21.6 (* 2003): 1124-30. Print.

Albert, C., et al. "Bone Properties by Nanoindentation in Mild and Severe Osteogenesis Imperfecta." *Clinical Biomechanics (Bristol, Avon)* 28.1 (2013): 110-6. Print.

Albert, C.I., J. Jameson, and G. Harris. "Design and Validation of Bending Test Method for Characterization of Miniature Pediatric Cortical Bone Specimens." *Proceedings of the Institution of Mechanical Engineering, Part H:Juornal of Engineering in Medicine* 227.2 (2013): 105-13. Print.

"Astm D638-14, Standard Test Method for Tensile Properties of Plastics." West Conshohocken, PA: ASTM International, 2014. Print.

Atkinson, T.S., B.J. Ewers, and R.C. Haut. "The Tensile and Stress Relaxation Responses of Human Patellar Tendon Varies with Specimen Cross-Sectional Area." *Journal of Biomechanics* 32.9 (1999): 907-14. Print.

Aurell, Y., et al. "Ultrasound Anatomy in the Neonatal Clubfoot." *European Radiology* 12.10 (2002): 2509-17. Print.

Berman, A.T., and B.G. Parks. "A Comparison of the Mechanical Properties of Fiberglass Cast Materials and Their Clinical Relevance." *Journal of Orthopaedic Trauma* 4.1 (1990): 85-92. Print.

Box, T.E.T. "Tensile Modulus - Modulus of Elasticity or Young's Modulus - for Some Common Materials". 7/24/15. <http://www.engineeringtoolbox.com/young-modulus-d_417.html>.

Brewster, M.B.S., et al. "Ponseti Casting: A New Soft Option." *Journal of Bone and Joint Surgery – British Volume* 90-B.11 (2008): 1512-15. Print.

Butler, A.M., et al. "Mechanical Response of Ankle Ligaments at Low Loads." *Foot & Ankle International* 25.1 (2004): 8-12. Print.

Callahan, D.J., et al. "A Comparative Study of Synthetic Cast Material Strength." *Orthopedics* 9.5 (1986): 679-81. Print.

Carew, E.O., et al. "Effect of Specimen Size and Aspect Ratio on the Tensile Properties of Porcine Aortic Valve Tissues." *Annals of Biomedical Engineering* 31.5 (2003): 526-35. Print.

Cassis, N., and A. Torres-Gomez. "Treatment Options for Clubfoot: An Update." *Pediatric Health* 3.5 (2009): 473-78. Print.

Creep Evaluation of (Orthotic) Cast Materials During Simulated Clubfoot Correction. Engineering in Medicine and Biology Society (EMBC), 2012 Annual International Conference of the IEEE. Aug. 28 2012-Sept. 1 2012 2012. Print.

Cohen, T.L., et al. "Evaluation of Cast Creep Occurring During Simulated Clubfoot Correction." *Proceedings of the Institution of Mechanical Engineering, Part H:Juornal of Engineering in Medicine* 227.8 (2013): 919-27. Print.

Coss, H.S., and W.L. Hennrikus. "Parent Satisfaction Comparing Two Bandage Materials Used During Serial Casting in Infants." *Foot & Ankle International* 17.8 (1996): 483-6. Print.

"Cure Clubfoot". 11/29/15 2015. <https://cure.org/clubfoot/>.

Currey, J. "The Structure and Mechanics of Bone." *Journal of Materials Science* 47.1 (2012): 41-54. Print.

Davids, J.R., et al. "Skin Surface Pressure beneath an above-the-Knee Cast: Plaster Casts Compared with Fiberglass Casts." *Journal of Bone and Joint Surgery - American Volume* 79.4 (1997): 565-9. Print.

Deshpande, S.V., and S.V. Deshpande. "An Experimental Study of Pressure-Volume Dynamics of Casting Materials." *Injury* 36.9 (2005): 1067-74. Print.

Dimeglio, A., et al. "Classification of Clubfoot." *Journal of Pediatric Orthopaedics B* 4.2 (1995): 129-36. Print.

Dobbs, M.B., et al. "Update on Clubfoot: Etiology and Treatment." *Clinical Orthopaedics and Related Research* 467.5 (2009): 1146-53. Print.

Docker, C.E., et al. "Ponseti Treatment in the Management of Clubfoot Deformity - a Continuing Role for Paediatric Orthopaedic Services in Secondary Care Centres." *Annals of the Royal College of Surgeons of England* 89.5 (2007): 510-2. Print.

Dortmans, L.J., A.A. Sauren, and E.P. Rousseau. "Parameter Estimation Using the Quasi-Linear Viscoelastic Model Proposed by Fung." *Journal of Biomechanical Engineering* 106.3 (1984): 198-203. Print.

Duenwald, S.E., R. Vanderby, Jr., and R.S. Lakes. "Stress Relaxation and Recovery in Tendon and Ligament: Experiment and Modeling." *Biorheology* 47.1 (2010): 1-14. Print.

Dyer, P.J., and N. Davis. "The Role of the Pirani Scoring System in the Management of Club Foot by the Ponseti Method." *Journal of Bone and Joint Surgery - British Volume* 88.8 (2006): 1082-4. Print.

Elliott, D.M., et al. "Effect of Altered Matrix Proteins on Quasilinear Viscoelastic Properties in Transgenic Mouse Tail Tendons." *Annals of Biomedical Engineering* 31.5 (2003): 599-605. Print.

Faulks, S., and B.S. Richards. "Clubfoot Treatment: Ponseti and French Functional Methods Are Equally Effective." *Clinical Orthopaedics and Related Research* 467.5 (2009): 1278-82. Print.

Feola, A., et al. "Impact of Pregnancy and Vaginal Delivery on the Passive and Active Mechanics of the Rat Vagina." *Annals of Biomedical Engineering* 39.1 (2011): 549-58. Print.

Flynn, J.M.M.D., M.P.T. Donohoe, and W.G.M.D. Mackenzie. "An Independent Assessment of Two Clubfoot-Classification Systems." *Journal of Pediatric Orthopaedics May/June* 18.3 (1998): 323-27. Print.

Frank, C.B. "Ligament Structure, Physiology and Function." *Journal of Musculoskeletal Neuronal Interaction* 4.2 (2004): 199-201. Print.

Fukuhara, K., G. Schollmeier, and H. Uhthoff. "The Pathogenesis of Club Foot. A Histomorphometric and Immunohistochemical Study of Fetuses." *Journal of Bone and Joint Surgery – British Volume* 76-B.3 (1994): 450-57. Print.

Fung, Y.C. *Biomechanics : Mechanical Properties of Living Tissues*. 2nd ed. New York: Springer-Verlag, 1993. Print.

Fung, Y.C., et al. *Biomechanics, Its Foundations and Objectives*. Englewood Cliffs, N.J.,: Prentice-Hall, 1972. Print.

Funk, J.R., et al. "Linear and Quasi-Linear Viscoelastic Characterization of Ankle Ligaments." *Journal of Biomechanical Engineering* 122.1 (2000): 15-22. Print.

Galloway, M.T., A.L. Lalley, and J.T. Shearn. "The Role of Mechanical Loading in Tendon Development, Maintenance, Injury, and Repair." *Journal of Bone and Joint Surgery* 95.17 (2013): 1620-28. Print.

Gere, J.M., and S.P. Timoshenko. *Mechanics of Materials*. PWS Pub Co., 1997. p. 889.Print.

Graf, A., et al. "Comprehensive Review of the Functional Outcome Evaluation of Clubfoot Treatment: A Preferred Methodology." *Journal of Pediatric Orthopaedics B* 21.1 (2012): 20-7. Print.

Bose Corporation - ElectroForce Systems Group. ElectroForce® 3100 Test Instrument. MN, USA: Bose Corporation.

Hattori, K.a., et al. "Measurement of Soft Tissue Elasticity in the Congenital Clubfoot Using Scanning Acoustic Microscope." *Journal of Pediatric Orthopaedics B* 16.5 (2007): 357-62. Print.

Haut, R.C. "Age-Dependent Influence of Strain Rate on the Tensile Failure of Rat-Tail Tendon." *Journal of Biomechanical Engineering* 105.3 (1983): 296-9. Print.

---. "The Influence of Specimen Length on the Tensile Failure Properties of Tendon Collagen." *Journal of Biomechanics* 19.11 (1986): 951-5. Print.

Haut, T.L., and R.C. Haut. "The State of Tissue Hydration Determines the Strain-Rate-Sensitive Stiffness of Human Patellar Tendon." *Journal of Biomechanics* 30.1 (1997): 79-81. Print.

Hersh, A. "The Role of Surgery in the Treatment of Club Feet." *Journal of Bone & Joint Surgery - American Volume* 49.8 (1967): 1684-96. Print.

Herzenberg, J.E., C. Radler, and N. Bor. "Ponseti Versus Traditional Methods of Casting for Idiopathic Clubfoot." *Journal of Pediatric Orthopedics* 22.4 (2002): 517-21. Print.

Illinois Tool Works Inc. *Instron® 3340 Series Single Column Model*. USA: Illinois Tool Works Inc..

Ippolito, E. "Update on Pathologic Anatomy of Clubfoot." *Journal of Pediatric Orthopaedics B* 4.1 (1995): 17-24. Print.

Ippolito, E., et al. "Long-Term Comparative Results in Patients with Congenital Clubfoot Treated with Two Different Protocols." *Journal of Bone and Joint Surgery – American Volume* 85-A.7 (2003): 1286-94. Print.

Ippolito, E., and I.V. Ponseti. "Congenital Club Foot in the Human Fetus. A Histological Study." *Journal of Bone and Joint Surgery – American Volume* 62.1 (1980): 8-22. Print.

Johnson, G.A., et al. "Tensile and Viscoelastic Properties of Human Patellar Tendon." *Journal of Orthopaedic Research* 12.6 (1994): 796-803. Print.

Jung, H.J., M.B. Fisher, and S.L. Woo. "Role of Biomechanics in the Understanding of Normal, Injured, and Healing Ligaments and Tendons." *Sports Medicine, Arthroscopy, Rehabilitation, Therapy and Technology* 1.1 (2009): 9. Print.

Laaveg, S.J., and I.V. Ponseti. "Long-Term Results of Treatment of Congenital Club Foot." *Journal of Bone & Joint Surgery - American Volume* 62.1 (1980): 23-31. Print.

Manley, E., et al. *Required Test Duration for Group Comparisons in Ligament Viscoelasticity: A Statistical Approach*: IOS Press. Print.

Martin, P.J., et al. "A Comparative Evaluation of Modern Fracture Casting Materials." *Engineering in Medicine* 17.2 (1988): 63-70. Print.

Martin, R.B., D.B. Burr, and N.A. Sharkey. *Skeletal Tissue Mechanics*. New York: Springer, 1998. Print.

Mihalko, W.M., A.J. Beaudoin, and W.R. Krause. "Mechanical Properties and Material Characteristics of Orthopaedic Casting Material." *Journal of Orthopaedic Trauma* 3.1 (1989): 57-63. Print.

Miller, K.S., et al. "Examining Differences in Local Collagen Fiber Crimp Frequency Throughout Mechanical Testing in a Developmental Mouse Supraspinatus Tendon Model." *Journal of Biomechanical Engineering* 134.4 (2012): 041004-04. Print.

Moalli, P.A., et al. "A Rat Model to Study the Structural Properties of the Vagina and Its Supportive Tissues." *Amerocan Journal of Obstetrics and Gynecology* 192.1 (2005): 80-8. Print.

Moon, D.K., et al. "The Effects of Refreezing on the Viscoelastic and Tensile Properties of Ligaments." *Journal of Biomechanics* 39.6 (2006): 1153-7. Print.

Morcuende, J.A. "Congenital Idiopathic Clubfoot: Prevention of Late Deformity and Disability by Conservative Treatment with the Ponseti Technique." *Pediatric Annals* 35.2 (2006): 128-30, 32-6. Print.

Morcuende, J.A.M.D.P., et al. "Results of an Accelerated Ponseti Protocol for Clubfoot." *Journal of Pediatric Orthopaedics September/October* 25.5 (2005): 623-26. Print.

MTS. *Acumen™ Electrodynamic Test Systems*. USA: MTS Corporation..

Ng, B.K., T.P. Lam, and J.C. Cheng. "Treatment of Severe Clubfoot with Manipulation Using Synthetic Cast Material and a Foam-Casting Platform: A Preliminary Report." *Journal of Pediatric Orthopaedics B* 19.2 (2010): 164-70. Print.

Nordin, M., and V.H. Frankel. *Basic Biomechanics of the Musculoskeletal System*. 4th ed. Philadelphia: Wolters Kluwer Health/Lippincott Williams & Wilkins, 2012. Print.

Owen, R.M., et al. "A Collaborative Public Health Approach to Clubfoot Intervention in 10 Low-Income and Middle-Income Countries: 2-Year Outcomes and Lessons Learnt." *Journal of Pediatric Orthopaedics B* 21.4 (2012): 361-5. Print.

Oza, A.L., R. Vanderby, and R.S. Lakes. "Creep and Relaxation in Ligament: Theory, Methods, and Experiment." *Mechanics of Biological Tissue*. Eds. Holzapfel, G.A. and R.W. Ogden. Berlin: Springer, 2006. 379-97. Print.

Parker, S.E., et al. "Multistate Study of the Epidemiology of Clubfoot." *Birth Defects Research Part A: Clinical and Molecular Teratology* 85.11 (2009): 897-904. Print.

Philbin, T.M., and M.E. Gittins. "Hybrid Casts: A Comparison of Different Casting Materials." *Journal of the American Osteopathic Association* 99.6 (1999): 311-2. Print.

Pittner, D.E., et al. "Treatment of Clubfoot with the Ponseti Method: A Comparison of Casting Materials." *Journal of Pediatric Orthopedics* 28.2 (2008): 250-3. Print.

"Ponseti International". *What is Clubfoot? - clubfoot facts and information*. 11/29/15 2015. <http://www.ponseti.info/what-is-clubfoot.html>.

Ponseti, I.V. "Clubfoot Management." *Journal of Pediatric Orthopedics* 20.6 (2000): 699-700. Print.

Ponseti, I.V "Relapsing Clubfoot: Causes, Prevention, and Treatment." *Iowa Orthopaedic Journal* 22 (2002): 55-6. Print.

Ponseti, I.V., and J. Campos. "Observations on Pathogenesis and Treatment of Congenital Clubfoot." *Clinical Orthopaedics and Related Research* 84 (1972): 50-60. Print.

Ponseti, I.V., and J.A. Morcuende. "Current Management of Idiopathic Clubfoot Questionnaire: A Multicenter Study." *Journal of Pediatric Orthopedics* 24.4 (2004): 448. Print.

Purslow, P.P., T.J. Wess, and D.W. Hukins. "Collagen Orientation and Molecular Spacing During Creep and Stress-Relaxation in Soft Connective Tissues." *Journal of Experimental Biology* 201.Pt 1 (1998): 135-42. Print.

Radler, C., et al. "Radiographic Evaluation of Idiopathic Clubfeet Undergoing Ponseti Treatment." *Journal of Bone and Joint Surgery – American Volume* 89.6 (2007): 1177-83. Print.

Richards, B.S., et al. "A Comparison of Two Nonoperative Methods of Idiopathic Clubfoot Correction: The Ponseti Method and the French Functional (Physiotherapy) Method *Journal of Bone and Joint Surgery – American Volume* 90.11 (2008): 2313-21. Print.

Rowley, D.I., et al. "The Comparative Properties of Plaster of Paris and Plaster of Paris Substitutes." *Archives of Orthopaedic and Trauma Surgery* 103.6 (1985): 402-07. Print.

Roye, B.D., J. Hyman, and D.P. Roye, Jr. "Congenital Idiopathic Talipes Equinovarus." *Pediatrics in Review* 25.4 (2004): 124-30. Print.

Roye, D.P., Jr., and B.D. Roye. "Idiopathic Congenital Talipes Equinovarus." *Journal of the American Academy of Orthopaedic Surgeons* 10.4 (2002): 239-48. Print.

Sano, H., et al. "Pathogenesis of Soft-Tissue Contracture in Club Foot." *Journal of Bone and Joint Surgery –British Volume* 80.4 (1998): 641-4. Print.

Schechtman, H., and D.L. Bader. "In Vitro Fatigue of Human Tendons." *Journal of Biomechanics* 30.8 (1997): 829-35. Print.

Scher, D.M. "Predicting the Need for Tenotomy in the Ponseti Method for Correction of Clubfeet." *Journal of Pediatric Orthopaedics July/August* 24.4 (2004): 349-52. Print.

Schmidt, V.E., J.H. Somerset, and R.E. Porter. "Mechanical Properties of Orthopedic Plaster Bandages." *Journal of Biomechanics* 6.2 (1973): 173-76, IN5, 77-85. Print.

Selected Pediatric Conditions. OrthopaedicsOne Clerkship. In: OrthopaedicsOne - The Orthopaedic Knowledge Network. Created Nov 27, 2010 17:46. Last modified Jan 05, 2011 13:26 ver.11. Retrieved 2015-12-02, from http://www.orthopaedicsone.com/x/JQbMAg.

Shabtai, L., S.C. Specht, and J.E. Herzenberg. "Worldwide Spread of the Ponseti Method for Clubfoot." *World Journal of Orthopaedics* 5.5 (2014): 585-90. Print.

Smith, B.A., G.A. Livesay, and S.L. Woo. "Biology and Biomechanics of the Anterior Cruciate Ligament." *Clinics in Sports Medicine* 12.4 (1993): 637-70. Print.

Smith, P.A., et al. "Long-Term Results of Comprehensive Clubfoot Release Versus the Ponseti Method: Which Is Better?" *Clinical Orthopaedics and Related Research* (2013). Print.

Tanaka, E., and T. van Eijden. "Biomechanical Behavior of the Temporomandibular Joint Disc." *Critical Reviews in Oral Biology & Medicine* 14.2 (2003): 138-50. Print.

Terrazas-Lafargue, G., et al. "Effect of Cast Removal Timing in the Correction of Idiopathic Clubfoot by the Ponseti Method." *Iowa Orthopaedic Journal* 27 (2007): 24-7. Print.

Thornton, G.M., et al. "Ligament Creep Cannot Be Predicted from Stress Relaxation at Low Stress: A Biomechanical Study of the Rabbit Medial Collateral Ligament." *Journal of Orthopaedic Research* 15.5 (1997): 652-6. Print.

Thornton, G.M., N.G. Shrive, and C.B. Frank. "Altering Ligament Water Content Affects Ligament Pre-Stress and Creep Behaviour." *Journal of Orthopaedic Research* 19.5 (2001): 845-51. Print.

Toms, S.R., et al. "Quasi-Linear Viscoelastic Behavior of the Human Periodontal Ligament." *Journal of Biomechanics* 35.10 (2002): 1411-5. Print.

Turco, V.J. "Surgical Correction of the Resistant Club Foot. One-Stage Posteromedial Release with Internal Fixation: A Preliminary Report." *Journal of Bone and Joint Surgery – American Volume* 53.3 (1971): 477-97. Print.

Wallander, H.M. "Congenital Clubfoot. Aspects on Epidemiology, Residual Deformity and Patient Reported Outcome." *Acta Orthopaedica Supplementum* 81.339 (2010): 1-25. Print.

Wang, J.H., Q. Guo, and B. Li. "Tendon Biomechanics and Mechanobiology--a Minireview of Basic Concepts and Recent Advancements." *Journal of Hand Therapy* 25.2 (2012): 133-40; quiz 41. Print.

Weiss, J.A., and L.E. Paulos. "Mechanical Testing of Ligament Fixation Devices." *Techniques in Orthopaedics* 14.1 (1999): 14-21. Print.

Wills, D.J., D.C.A. Picton, and W.I.R. Davies. "An Investigation of the Viscoelastic Properties of the Periodontium in Monkeys." *Journal of Periodontal Research* 7.1 (1972): 42-51. Print.

Windisch, G., et al. "Anatomical Study for an Updated Comprehension of Clubfoot. Part Ii: Ligaments, Tendons and Muscles." *Journal of Children's Orthopaedics* 1.1 (2007): 79-85. Print.

Winkelstein, B.A. *Orthopaedic Biomechanics*. Boca Raton, FL: CRC Press, 2013. Print.

Woo, S.L., G.A. Johnson, and B.A. Smith. "Mathematical Modeling of Ligaments and Tendons." *Journal of Biomechanical Engineering* 115.4B (1993): 468-73. Print.

Woo, S.L., Lee T.Q., Abramowitch, S.D., Gilbert, T.W. "Structure and Function of Ligaments and Tendons." *Basic Orthopaedic Biomechanics & Mechano-Biology*. Ed. Mow, V.C., Huiskes, R. 3rd Ed. ed. Philadelphia, PA: Lippincott Williams & Wilkins, 2005. 301-42. Print.

Woo, S.L., et al. "Temperature Dependent Behavior of the Canine Medial Collateral Ligament." *Journal of Biomechanical Engineering* 109.1 (1987): 68-71. Print.

Woo, S.L., K.J. Ohland, and J.A. Weiss. "Aging and Sex-Related Changes in the Biomechanical Properties of the Rabbit Medial Collateral Ligament." *Mechanisms in Ageing and Development* 56.2 (1990): 129-42. Print.

Woo, S.L., et al. "Tensile Properties of the Medial Collateral Ligament as a Function of Age." *Journal of Orthopaedic Research* 4.2 (1986): 133-41. Print.

Woo, S.L., et al. "The Effects of Strain Rate on the Properties of the Medial Collateral Ligament in Skeletally Immature and Mature Rabbits: A Biomechanical and Histological Study." *Journal of Orthopaedic Research* 8.5 (1990): 712-21. Print.

Zhang, T.X., et al. "Genome-Wide Association Study Identifies New Disease Loci for Isolated Clubfoot." *Journal of Medical Genetics* 51.5 (2014): 334-9. Print.

Zionts, L.E., et al. "Has the Rate of Extensive Surgery to Treat Idiopathic Clubfoot Declined in the United States?" *Journal of Bone & Joint Surgery - American Volume* 92.4 (2010): 882-9. Print.

Zmurko, M.G., S.M. Belkoff, and J.E. Herzenberg. "Mechanical Evaluation of a Soft Cast Material." *Orthopedics* 20.8 (1997): 693-8. Print.

APPENDIX A: MFMT TESTING AND MODELING OUTPUTS

Table A-1: Patient/specimen demographics. Age (months), affected side (left (L)/right(R)), bilateral (B)/unilateral (U), gender (male (M)/female (F)), height (mm), weight (kg), idiopathic (yes (Y)/no (N)), Dimèglio severity score (1-4), previous treatment (none, casting, Ponseti method (with percutaneous Achilles tenotomy), surgery).

Sp	Age (mths)	Side (L/R)	B/U	Gender (M/F)	Height (mm)	Weight (kg)*	Idiop	Severity	Treatment
S1	83	L	B	M	1230.88	22	Y	3	Casting/Surgery
S3	51	L	U	F	1143.00	20.6	Y	4	Ponseti/Surgery
S6	72	R	B	M	1310.64	26	Y	3	Casting/Surgery
S7	84	L	B	M	1219.20	25	Y	3	Casting/Surgery
S8	36	R	U	M	962.00	17.2	N[a]	2	Ponseti/Surgery
C1	12	R	B	M	NA	8	N[b]	4	Ponseti
C2B	NA	NA	NA	NA	NA	NA	NA	NA	NA
C3	38	L	U	M	NA	13	Y	3	Casting
C4.1	48	R	U	F	NA	12	N[c]	4	Casting
C4.2	48	R	U	F	NA	12	N[c]	4	Casting
C6	31	L	B	M	NA	11.4	Y	3	Ponseti
C7.2	19	R	B	M	NA	11.3	N[d]	3	Ponseti
C8R	NA	NA	NA	NA	NA	NA	NA	NA	NA
C9	19	R	B	M	NA	9	N[e]	4	Ponseti
C11	60	L	B	M	NA	10	N[f]	4	None
C12	19	L	U	M	NA	7.8	N[g]	2 OR 3	Ponseti
C13	14	L	B	F	NA	9	Y	3	Ponseti
C15	31	L	B	M	NA	13	Y	3	Ponseti

*Weight only reported by Shriner's Hospitals for Children – Chicago.

[a]Myelomeningocele and Neuromuscular Clubfoot

[b]Bilateral Arthrogypotic Clubfoot with absent toenail plates

[c]Same patient, Right Arthrogypotic Clubfoot, Hand Congenital Band Syndrome

[d]Moebius Syndrome, Hand Congenital Band Syndrome

[e]Bilateral Arthrogypotic Clubfoot

[f]Bilateral Arthrogypotic Clubfoot

[g]Left Idiopathic Clubfoot, Preacial Hand Polydactyl

Table A-2: Preconditioning strain rates. Median preconditioning strain rate for each specimen undergoing preconditioning

Specimen #	Displacement Rate (mm/s)	Strain Rate (mm/mm/s)	% Strain Rate
C11	0.164516	0.017671	1.767086
C12	0.15621	0.020235	2.023452
C15	0.161999	0.021428	2.142841
C3	0.162679	0.023871	2.387077
C4.1	0.163188	0.01678	1.678022
C6	0.160348	0.017122	1.7122
C7.2	0.147483	0.017101	1.710141
C8R	0.160459	0.019881	1.988096
C9	0.157908	0.028868	2.886796
S1	0.16146	0.022866	2.28664
S3	0.163069	0.020407	2.040662
S7	0.15975	0.027187	2.718693
S8	0.16221	0.017021	1.702099
Median	**0.16146**	**0.020235**	**2.023452**
Min	**0.147483**	**0.01678**	**1.678022**
Max	**0.164516**	**0.028868**	**2.886796**

Table A-3: Preconditioning areas of hysteresis. Areas of hysteresis for 13 specimens undergoing 20 preconditioning cycles. A) Values represent areas (Nmm) calculated from the force-displacement preconditioning data. B) Values represent areas (MPa) calculated from stress-strain preconditioning data.

A	Specimen												
Cycles	C11	C12	C15	C3	C4.1	C6	C7.2	C8R	C9	S1	S3	S7	S8
1	2.80E-01	1.94E-01	1.08E-01	4.98E-01	2.56E-01	2.22E-01	2.99E-02	2.20E-01	8.34E-02	6.11E-01	2.73E-01	1.05E-01	2.13E-01
2	1.17E-01	7.81E-02	6.32E-02	1.50E-01	1.00E-01	7.18E-02	1.03E-02	8.45E-02	5.59E-02	8.90E-02	6.58E-02	5.74E-02	7.91E-02
3	9.09E-02	1.20E-01	5.33E-02	1.35E-01	7.84E-02	5.03E-02	4.26E-03	7.27E-02	4.21E-02	7.52E-02	5.51E-02	4.06E-02	5.31E-02
4	7.47E-02	5.20E-02	4.40E-02	1.24E-01	6.83E-02	4.48E-02	3.54E-03	8.24E-02	3.87E-02	6.26E-02	3.38E-02	3.29E-02	4.95E-02
5	7.89E-02	3.26E-02	4.50E-02	1.21E-01	6.77E-02	3.50E-02	1.56E-03	6.17E-02	3.69E-02	4.03E-02	4.09E-02	2.92E-02	4.53E-02
6	5.98E-02	3.40E-02	3.69E-02	1.73E-01	5.67E-02	3.94E-02	2.72E-03	6.36E-02	3.69E-02	3.88E-02	2.68E-02	2.81E-02	4.44E-02
7	6.41E-02	3.26E-02	3.13E-02	1.51E-01	5.15E-02	2.68E-02	1.13E-03	6.01E-02	2.56E-02	4.39E-02	3.81E-02	2.83E-02	4.49E-02
8	5.86E-02	2.98E-02	3.35E-02	1.20E-01	5.55E-02	2.71E-02	-2.37E-03	5.81E-02	3.20E-02	4.03E-02	2.19E-02	2.51E-02	3.88E-02
9	5.89E-02	2.39E-02	3.05E-02	8.81E-02	5.21E-02	3.65E-02	8.14E-04	4.19E-02	2.61E-02	2.81E-02	3.05E-02	2.19E-02	4.75E-02
10	5.46E-02	2.21E-02	2.97E-02	8.87E-02	5.55E-02	3.21E-02	-3.02E-04	5.15E-02	2.72E-02	2.96E-02	2.66E-02	2.71E-02	4.43E-02
11	5.47E-02	1.74E-02	2.95E-02	8.42E-02	5.12E-02	2.03E-02	-1.06E-03	3.48E-02	3.09E-02	4.18E-02	3.12E-02	2.45E-02	4.24E-02
12	4.37E-02	2.20E-02	3.33E-02	8.27E-02	4.27E-02	2.20E-02	-1.72E-03	2.56E-02	2.59E-02	2.28E-02	2.05E-02	2.67E-02	4.25E-02
13	5.22E-02	1.49E-02	2.66E-02	7.68E-02	5.30E-02	2.37E-02	-1.67E-03	3.03E-02	2.30E-02	3.06E-02	2.80E-02	2.22E-02	4.32E-02
14	5.16E-02	2.16E-02	2.55E-02	7.06E-02	4.49E-02	2.89E-02	-2.52E-04	3.09E-02	2.58E-02	1.61E-02	2.72E-02	3.29E-02	4.38E-02
15	3.64E-02	2.46E-02	2.74E-02	6.22E-02	4.30E-02	1.35E-02	-2.35E-03	2.04E-02	2.11E-02	2.83E-02	2.48E-02	2.44E-02	4.91E-02
16	5.32E-02	5.96E-03	2.83E-02	5.56E-02	4.77E-02	2.14E-02	-2.08E-03	2.09E-02	2.54E-02	2.76E-02	2.25E-02	2.93E-02	3.23E-02
17	4.84E-02	1.67E-02	2.20E-02	6.47E-02	4.54E-02	2.04E-02	-3.50E-03	1.96E-02	2.02E-02	1.40E-02	1.93E-02	2.50E-02	3.67E-02
18	4.20E-02	1.61E-02	2.07E-02	6.42E-02	5.04E-02	1.99E-02	-2.43E-03	2.40E-02	2.44E-02	3.41E-02	2.93E-02	3.06E-02	4.13E-02
19	4.38E-02	2.09E-02	2.32E-02	4.71E-02	3.80E-02	2.58E-02	-1.66E-03	1.71E-02	1.90E-02	1.72E-02	2.14E-02	2.08E-02	4.35E-02
20	4.61E-02	1.60E-02	1.95E-02	6.61E-02	4.41E-02	1.64E-02	-2.89E-03	1.98E-02	2.35E-02	4.16E-02	2.95E-02	2.51E-02	2.38E-02
mean	7.05E-02	3.98E-02	3.66E-02	1.16E-01	6.51E-02	3.99E-02	1.60E-03	5.20E-02	3.22E-02	6.66E-02	4.33E-02	3.29E-02	5.29E-02
std	5.29E-02	4.47E-02	2.02E-02	9.69E-02	4.72E-02	4.49E-02	7.41E-03	4.54E-02	1.50E-02	1.29E-01	5.53E-02	1.89E-02	3.91E-02
me	5.46E-02	2.30E-02	3.01E-02	8.61E-02	5.18E-02	2.69E-02	-6.81E-04	3.84E-02	2.60E-02	3.65E-02	2.86E-02	2.76E-02	4.41E-02
max	2.80E-01	1.94E-01	1.08E-01	4.98E-01	2.56E-01	2.22E-01	2.99E-02	2.20E-01	8.34E-02	6.11E-01	2.73E-01	1.05E-01	2.13E-01
min	3.64E-02	5.96E-03	1.95E-02	4.71E-02	3.80E-02	1.35E-02	-3.50E-03	1.71E-02	1.90E-02	1.40E-02	1.93E-02	2.08E-02	2.38E-02
C1-20	2.34E-01	1.78E-01	8.89E-02	4.32E-01	2.12E-01	2.06E-01	3.28E-02	2.01E-01	5.99E-02	5.69E-01	2.44E-01	8.04E-02	1.89E-01
C2-20	7.07E-02	6.21E-02	4.37E-02	8.37E-02	5.60E-02	5.54E-02	1.32E-02	6.47E-02	3.24E-02	4.74E-02	3.63E-02	3.23E-02	5.53E-02

Table A-3: Preconditioning areas of hysteresis. Areas of hysteresis for 13 specimens undergoing 20 preconditioning cycles. A) Values represent areas calculated from the force-displacement preconditioning data. B) Values represent areas calculated from stress-strain preconditioning data.

B	Specimen												
Cycles	C11	C12	C15	C3	C4.1	C6	C7.2	C8R	C9	S1	S3	S7	S8
1	1.10E-02	8.61E-03	2.64E-03	1.02E-02	4.95E-03	4.07E-03	1.02E-03	6.71E-03	3.79E-03	2.51E-02	6.92E-03	8.44E-03	5.20E-03
2	4.60E-03	3.46E-03	1.54E-03	3.07E-03	1.94E-03	1.32E-03	3.50E-04	2.57E-03	2.54E-03	3.66E-03	1.67E-03	4.59E-03	1.93E-03
3	3.58E-03	5.33E-03	1.30E-03	2.78E-03	1.52E-03	9.22E-04	1.45E-04	2.21E-03	1.91E-03	3.09E-03	1.39E-03	3.25E-03	1.30E-03
4	2.94E-03	2.30E-03	1.07E-03	2.54E-03	1.32E-03	8.21E-04	1.20E-04	2.51E-03	1.76E-03	2.57E-03	8.55E-04	2.63E-03	1.21E-03
5	3.10E-03	1.44E-03	1.10E-03	2.48E-03	1.31E-03	6.42E-04	5.30E-05	1.88E-03	1.68E-03	1.66E-03	1.04E-03	2.34E-03	1.10E-03
6	2.35E-03	1.51E-03	8.98E-04	3.56E-03	1.10E-03	7.21E-04	9.24E-05	1.94E-03	1.68E-03	1.60E-03	6.78E-04	2.25E-03	1.08E-03
7	2.52E-03	1.44E-03	7.63E-04	3.09E-03	9.96E-04	4.90E-04	3.84E-05	1.83E-03	1.16E-03	1.80E-03	9.66E-04	2.26E-03	1.10E-03
8	2.31E-03	1.32E-03	8.16E-04	2.47E-03	1.07E-03	4.96E-04	-8.07E-05	1.77E-03	1.45E-03	1.66E-03	5.55E-04	2.01E-03	9.46E-04
9	2.32E-03	1.06E-03	7.44E-04	1.81E-03	1.01E-03	6.69E-04	2.77E-05	1.28E-03	1.19E-03	1.16E-03	7.72E-04	1.76E-03	1.16E-03
10	2.15E-03	9.80E-04	7.24E-04	1.82E-03	1.07E-03	5.88E-04	-1.03E-05	1.57E-03	1.24E-03	1.22E-03	6.74E-04	2.17E-03	1.08E-03
11	2.15E-03	7.69E-04	7.18E-04	1.73E-03	9.89E-04	3.73E-04	-3.60E-05	1.06E-03	1.40E-03	1.72E-03	7.91E-04	1.96E-03	1.03E-03
12	1.72E-03	9.75E-04	8.10E-04	1.70E-03	8.25E-04	4.02E-04	-5.83E-05	7.79E-04	1.18E-03	9.37E-04	5.18E-04	2.14E-03	1.04E-03
13	2.05E-03	6.62E-04	6.49E-04	1.58E-03	1.02E-03	4.34E-04	-5.69E-05	9.22E-04	1.05E-03	1.26E-03	7.08E-04	1.78E-03	1.05E-03
14	2.03E-03	9.57E-04	6.21E-04	1.45E-03	8.69E-04	5.30E-04	-8.58E-06	9.39E-04	1.17E-03	6.61E-04	6.89E-04	2.63E-03	1.07E-03
15	1.43E-03	1.09E-03	6.68E-04	1.28E-03	8.31E-04	2.47E-04	-7.99E-05	6.20E-04	9.58E-04	1.16E-03	6.29E-04	1.95E-03	1.20E-03
16	2.09E-03	2.64E-04	6.89E-04	1.14E-03	9.22E-04	3.93E-04	-7.06E-05	6.35E-04	1.16E-03	1.13E-03	5.71E-04	2.35E-03	7.87E-04
17	1.90E-03	7.41E-04	5.36E-04	1.33E-03	8.78E-04	3.74E-04	-1.19E-04	5.98E-04	9.20E-04	5.74E-04	4.88E-04	2.00E-03	8.94E-04
18	1.65E-03	7.15E-04	5.04E-04	1.32E-03	9.74E-04	3.64E-04	-8.24E-05	7.30E-04	1.11E-03	1.40E-03	7.42E-04	2.45E-03	1.01E-03
19	1.72E-03	9.24E-04	5.66E-04	9.67E-04	7.35E-04	4.73E-04	-5.63E-05	5.20E-04	8.62E-04	7.06E-04	5.42E-04	1.66E-03	1.06E-03
20	1.81E-03	7.08E-04	4.75E-04	1.36E-03	8.53E-04	3.00E-04	-9.81E-05	6.04E-04	1.07E-03	1.71E-03	7.48E-04	2.01E-03	5.80E-04
mean	2.77E-03	1.76E-03	8.91E-04	2.38E-03	1.26E-03	7.31E-04	5.42E-05	1.58E-03	1.46E-03	2.74E-03	1.10E-03	2.63E-03	1.29E-03
std	2.08E-03	1.98E-03	4.92E-04	1.99E-03	9.13E-04	8.24E-04	2.52E-04	1.38E-03	6.81E-04	5.32E-03	1.40E-03	1.51E-03	9.53E-04
med	2.15E-03	1.02E-03	7.34E-04	1.77E-03	1.00E-03	4.93E-04	-2.31E-05	1.17E-03	1.18E-03	1.50E-03	7.25E-04	2.21E-03	1.07E-03
max	1.10E-02	8.61E-03	2.64E-03	1.02E-02	4.95E-03	4.07E-03	1.02E-03	6.71E-03	3.79E-03	2.51E-02	6.92E-03	8.44E-03	5.20E-03
min	1.43E-03	2.64E-04	4.75E-04	9.67E-04	7.35E-04	2.47E-04	-1.19E-04	5.20E-04	8.62E-04	5.74E-04	4.88E-04	1.66E-03	5.80E-04
C1-20	9.21E-03	7.90E-03	2.17E-03	8.86E-03	4.10E-03	3.77E-03	1.11E-03	6.10E-03	2.72E-03	2.34E-02	6.17E-03	6.43E-03	4.62E-03
C2-20	2.78E-03	2.75E-03	1.06E-03	1.72E-03	1.08E-03	1.02E-03	4.48E-04	1.97E-03	1.47E-03	1.95E-03	9.19E-04	2.58E-03	1.35E-03

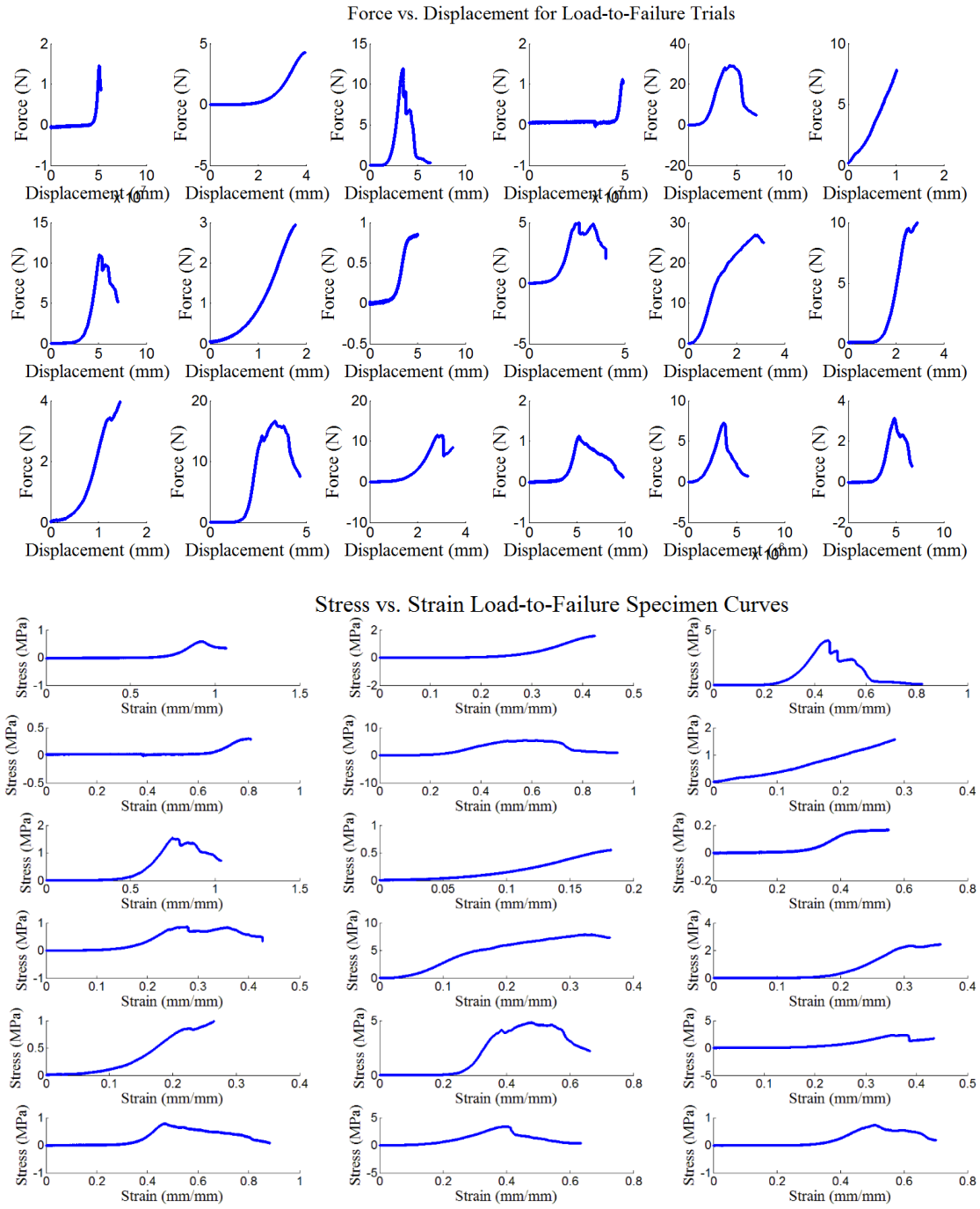

Figure A-1:Load-to-failure curves. A) force vs. displacement, B) stress vs. strain

Table A-4: Stress relaxation strain rates. Median (min/max) and per-trial stress-relaxation strain rate for each specimen undergoing stress-relaxation

Specimen #	Strain Rate (mm/mm/s)	% Strain Rate	Median strain rate for each individual trial (%/s)										
C1	0.01841	1.841022	1.84	1.84	1.84	1.84							
C11	0.017825	1.782509	1.77	1.78	1.78	1.78							
C12	0.021507	2.150682	2.125	2.15	2.15	2.15	2.155	2.15	2.15	2.15	2.155	2.15	
C15	0.021968	2.196839	2.19	2.20	2.20	2.19	2.20	2.20	2.20	2.20			
C3	0.024397	2.439658	2.41	2.43	2.44	2.43	2.45	2.45	2.44	2.44	2.43	2.43	
C4.1	0.017032	1.703246	1.70	2.70	1.71								
C4.2	0.018353	1.835251	1.83	1.835									
C6	0.01773	1.773026	1.76	1.76	1.77	1.77	1.78	1.78	1.79	1.78	1.77		
C7.2	0.019252	1.925184	1.88	1.92	1.92	1.93	1.93	1.93	1.92	1.93	1.92	1.925	
C8R	0.020588	2.05877	2.045	2.05	2.06	2.06	2.06	2.06	2.06	2.06	2.06	2.06	
C9	0.030054	3.005356	2.99	3.02									
S1	0.023545	2.354549	2.32	2.35	2.36	2.36	2.35	2.35	2.36	2.35	2.35	2.35	2.355
S3	0.020816	2.081594	2.08	2.08	2.08	2.08	2.08	2.08	2.08	2.08	2.08	2.08	
S6	0.014832	1.483212	1.49	1.48	1.48								
S7	0.028178	2.817752	2.81	2.81	2.81	2.82	2.81	2.82	2.84	2.84			
S8	0.017437	1.743716	1.74	1.75	1.74	1.74	1.74	1.74					
Median	**0.01992**	**1.991977**											
Min	**0.014832**	**1.483212**											
Max	**0.030054**	**3.005356**											

Table A-5: Stress Relaxation Outcomes. Percent relaxation, 80% of relaxation, and corresponding time (s) for each trial, as well as mean and standard deviation. *Outliers based on 3std.

Specimen	Time (s)	% Relaxation	Time (s) to 80% of Relaxation	80% of Relaxation
C1	181.68*	62.38*	54.63	0.70
C1	99.96	64.55	29.59	0.72
C1	99.95	63.02	29.78	0.71
C1	99.96	53.69	26.32	0.63
C11	99.95	75.41	27.63	0.81
C11	99.98	64.07	23.24	0.71
C11	100.00	59.51	19.98	0.68
C11	174.60*	49.33*	22.98	0.59
C12	99.95	71.53	39.08	0.77
C12	99.98	57.16	25.97	0.66
C12	99.96	60.36	26.63	0.68
C12	99.97	64.37	25.24	0.72
C12	99.97	66.88	26.09	0.74
C12	99.97	69.75	28.63	0.76
C12	99.97	71.58	24.38	0.77
C12	99.98	68.64	22.04	0.75
C12	99.98	68.93	22.25	0.75
C12	99.97	71.40	24.69	0.77
C15	99.95	78.29	42.22	0.83
C15	99.95	74.43	37.82	0.80
C15	99.96	74.19	37.28	0.79
C15	99.96	73.79	32.50	0.79
C15	99.97	77.40	33.61	0.82
C15	99.96	79.45	32.01	0.84
C15	99.97	79.62	32.11	0.84
C15	99.96	80.16	32.87	0.84
C3	99.95	79.31	46.30	0.83
C3	99.95	72.96	38.19	0.78
C3	99.96	73.76	38.43	0.79
C3	98.71	74.71	36.54	0.80
C3	99.96	73.71	37.85	0.79
C3	99.97	74.22	36.47	0.79
C3	99.96	74.40	36.71	0.80
C3	99.97	72.65	32.19	0.78
C3	99.97	70.42	27.02	0.76
C3	99.98	72.66	26.45	0.78
C4.1	99.95	83.36	44.37	0.87

C4.1	99.95	74.49	26.76	0.80
C4.1	7.30*	53.92*	4.12*	0.63*
C4.2	100.01	50.76	22.80	0.61
C4.2	133.06	47.90	27.56	0.58
C6	99.96	76.40	49.27	0.81
C6	99.96	69.36	34.30	0.76
C6	99.98	68.56	32.37	0.75
C6	99.96	68.52	32.50	0.75
C6	99.96	69.70	32.18	0.76
C6	99.97	70.50	32.74	0.76
C6	99.96	71.33	32.73	0.77
C6	99.97	68.69	44.57	0.75
C6*	99.97	55.64	85.97*	0.65*
C7.2	99.96	77.38	38.82	0.82
C7.2	99.96	72.73	31.96	0.78
C7.2	99.97	74.23	31.71	0.79
C7.2	99.96	74.39	32.55	0.80
C7.2	99.97	75.22	27.06	0.80
C7.2	99.96	76.01	30.97	0.81
C7.2	99.96	77.45	29.83	0.82
C7.2	99.96	77.29	29.40	0.82
C7.2	99.99	75.69	28.18	0.81
C7.2	99.96	76.71	31.26	0.81
C8R	99.94	75.18	36.71	0.80
C8R	100.02	67.69	30.35	0.74
C8R	99.97	62.41	28.78	0.70
C8R	99.97	67.18	32.17	0.74
C8R	99.97	71.01	31.93	0.77
C8R	99.97	73.26	23.26	0.79
C8R	99.96	75.64	30.26	0.81
C8R	99.97	72.86	25.23	0.78
C8R	99.97	70.59	25.47	0.76
C8R	99.97	70.32	24.69	0.76
C9	99.96	75.50	39.28	0.81
C9	99.98	63.13	25.07	0.71
S1	99.97	71.02	47.09	0.77
S1	99.98	65.71	23.89	0.73
S1	99.95	66.51	24.96	0.73
S1	99.96	67.07	20.92	0.74
S1	99.96	69.01	23.55	0.75
S1	99.97	68.51	21.86	0.75

S1	99.97	64.98	19.83	0.72
S1	99.97	67.57	24.64	0.74
S1	99.97	61.56	27.09	0.69
S1	99.97	64.89	25.87	0.72
S1	99.97	67.46	30.08	0.74
S3	99.95	84.02	48.58	0.87
S3	99.95	78.51	33.15	0.83
S3	99.94	77.92	32.21	0.82
S3	99.96	76.26	30.87	0.81
S3	99.94	74.73	29.92	0.80
S3	99.95	75.02	30.02	0.80
S3	99.96	75.81	29.25	0.81
S3	99.97	73.95	28.21	0.79
S3	99.98	71.24	29.47	0.77
S3	99.97	75.00	27.79	0.80
S6	3.56*	85.06*	2.65*	0.88*
S6	99.96	64.97	35.40	0.72
S6	99.98	59.40	30.67	0.68
S7	99.96	82.10	45.65	0.86
S7	99.96	74.93	32.25	0.80
S7	99.95	74.82	30.98	0.80
S7	99.95	75.93	33.70	0.81
S7	99.96	76.56	31.96	0.81
S7	99.96	75.70	28.24	0.81
S7	99.96	77.21	30.55	0.82
S7	99.98	75.65	31.92	0.81
S8	99.94	81.08	42.04	0.85
S8	99.96	42.61	4.42*	0.54*
S8	99.99	63.59	35.41	0.71
S8	219.65*	46.07*	30.62	0.57
S8	193.42*	70.96*	52.55	0.77
S8	99.96	74.24	36.55	0.80
Mean	100.27	70.96	31.61	0.77
Std.	3.25	7.25	7.04	0.06

Table A-6: Parametric statistics of parameters predicted using the strain history approach. Mean and standard deviation (mean (std)) values of parameters from Eqs. 5 and 6, and corresponding goodness of fit measure R^2.

Sample	A	B	G_1	λ_1	G_2	λ_2	G_3	λ_3	R^2
C1	0.0002	10.0238	1.5067	0.0019	1.8894	0.3422	-0.8021	8.9221	0.9744
	(0.0003)	(1.9789)	(0.1709)	(0.0008)	(0.3744)	(0.1183)	(0.2339)	(1.0921)	(0.0175)
C11	3.1739	8.0348	1.3930	2.7967	2.8299	0.0179	9.5684	0.9753	0.9129
	(6.3357)	(5.8482)	(6.5156)	(5.5372)	(2.6932)	(0.0311)	(14.9075)	(0.5775)	(0.0871)
C12	0.2917	18.6266	-2.4927	7.2654	18.7085	0.0761	-4.9720	5.7165	0.9818
	(0.8891)	(8.1183)	(10.8591)	(18.4422)	(29.4181)	(0.2346)	(7.3761)	(4.0788)	(0.0111)
C15	5.6072	9.7837	0.2781	2.1029	12.4498	0.0220	9.5491	7.5729	0.9474
	(9.1443)	(8.1226)	(8.3997)	(5.2336)	(21.8975)	(0.0377)	(16.7470)	(6.9798)	(0.1081)
C3	0.1417	7.8500	2.2421	0.0185	4.4144	0.1315	-10.7459	5.7997	0.9903
	(0.4343)	(1.9720)	(1.2283)	(0.0401)	(8.7216)	(0.2267)	(23.3556)	(2.1833)	(0.0058)
C4.1	5.8112	6.7734	8.1677	1.3558	1.6734	0.0008	-14.1710	7.3846	0.9842
	(5.9104)	(11.1737)	(9.0430)	(2.0155)	(2.8535)	(0.0019)	(46.8812)	(10.6001)	(0.0089)
C4.2	0.0023	9.9286	2.6021	0.0886	-1.0982	0.5005	-5.6554	4.1740	0.8667
	(0.0025)	(4.3066)	(3.2064)	(0.1220)	(2.8130)	(0.7049)	(14.0010)	(5.9072)	(0.1446)
C6	10.6132	8.0677	3.3118	1.8011	12.9190	0.0595	21.3831	5.7235	0.9694
	(11.9643)	(9.4814)	(7.2072)	(4.6379)	(27.7566)	(0.1473)	(21.8929)	(5.1444)	(0.0272)
C7.2	17.9533	9.2096	16.5375	0.3914	-0.6469	0.0012	18.3126	79.9924	0.9833
	(12.7888)	(28.6850)	(32.9840)	(0.3306)	(1.6811)	(0.0003)	(12.1870)	(250.8160)	(0.0036)
C8R	8.0842	11.7284	-3.8514	13.3959	18.0939	0.0141	3.9788	5.5407	0.9115
	(16.3781)	(8.6509)	(9.7750)	(29.9334)	(19.6619)	(0.0386)	(8.0810)	(4.9741)	(0.1762)
C9	0.9020	5.7386	1.7916	0.1374	1.3567	0.0005	1.4085	0.0976	0.9431
	(1.2551)	(4.2709)	(0.1258)	(0.0862)	(2.6148)	(0.0009)	(0.6719)	(0.1542)	(0.0708)
S1	7.1288	20.1780	-2.2541	8.5464	17.8820	0.0023	2.7807	5.5549	0.9657
	(22.6606)	(6.8815)	(5.1336)	(11.7213)	(10.6697)	(0.0006)	(18.8552)	(4.0181)	(0.0397)
S3	9.1321	8.6264	-2.0246	9.3131	11.1942	0.0215	1.7012	3.2925	0.9767
	(14.3481)	(7.1637)	(9.0941)	(21.4580)	(15.1670)	(0.0640)	(10.1664)	(2.9094)	(0.0150)
S6	0.5946	11.6763	3.9057	-0.0017	2.0101	2.2406	-0.5979	17.9110	0.9121
	(1.0284)	(10.2052)	(2.7041)	(0.0028)	(1.1968)	(3.8296)	(3.3889)	(19.3552)	(0.1345)
S7	23.6442	3.0207	1.7517	0.4636	0.6983	0.0011	14.1633	3.5921	0.9833
	(19.3812)	(4.8064)	(1.0014)	(0.2509)	(2.0405)	(0.0003)	(13.0860)	(5.7493)	(0.0067)
S8	10.0987	8.9550	4.4586	0.3207	7.1517	0.0009	-0.6397	4.2681	0.9469
	(19.3124)	(7.0725)	(7.5469)	(0.3604)	(15.4407)	(0.0007)	(14.9043)	(4.6828)	(0.0507)

APPENDIX B: ANALYTICAL INTEGRATION OF QUASI-LINEAR VISCOELASTIC MODEL

$$\sigma(t)$$

$$= \int_{-t}^{t} \bar{G}(t-\tau)\frac{\partial \sigma^e(\varepsilon)}{\partial \varepsilon}\frac{\partial \varepsilon}{\partial \tau}\partial\tau \tag{B.1}$$

$$\overline{G}(t) = G_1 e^{-\boldsymbol{\lambda}_1 t} + G_2 e^{-\boldsymbol{\lambda}_2 t} + G_5 e^{-\boldsymbol{\lambda}_3 t} \tag{B.2}$$

$$\sigma^e(\varepsilon) = A(e^{B\varepsilon} - 1) \tag{B.3}$$

$$\frac{\partial \sigma^e(\varepsilon)}{\partial \varepsilon} = ABe^{B\varepsilon} \tag{B.4}$$

$$0 \le t \le t_0 \colon \frac{\partial \varepsilon}{\partial \tau} = \gamma \tag{B.5}$$

$$t > t_0 \colon \frac{\partial \varepsilon}{\partial \tau} = 0 \tag{B.6}$$

$$\sigma(0 \le t \le t_0) = AB\gamma \int_0^t \{G_1 e^{-\boldsymbol{\lambda}_1(t-\tau)} + G_2 e^{-\boldsymbol{\lambda}_2(t-\tau)} + G_3 e^{-\boldsymbol{\lambda}_3(t-\tau)}\} e^{B\gamma\tau}\, \partial\tau \tag{B.7}$$

$$= AB\gamma \left[\frac{G_1 e^{-\boldsymbol{\lambda}_1 t} e^{(\boldsymbol{\lambda}_1 + B\gamma)\tau}}{\boldsymbol{\lambda}_1 + B\gamma} + \frac{G_2 e^{-\boldsymbol{\lambda}_2 t} e^{(\boldsymbol{\lambda}_2 + B\gamma)\tau}}{\boldsymbol{\lambda}_2 + B\gamma} + \frac{G_3 e^{-\boldsymbol{\lambda}_3 t} e^{(\boldsymbol{\lambda}_3 + B\gamma)\tau}}{\boldsymbol{\lambda}_3 + B\gamma}\right]_0^t \tag{B.8}$$

$$= AB\gamma \left[\frac{G_1 e^{-\boldsymbol{\lambda}_1 t} e^{(\boldsymbol{\lambda}_1 + B\gamma)t}}{\boldsymbol{\lambda}_1 + B\gamma} + \frac{G_2 e^{-\boldsymbol{\lambda}_2 t} e^{(\boldsymbol{\lambda}_2 + B\gamma)t}}{\boldsymbol{\lambda}_2 + B\gamma} + \frac{G_3 e^{-\boldsymbol{\lambda}_3 t} e^{(\boldsymbol{\lambda}_3 + B\gamma)t}}{\boldsymbol{\lambda}_3 + B\gamma}\right] - AB\gamma \left[\frac{G_1 e^{-\boldsymbol{\lambda}_1 t}}{\boldsymbol{\lambda}_1 + B\gamma} + \frac{G_2 e^{-\boldsymbol{\lambda}_2 t}}{\boldsymbol{\lambda}_2 + B\gamma} + \frac{G_3 e^{-\boldsymbol{\lambda}_3 t}}{\boldsymbol{\lambda}_3 + B\gamma}\right] \tag{B.9}$$

$$= AB\gamma \left[\frac{G_1 e^{B\gamma t}}{\boldsymbol{\lambda}_1 + B\gamma} + \frac{G_2 e^{B\gamma t}}{\boldsymbol{\lambda}_2 + B\gamma} + \frac{G_3 e^{B\gamma t}}{\boldsymbol{\lambda}_3 + B\gamma}\right] - AB\gamma \left[\frac{G_1 e^{-\boldsymbol{\lambda}_1 t}}{\boldsymbol{\lambda}_1 + B\gamma} + \frac{G_2 e^{-\boldsymbol{\lambda}_2 t}}{\boldsymbol{\lambda}_2 + B\gamma} + \frac{G_3 e^{-\boldsymbol{\lambda}_3 t}}{\boldsymbol{\lambda}_3 + B\gamma}\right] \tag{B.10}$$

$$\sigma(t > t_0) = AB\gamma \int_0^{t_0} \{G_1 e^{-\boldsymbol{\lambda}_1(t-\tau)} + G_2 e^{-\boldsymbol{\lambda}_2(t-\tau)} + G_3 e^{-\boldsymbol{\lambda}_3(t-\tau)}\} e^{B\gamma\tau}\, \partial\tau \tag{B.11}$$

$$= AB\gamma \left[\frac{G_1 e^{-\lambda_1 t} e^{(\lambda_1 + B\gamma)\tau}}{\boldsymbol{\lambda}_1 + B\gamma} + \frac{G_2 e^{-\lambda_2 t} e^{(\lambda_2 + B\gamma)\tau}}{\boldsymbol{\lambda}_2 + B\gamma} \right.$$

$$\left. + \frac{G_3 e^{-\lambda_3 t} e^{(\lambda_3 + B\gamma)\tau}}{\boldsymbol{\lambda}_3 + B\gamma} \right]_0^{t_0} \qquad \text{(B. 12)}$$

$$= AB\gamma \left[\frac{G_1 e^{-\lambda_1 t} e^{(\lambda_1 + B\gamma)t_0}}{\boldsymbol{\lambda}_1 + B\gamma} + \frac{G_2 e^{-\lambda_2 t} e^{(\lambda_2 + B\gamma)t_0}}{\boldsymbol{\lambda}_2 + B\gamma} + \frac{G_3 e^{-\lambda_3 t} e^{(\lambda_3 + B\gamma)t_0}}{\boldsymbol{\lambda}_3 + B\gamma} \right]$$

$$- AB\gamma \left[\frac{G_1 e^{-\lambda_1 t}}{\boldsymbol{\lambda}_1 + B\gamma} + \frac{G_2 e^{-\lambda_2 t}}{\boldsymbol{\lambda}_2 + B\gamma} + \frac{G_3 e^{-\lambda_3 t}}{\boldsymbol{\lambda}_3 + B\gamma} \right] \qquad \text{(B. 13)}$$

APPENDIX C: QLV STATISTICAL EXPLORATION

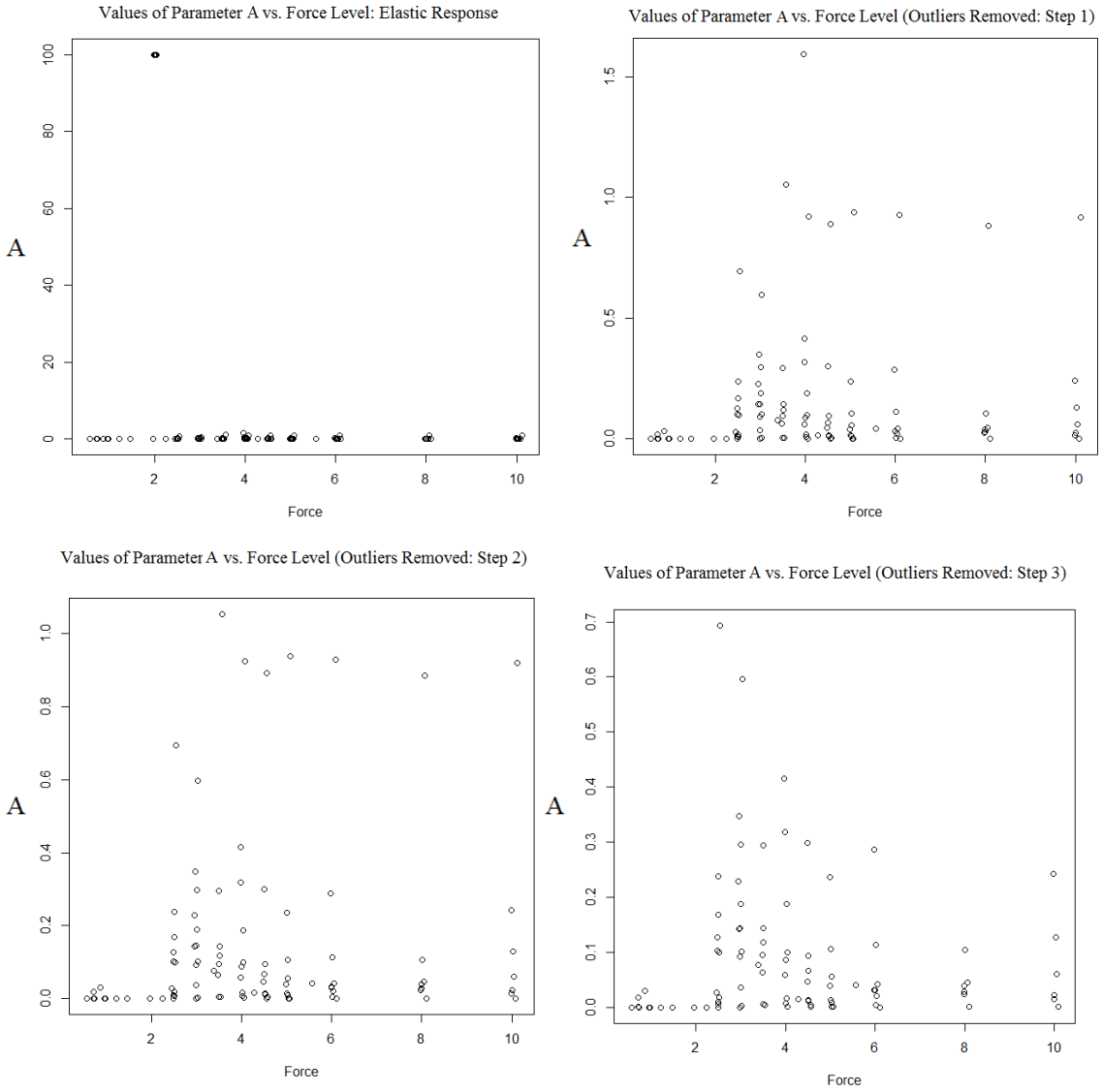

Figure B-1: Values of Parameter *A* vs. Force Level. Values of parameter *A* calculated from the elastic response data fitted with the equation $\sigma^e(\varepsilon) = A(e^{Bt} - 1)$.

```
Formula: b[[o]] ~ b[[v]] + (1 | b$ID)

REML criterion at convergence: -185.3

Scaled residuals:
    Min      1Q  Median      3Q     Max
-1.9089 -0.3937 -0.0642  0.1560  4.2172

Random effects:
 Groups   Name        Variance Std.Dev.
 b$ID     (Intercept) 0.028575 0.16904
 Residual             0.003282 0.05729
Number of obs: 89, groups:  b$ID, 16

Fixed effects:
             Estimate Std. Error t value
(Intercept)  0.1287123  0.0445295   2.890
b[[v]]      -0.0003138  0.0032195  -0.098

Correlation of Fixed Effects:
       (Intr)
b[[v]] -0.263
> 0.028575/(.028575+0.003282)
[1] 0.8969771
refitting model(s) with ML (instead of REML)
Data: NULL
Models:
fit0: b[[o]] ~ 1 + (1 | b$ID)
fit1: b[[o]] ~ b[[v]] + (1 | b$ID)
     Df     AIC     BIC logLik deviance  Chisq Chi Df Pr(>Chisq)
fit0  3 -193.39 -185.93 99.697  -199.39
fit1  4 -191.40 -181.45 99.702  -199.40 0.0097      1     0.9217
```

Figure B-2: Values of Parameter *A* vs. Force Level. R output of linear mixed model and likelihood ratio test.

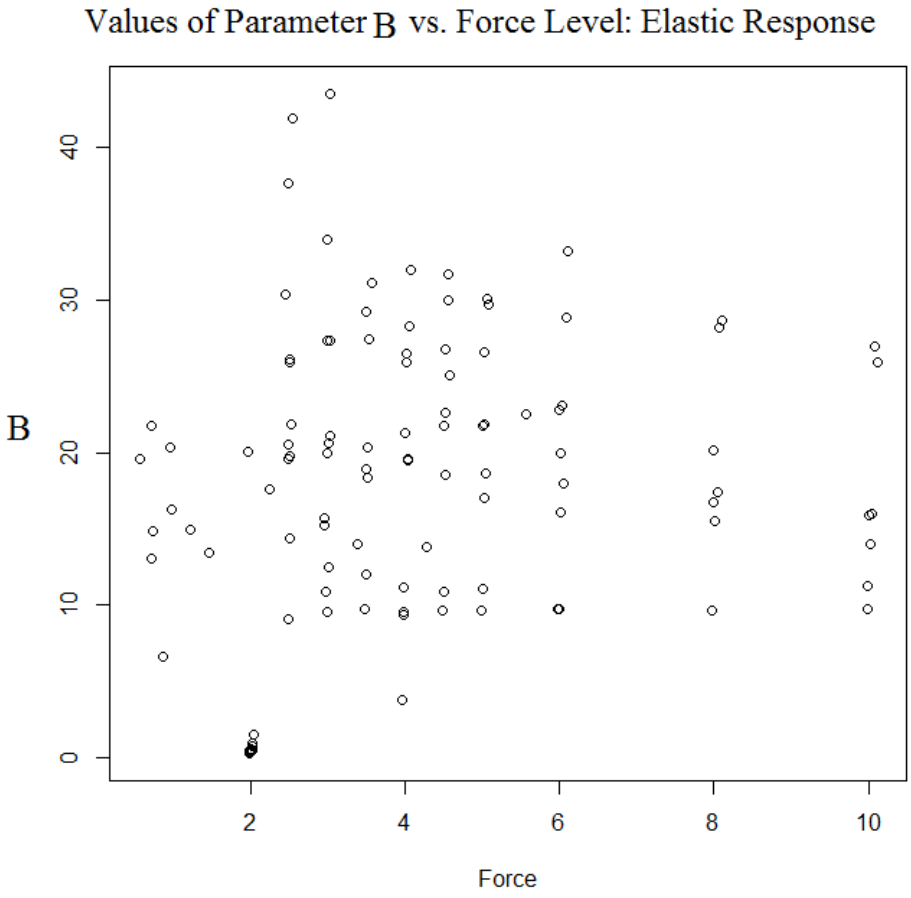

Figure B-3: Values of Parameter *B* vs. Force Level. Values of parameter *B* calculated from the elastic response data fitted with the equation $\sigma^e(\varepsilon) = A(e^{Bt} - 1)$.

```
Linear mixed model fit by REML ['lmerMod']
Formula: a[[o]] ~ a[[v]] + (1 | a$ID)

REML criterion at convergence: 782

Scaled residuals:
    Min      1Q  Median      3Q     Max
-3.2058 -0.2119  0.1207  0.4499  2.1931

Random effects:
 Groups   Name        Variance Std.Dev.
 a$ID     (Intercept) 33.70    5.805
 Residual             60.09    7.752
Number of obs: 110, groups:  a$ID, 16

Fixed effects:
            Estimate Std. Error t value
(Intercept)  14.9441     2.1177   7.057
a[[v]]        0.4175     0.3519   1.186

Correlation of Fixed Effects:
       (Intr)
a[[v]] -0.613
> 33.70/(33.70+60.09)
[1] 0.3593134
refitting model(s) with ML (instead of REML)
Data: NULL
Models:
fit0: a[[o]] ~ 1 + (1 | a$ID)
fit1: a[[o]] ~ a[[v]] + (1 | a$ID)
     Df    AIC    BIC  logLik deviance  Chisq Chi Df Pr(>Chisq)
fit0  3 792.04 800.14 -393.02   786.04
fit1  4 792.59 803.39 -392.30   784.59 1.4491      1     0.2287
```

Figure B-4: Values of Parameter *B* vs. Force Level. R output of linear mixed model and likelihood ratio test.

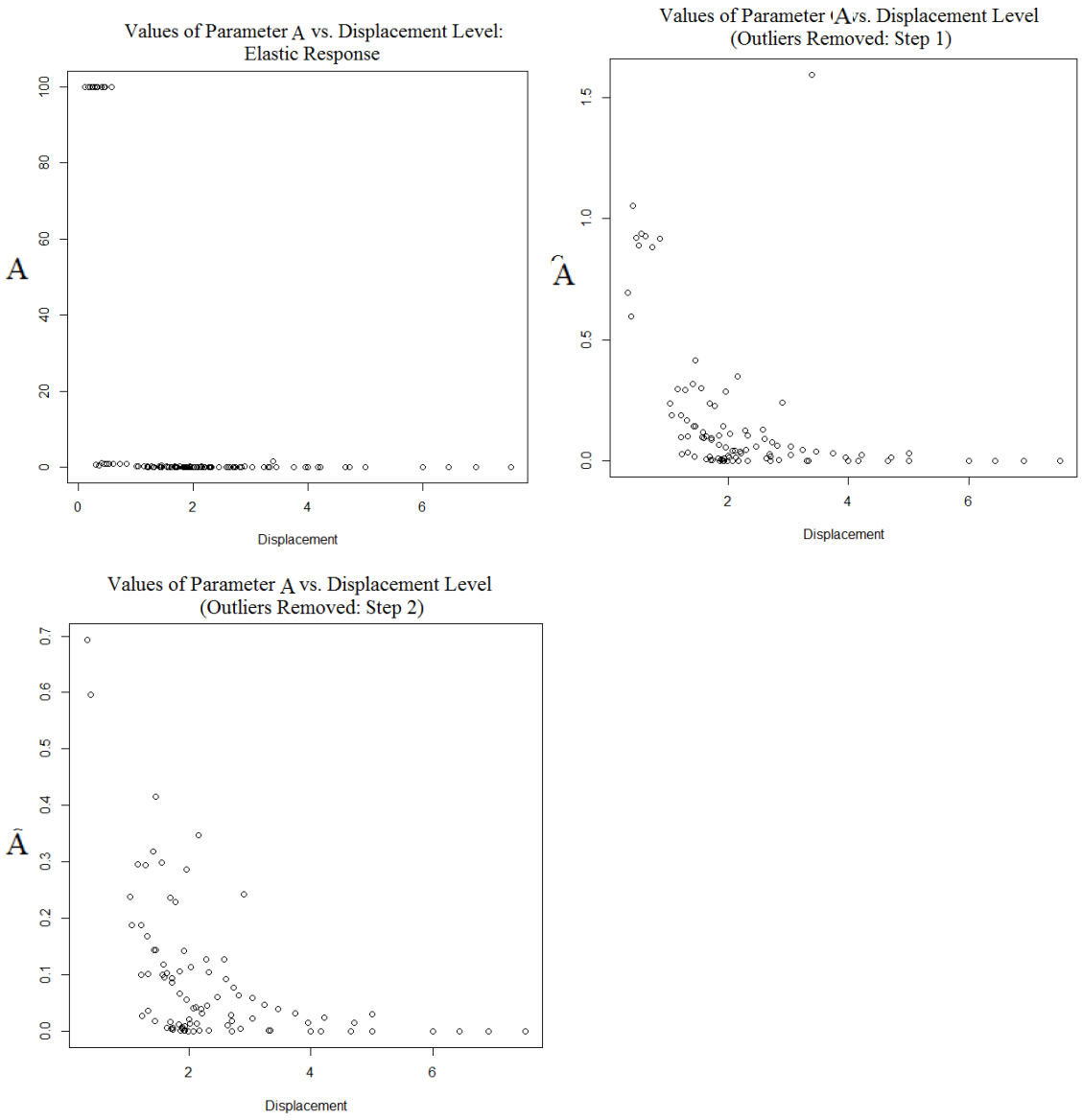

Figure B-5: Values of Parameter *A* vs. Displacement Level. Values of parameter A calculated from the elastic response data fitted with the equation $\sigma^e(\varepsilon) = A(e^{Bt} - 1)$.

```
Linear mixed model fit by REML ['lmerMod']
Formula: b[[o]] ~ b[[v]] + (1 | b$ID)

REML criterion at convergence: -203.7

Scaled residuals:
    Min      1Q  Median      3Q     Max
-1.7639 -0.5062 -0.0997  0.3599  4.2489

Random effects:
 Groups   Name        Variance Std.Dev.
 b$ID     (Intercept) 0.020203 0.14214
 Residual             0.002814 0.05305
Number of obs: 89, groups:  b$ID, 16

Fixed effects:
             Estimate Std. Error t value
(Intercept)  0.227369   0.043250   5.257
b[[v]]      -0.038951   0.009171  -4.247

Correlation of Fixed Effects:
       (Intr)
b[[v]] -0.546
>  0.020203/(0.020203+ 0.002814)
[1] 0.8777425
refitting model(s) with ML (instead of REML)
Data: NULL
Models:
fit0: b[[o]] ~ 1 + (1 | b$ID)
fit1: b[[o]] ~ b[[v]] + (1 | b$ID)
     Df     AIC     BIC  logLik deviance  Chisq Chi Df Pr(>Chisq)
fit0  3 -193.39 -185.93  99.697  -199.39
fit1  4 -208.08 -198.13 108.041  -216.08 16.689      1  4.404e-05 ***
---
Signif. codes:  0 '***' 0.001 '**' 0.01 '*' 0.05 '.' 0.1 ' ' 1
```

Figure B-6: Values of Parameter *A* vs. Displacement Level. R output of linear mixed model and likelihood ratio test.

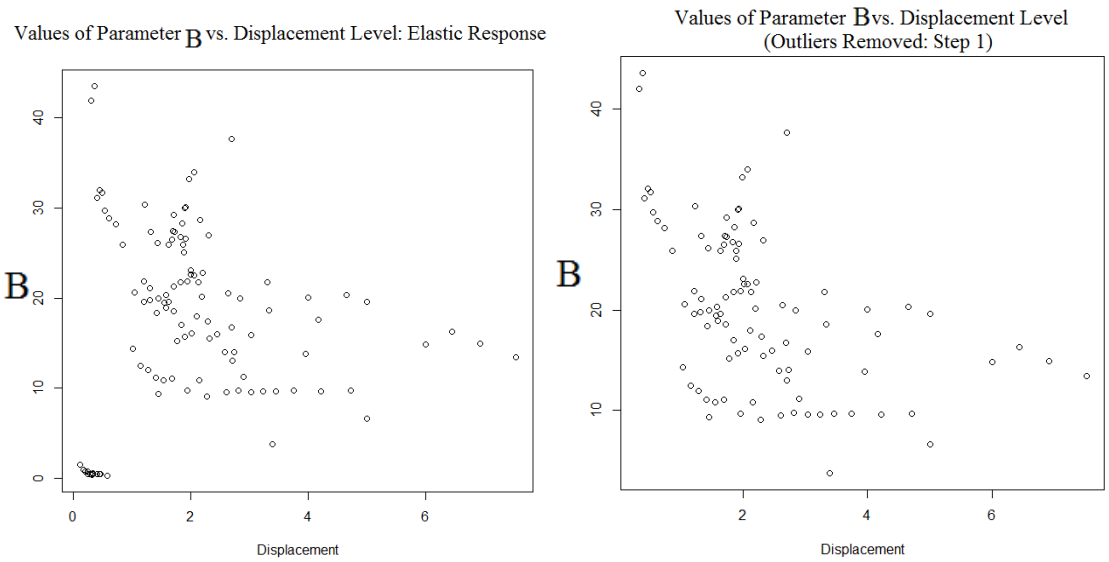

Figure B-7: Values of Parameter *B* vs. Displacement Level. Values of parameter B calculated from the elastic response data fitted with the equation $\sigma^e(\varepsilon) = A(e^{Bt} - 1)$.

```
Linear mixed model fit by REML ['lmerMod']
Formula: b[[o]] ~ b[[v]] + (1 | b$ID)

REML criterion at convergence: 579

Scaled residuals:
    Min      1Q  Median      3Q     Max
-2.4909 -0.4779 -0.0711  0.3754  3.4593

Random effects:
 Groups   Name        Variance Std.Dev.
 b$ID     (Intercept) 36.97    6.081
 Residual             15.92    3.989
Number of obs: 97, groups:  b$ID, 16

Fixed effects:
            Estimate Std. Error t value
(Intercept)  23.5951     2.2524  10.476
b[[v]]       -2.0367     0.6157  -3.308

Correlation of Fixed Effects:
       (Intr)
b[[v]] -0.705
> 36.97/(36.97+ 15.92)
[1] 0.6989979
refitting model(s) with ML (instead of REML)
Data: NULL
Models:
fit0: b[[o]] ~ 1 + (1 | b$ID)
fit1: b[[o]] ~ b[[v]] + (1 | b$ID)
     Df    AIC    BIC  logLik deviance  Chisq Chi Df Pr(>Chisq)
fit0  3 599.23 606.95 -296.61   593.23
fit1  4 590.62 600.92 -291.31   582.62 10.608      1   0.001126 **
---
Signif. codes:  0 '***' 0.001 '**' 0.01 '*' 0.05 '.' 0.1 ' ' 1
```

Figure B-8: Values of Parameter *B* vs. Displacement Level. R output of linear mixed model and likelihood ratio test.

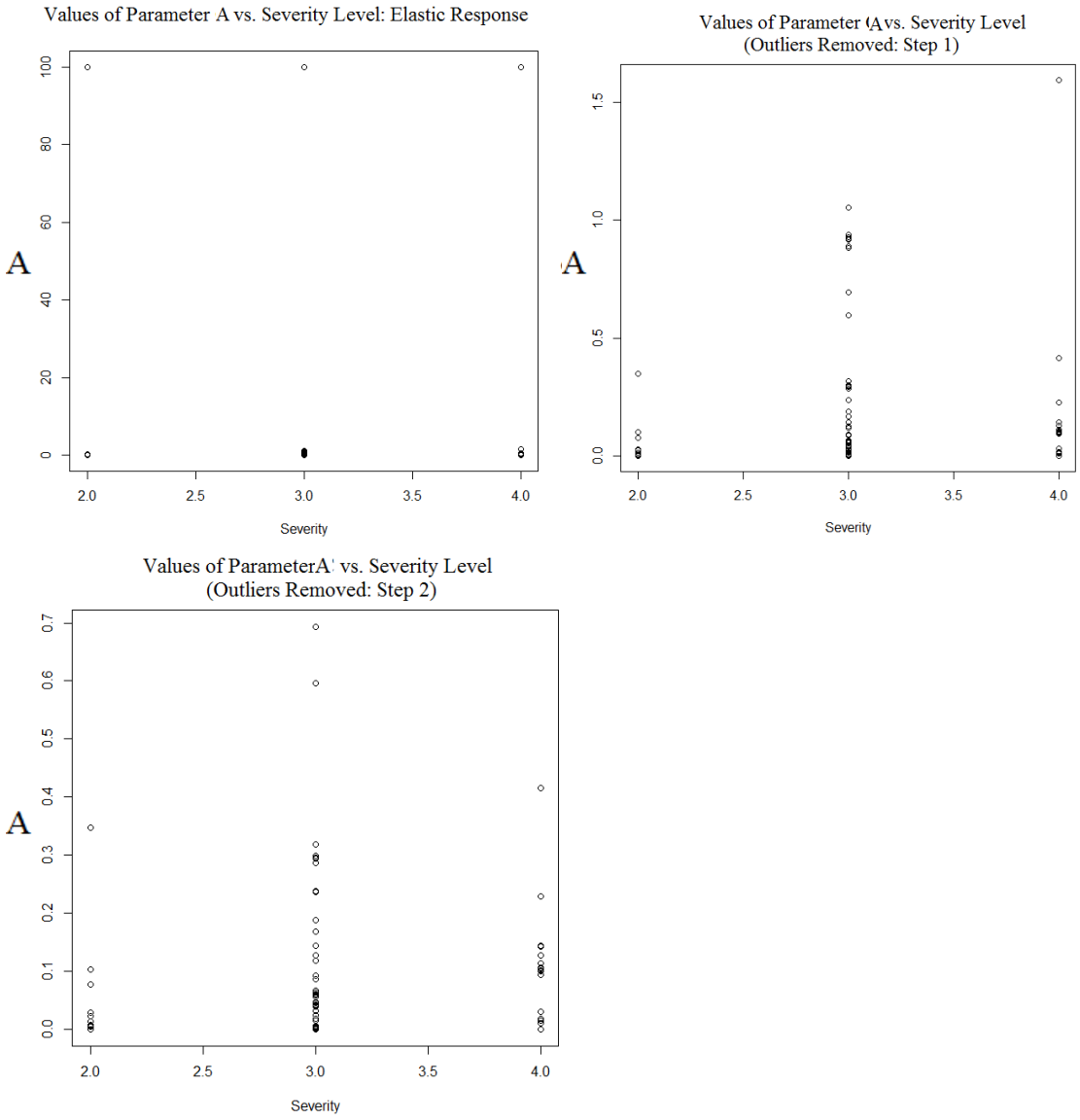

Figure B-9: Values of Parameter *A* vs. Severity Level. Values of parameter *A* calculated from the elastic response data fitted with the equation $\sigma^e(\varepsilon) = A(e^{Bt} - 1)$.

```
Linear mixed model fit by REML ['lmerMod']
Formula: b[[o]] ~ b[[v]] + (1 | b$ID)

REML criterion at convergence: -175

Scaled residuals:
    Min      1Q  Median      3Q     Max
-2.0233 -0.3166 -0.0573  0.1634  4.4547

Random effects:
 Groups   Name        Variance Std.Dev.
 b$ID     (Intercept) 0.033066 0.18184
 Residual             0.002946 0.05428
Number of obs: 80, groups:  b$ID, 15

Fixed effects:
            Estimate Std. Error t value
(Intercept)  0.09058    0.23303   0.389
b[[v]]       0.01299    0.06999   0.186

Correlation of Fixed Effects:
       (Intr)
b[[v]] -0.979
> 0.033066/(0.033066+ 0.002946)
[1] 0.9181939
refitting model(s) with ML (instead of REML)
Data: NULL
Models:
fit0: b[[o]] ~ 1 + (1 | b$ID)
fit1: b[[o]] ~ b[[v]] + (1 | b$ID)
     Df     AIC     BIC logLik deviance  Chisq Chi Df Pr(>Chisq)
fit0  3 -176.86 -169.71 91.429  -182.86
fit1  4 -174.90 -165.37 91.449  -182.90 0.0394      1     0.8427
```

Figure B-10: Values of Parameter *A* vs. Severity Level. R output of linear mixed model and likelihood ratio test.

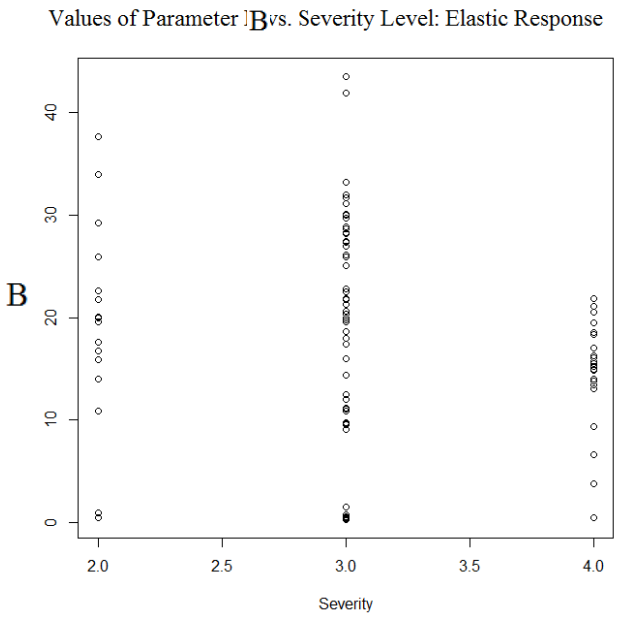

Figure B-11: Values of Parameter *B* vs. Severity Level. Values of parameter *B* calculated from the elastic response data fitted with the equation $\sigma^e(\varepsilon) = A(e^{Bt} - 1)$.

```
Linear mixed model fit by REML ['lmerMod']
Formula: a[[o]] ~ a[[v]] + (1 | a$ID)

REML criterion at convergence: 702.5

Scaled residuals:
    Min      1Q  Median      3Q     Max
-3.4631 -0.0800  0.1394  0.4551  2.1050

Random effects:
 Groups   Name        Variance Std.Dev.
 a$ID     (Intercept) 34.53    5.876
 Residual             57.10    7.556
Number of obs: 100, groups:  a$ID, 15

Fixed effects:
            Estimate Std. Error t value
(Intercept)   29.768      8.479   3.511
a[[v]]        -4.260      2.586  -1.647

Correlation of Fixed Effects:
       (Intr)
a[[v]] -0.979
> 34.53/(34.53+ 57.10)
[1] 0.3768416
refitting model(s) with ML (instead of REML)
Data: NULL
Models:
fit0: a[[o]] ~ 1 + (1 | a$ID)
fit1: a[[o]] ~ a[[v]] + (1 | a$ID)
     Df    AIC    BIC  logLik deviance  Chisq Chi Df Pr(>Chisq)
fit0  3 717.85 725.67 -355.93   711.85
fit1  4 717.01 727.43 -354.51   709.01 2.8397      1    0.09196
---
Signif. codes:  0 '***' 0.001 '**' 0.01 '*' 0.05 '.' 0.1 ' ' 1
```

Figure B-12: Values of Parameter *B* vs. Severity Level. R output of linear mixed model and likelihood ratio test.

APPENDIX D: TISSUE TESTING DEVICE PROTOCOL

Tissue Preparation:

1. Tissue sizing: A tissue cutter constructed from two 0.009 in single edge razor blades and a metal spacer of a 1.5 mm thickness, is used to size the tissue to an approximately 1.5 mm x 1.5 mm cross sectional area (figures below).

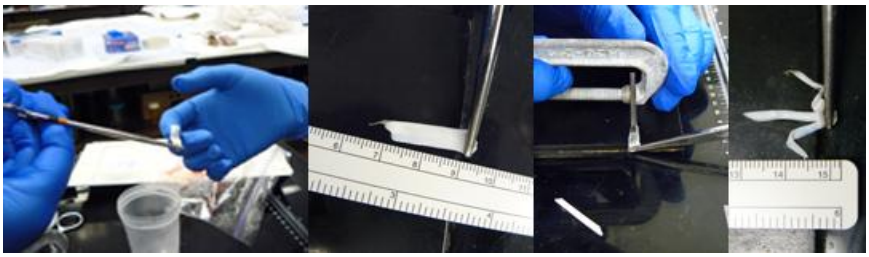

   a. Clamp one end of tissue with hemostat
   b. Lay ligament flat on cutting surface
   c. Press edge of cutting tool along length of tissue
   d. Drag cutting tool (with force) down the length of the tissue
   e. Separate sections of specimen
   f. Cut to length (approx. 1 cm) with scalpel
   g. Store in freezer in 0.9% saline solution until testing
2. Tissue testing preparation:
   a. Remove sized specimen from freezer
   b. Fill reservoir with 5 gallons of distilled water
   c. Turn on pump and plug in temperature controller. Set to 37^{o}C.
   d. Fill specimen container half way with 0.9% phosphate buffered saline solution
   e. Place specimen container in reservoir and thaw at a temperature of 37^{o}C for 30 minutes

Test Space Preparation:

1. Clean off cutting board, table, hardware (bolts, nuts, springs), test fixture, tissue applicator, tools, and scalpel with alcohol wipes
2. Remove gauze pad from individual wrapper and cut in half. One half is to be used with sprayer; the other to be used during tissue/grip setup.
3. Check to make sure nuts can be easily fastened on bolts (use socket head wrench, regular, wrench, and Allen wrench)
4. Have video calibration ruler available
5. Remove PBS solution filled spray bottle from heated reservoir just prior to testing

Grip Preparation:

1. Clean off grip surfaces with alcohol wipes to remove oils and debris
2. Cut and secure rectangular sections of paper, sized to fit between grip holes, to the roughened grip surface using double-sided tape (figure below)

Top row: Roughened surface extruded
Bottom row: Depressed roughened surface

3. Cut and secure 2 rectangular sections of paper to the smooth upper surface of one face of the upper and lower grip assembly, using double-sided tape (figure above)
4. Place these grip components in the grip fixture (figure below)

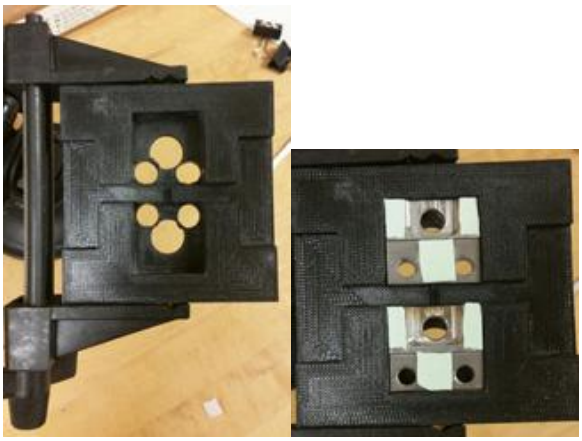

Tissue Clamping Protocol: (spray with heated PBS solution periodically to keep tissue hydrated)

1. Remove tissue from PBS solution and place, centered, on “I” shaped applicator, with at least 2 mm of overhang at each end of the specimen
2. Using the applicator, place the specimen on the grip surfaces so that the body is in line with the middle slot and ends of the specimen sit on the papered surface
3. Apply a small bead of cyanoacrylate on each end of the specimen, careful to keep the glue from reaching the grip edge
4. Insert 10-24 bolts, from underneath the fixture, into the two holes of the top grip and hold in place
5. Carefully slide the corresponding grip component into position, sandwiching the specimen between the two grip components
6. Place a spring around each bolt, then secure in place with a nut
7. Repeat steps 4, 5 and 6 for the bottom grip
8. Carefully torque each nut using a socket wrench head and Allen wrench until there is no space between the spring coils. Alternate between each nut/bolt, rotating the nut a little at a time.
9. Carefully remove the top and bottom grip assemblies, being mindful to keep the specimen tensionless
10. Holding the grips in alignment, clamp the assemblies in place with a quick grip clamp in the position shown in the figure

11. Place and secure the bottom grip to the bottom test fixture with bolt, socket head facing out
12. Using the Command.VI program, lower the actuator to insert the top test fixture lip into the slot of the top grip assembly (a few mm increments at a time). The clamp may need to be removed to properly mate these pieces.
13. Secure top grip in place with a bolt, socket head facing out
14. Tighten the clamping nut/bolts, alternating sides, to remove as much space between grip components as possible
15. Loosen the bolts of the base of the bottom grip fixture to align the specimen in the x, y and z axes (see figure). Secure the bottom fixture.
16. Change the velocity of the actuator to 0.166667 mm/s and move the actuator up to remove 95% of the slack in the specimen
17. Using a thin tipped brush and skin marker ink, apply a horizontal line at the grip tissue interfaces and at the mid line of the specimen
18. Rehydrate tissue.

APPENDIX E: TEST PROGRAM SETUP

1. Turn on computer, power strip, and signal conditioner
2. Open Matlab 2013a
3. Open PIMikroMove® Software
    a. Select C-863 controller and connect
    b. Select M230.25 stage, assign, and connect
    c. Select Positive reference button and follow directions (moves actuator down to furthest point (25 mm))
    d. Close PIMikroMove® Software
4. Open Mercury_GCS_Configuration_Setup_a.VI found in C:\Users\1375COHENT\Documents\LabVIEW Data
    a. Under Interface Settings
        i. Select RS-232 from pull-down menu
        ii. Select COM1 from portnumber pull-down menu
        iii. Select 115200 from Baudrate pull-down menu
    b. Under Referencing Mode
        i. Select Reference mode ON
    c. Under Move Settings
        i. Select All axes YES
        ii. Select Switch servo on YES
        iii. Select Limit switch selection POSITIVE (FPL)
        iv. Select Move to Middle NO
    d. RUN VI
5. Open Vis found in C:\Users\1375COHENT\Documents\LabVIEW Data:
    a. Tester Events Working11-17.VI
    b. Command.VI
    c. LEDrefresh.VI
    d. Deletevid.VI
    e. Deletetask.VI
6. Attach grips (unweighted)

7. Calibrate transducer (separate instructions)
8. Attach specimen to grips
9. Measure voltage with multimeter, record, and calculate weight of specimen
10. Recalibrate transducer to tare transducer
11. For **First Run**
    a. Press Initialize? pushbutton = TRUE
    b. Under Data Storage, input position, force, and video file paths and file names in the folder C:\Users\1375COHENT\Documents\LabVIEW Data\test\Validation(date)
        i. Position files have file extension .lvm
        ii. Force files have file extension .tdms
        iii. Video files have file extension .avi
    c. Under Sampling Rates:
        i. Force sampling rate = 1000 (Hz)
        ii. Position sampling rate = 100 (Hz)
        iii. Video FPT (frames per trigger) = Inf
    d. Input Actuator Velocity spec = .16667(mm/s)
        i. Max = 1.5 mm/s
        ii. Current = .5 mm/s
    e. Under Testing:
        i. Save as SP_a.__
        ii. Select “Gauge Length” in EVENT pull down menu
        iii. Input Force Threshold in newtons = __ (N)
        iv. Input Displacement in mm = _____ (mm)
    f. Start VI
12. For subsequent runs:
    a. Deselect Initialize? push button = FALSE
    b. Repeat steps 2b and 6c for setting up data storage and sampling rates
    c. Under Testing:
        i. For Preconditioning:
            1. Save as SP__b.__

2. Select “Force Precondition” in Event pull down menu
3. Input Displacement in mm = ___ (mm)
4. Input number of cycles to complete = ____ cycles

ii. For Stress Relaxation:

1. Save as SP__c.__
2. Select “Stress Relaxation” in Event pull down menu
3. Input Displacement in mm = ____ (mm)
4. Input Force Threshold in Newtons = ___ (N)
5. Input Time in seconds = ____ (s)

iii. For Move:

1. Select “Move” in Event pull down menu
2. Input Displacement in mm = ____ (mm)

d. Start VI

e. **For load to failure – use Gauge Length**

13. If program, actuator, data collection, etc. needs to be stopped, press **STOP** and stop the VI. (Refresh LED)
14. To view TDMS files
    a. Open ViewTDMS.VI
    b. Select correct file path
    c. Run VI

APPENDIX F: LABVIEW VIS

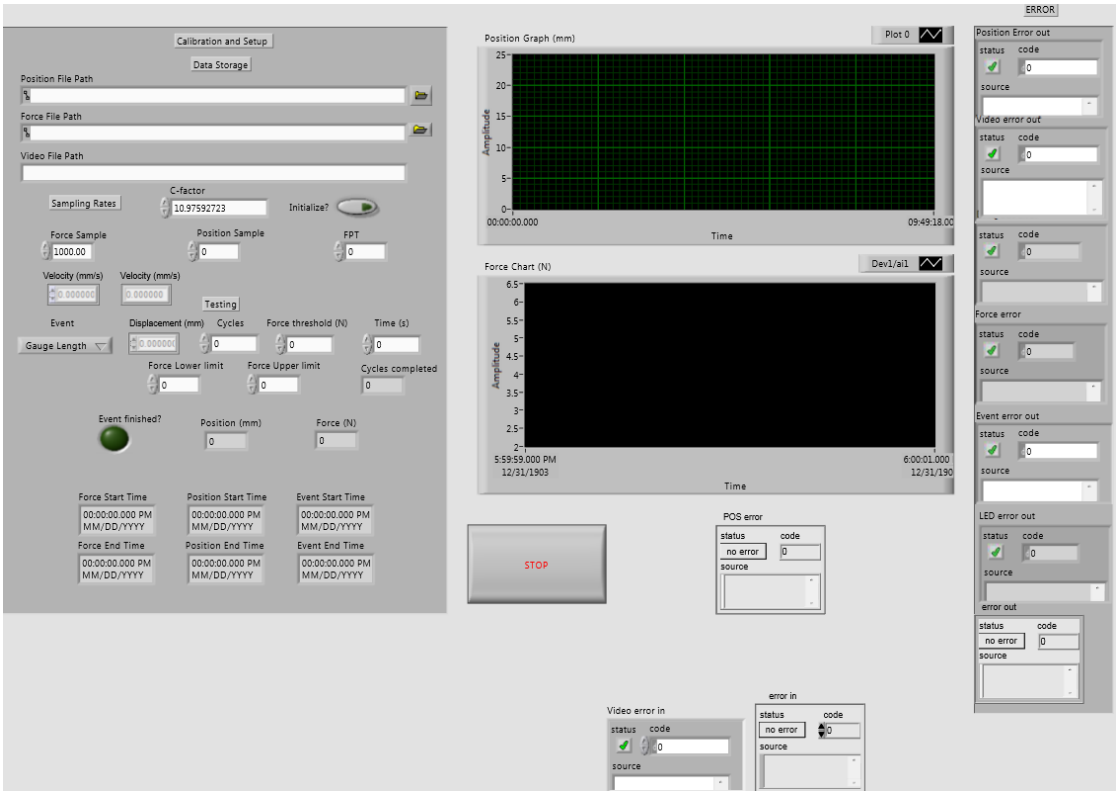

Figure D-1: Main Control VI Front Panel of PedsTES.

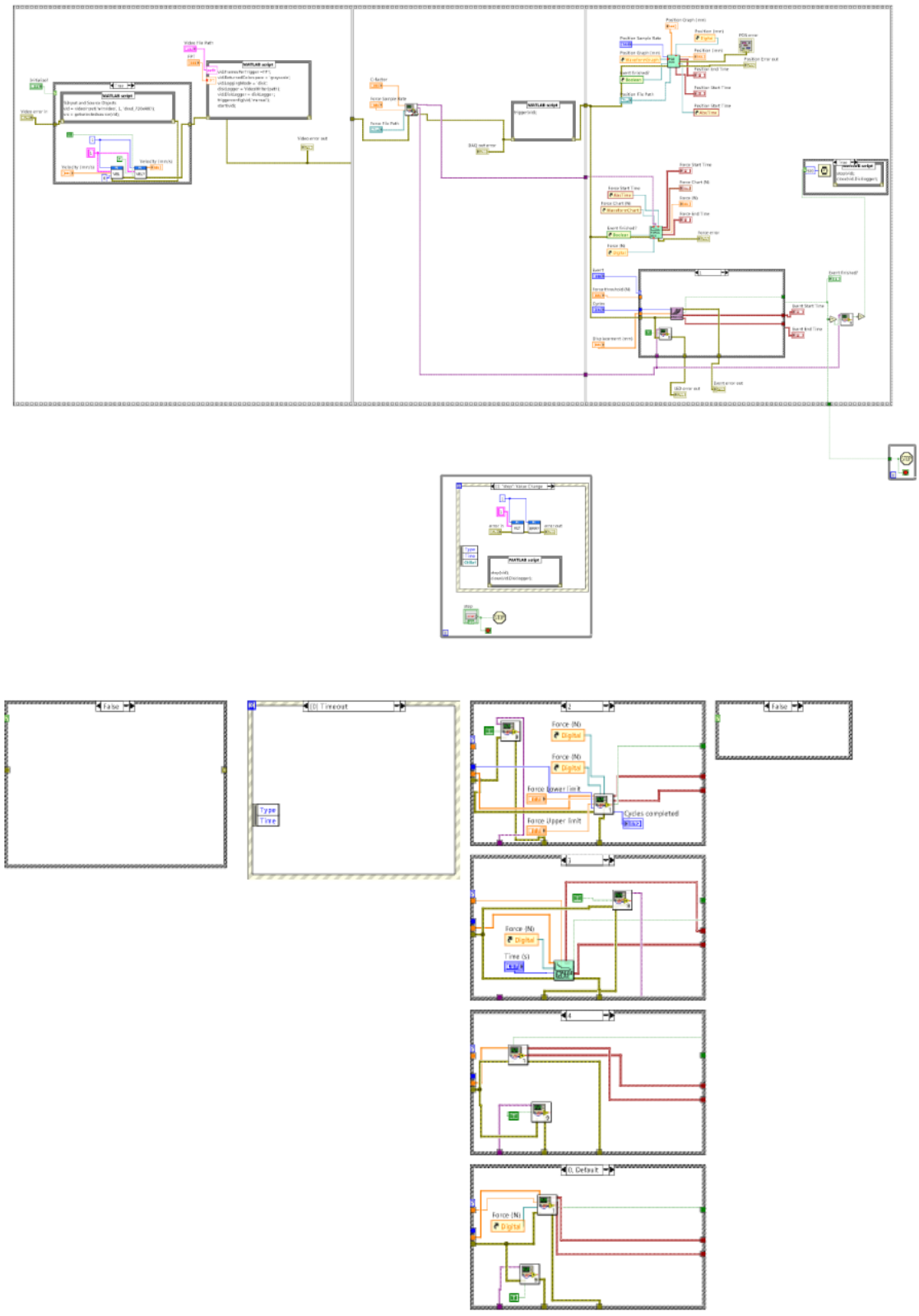

Figure D-2: Main control VI block diagram of PedsTES.

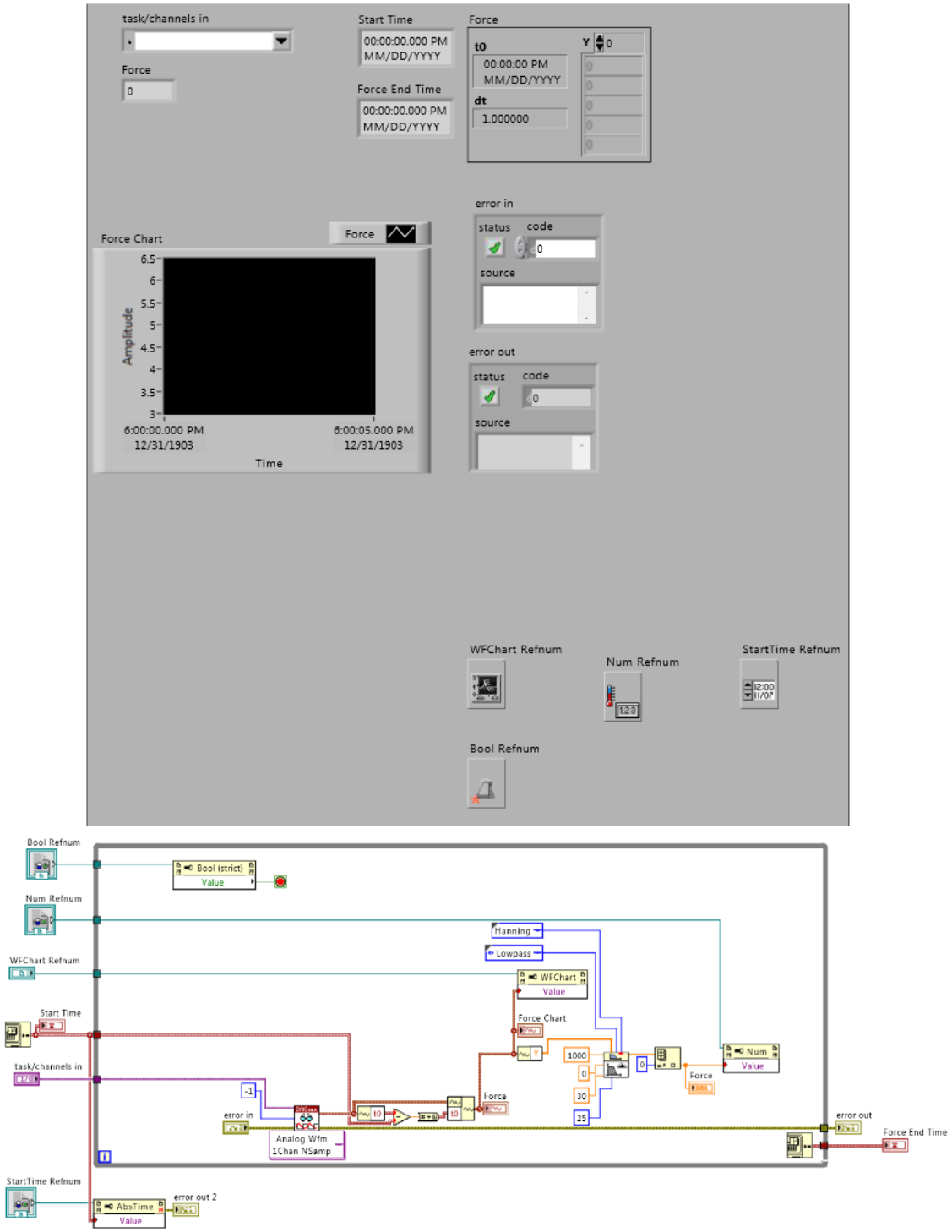

Figure D-3: Force acquisition subVI of PedsTES. Front panel and block diagram.

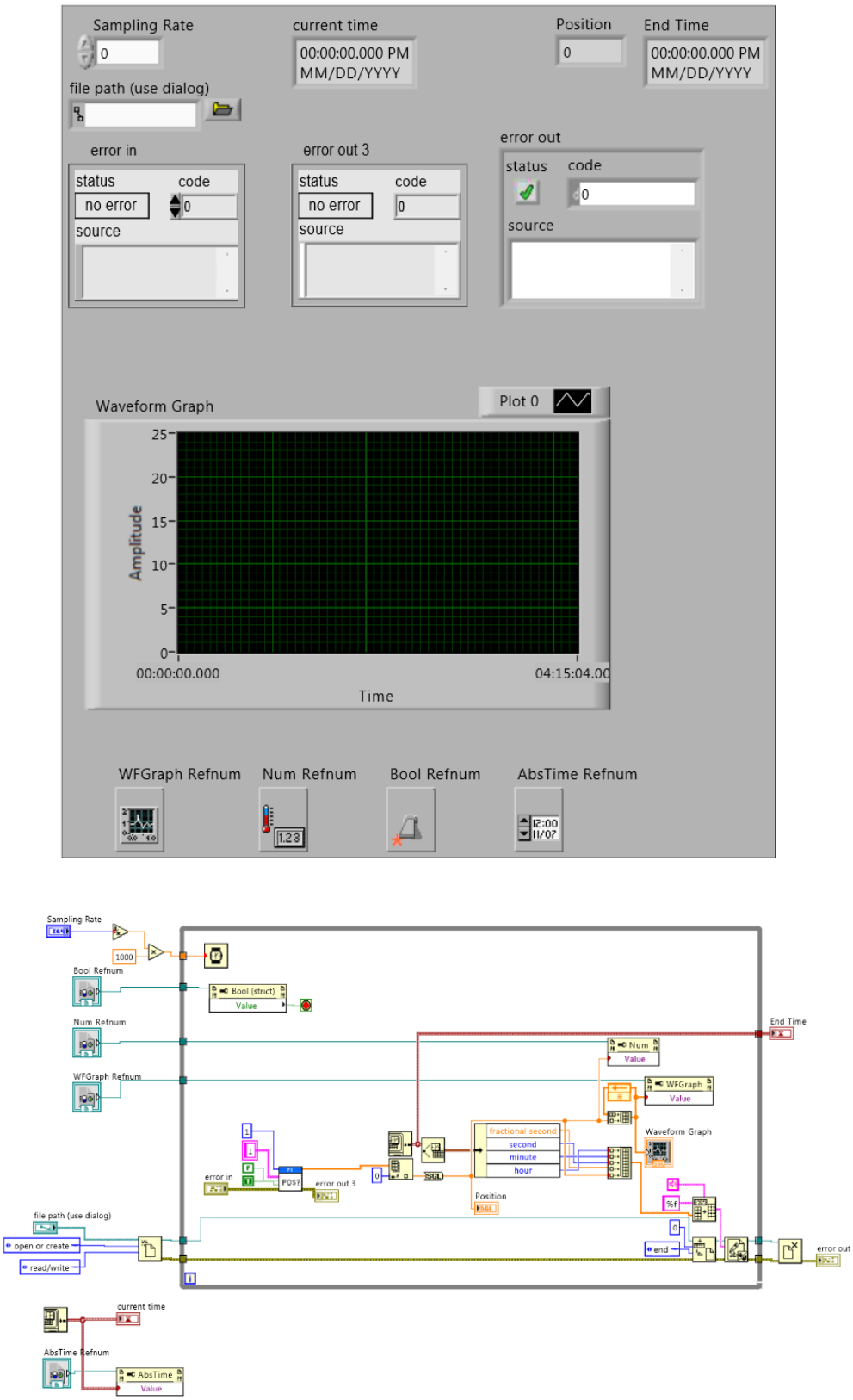

Figure D-4: Position acquisition subVI of PedsTES. Front panel and block diagram

DAQSetUPb.vi

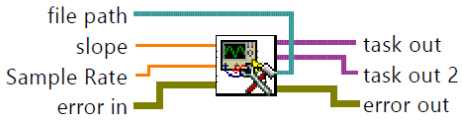

DAQmx Set up for force transducer voltage acquisition. Control input = sampling rate. Constant inputs= max and min expected values, physical channels, polymor info, sampling type (continuous, etc). Includes DAQ create channel, DAQ timing, and DAQ start task.

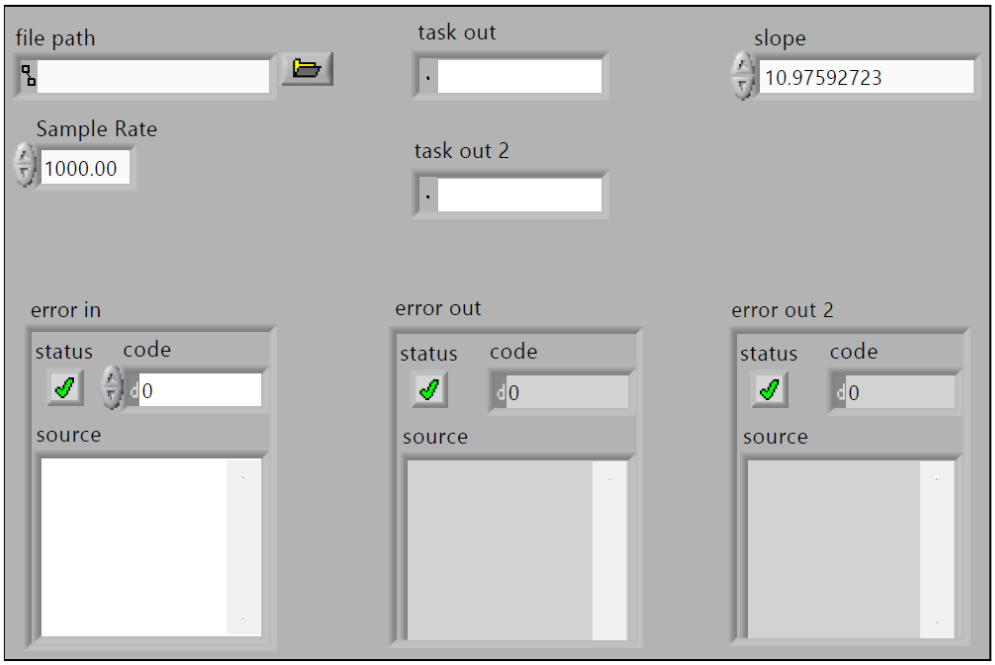

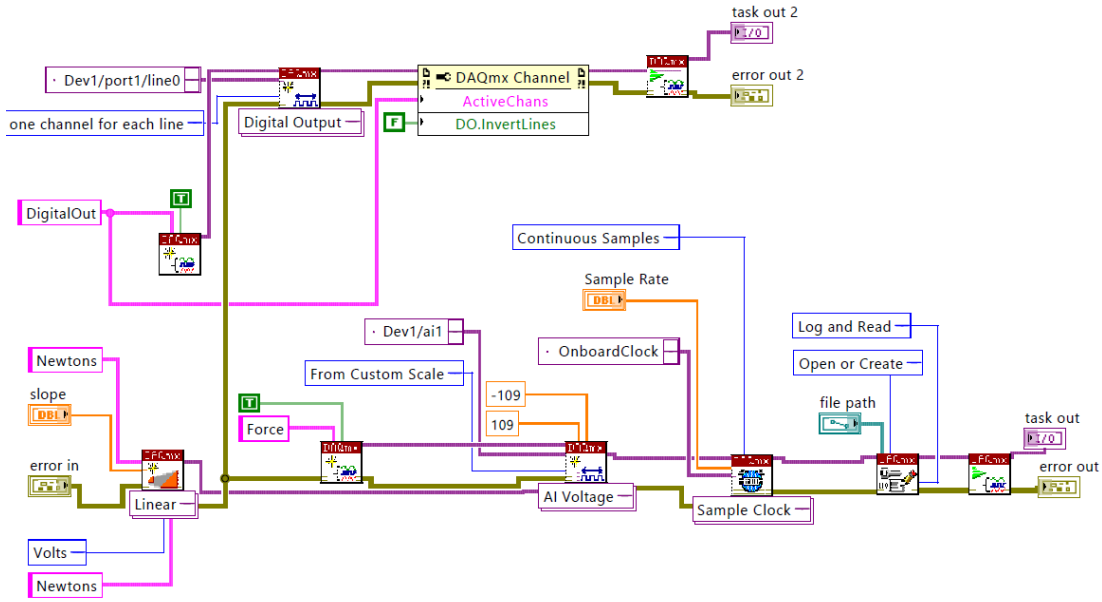

Figure D-5: DAQ setup subVI of PedsTES. Icon, front panel, and block diagram. SubVI includes scale to convert volts to Newtons, intake of analog data, and output of digital signal.

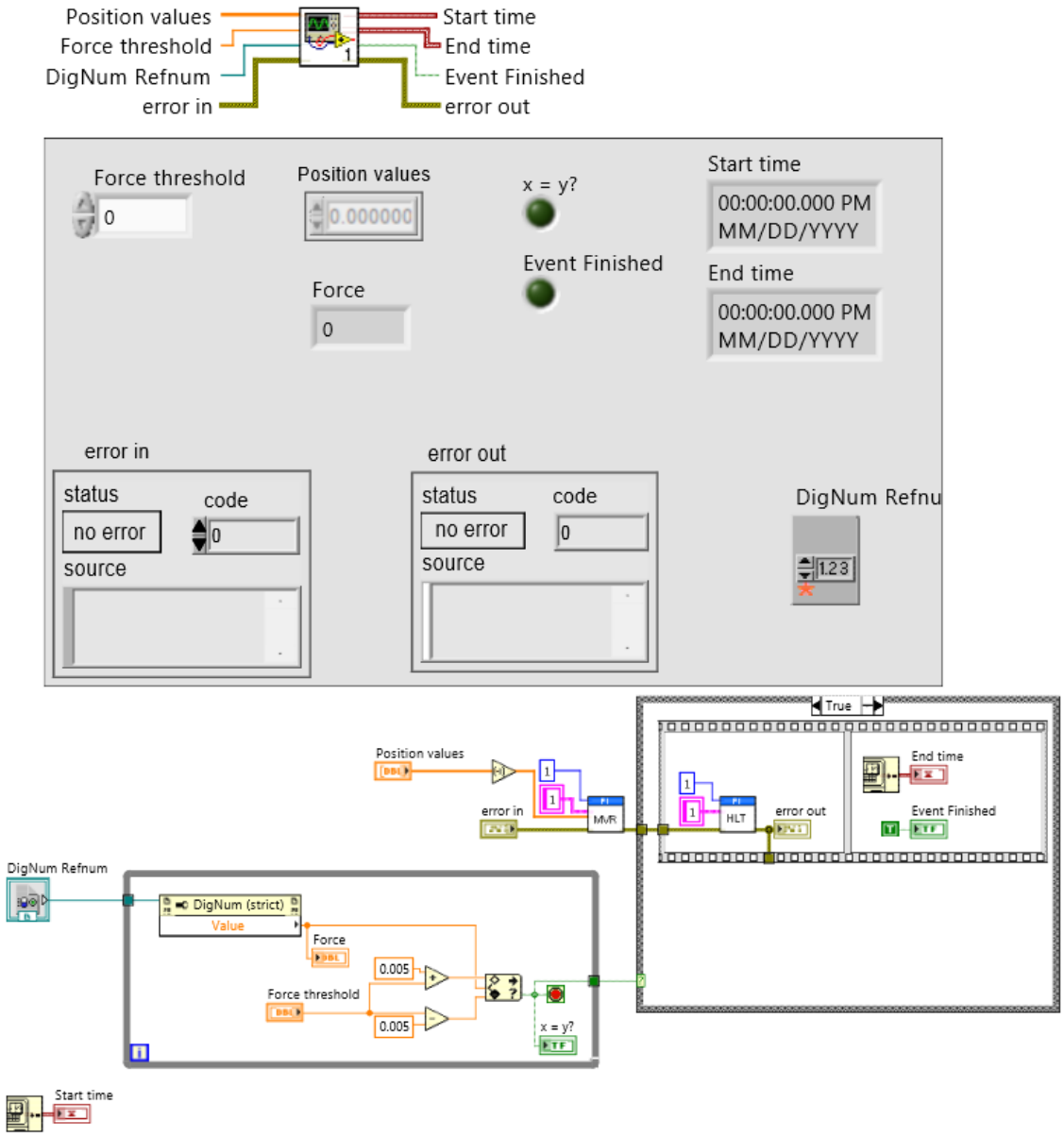

Figure D-4: Force control subVI of PedsTES. Icon, front panel, and bloc diagram. SubVI sets force threshold and sends signal to actuator to move a desired displacement until force value is reached.

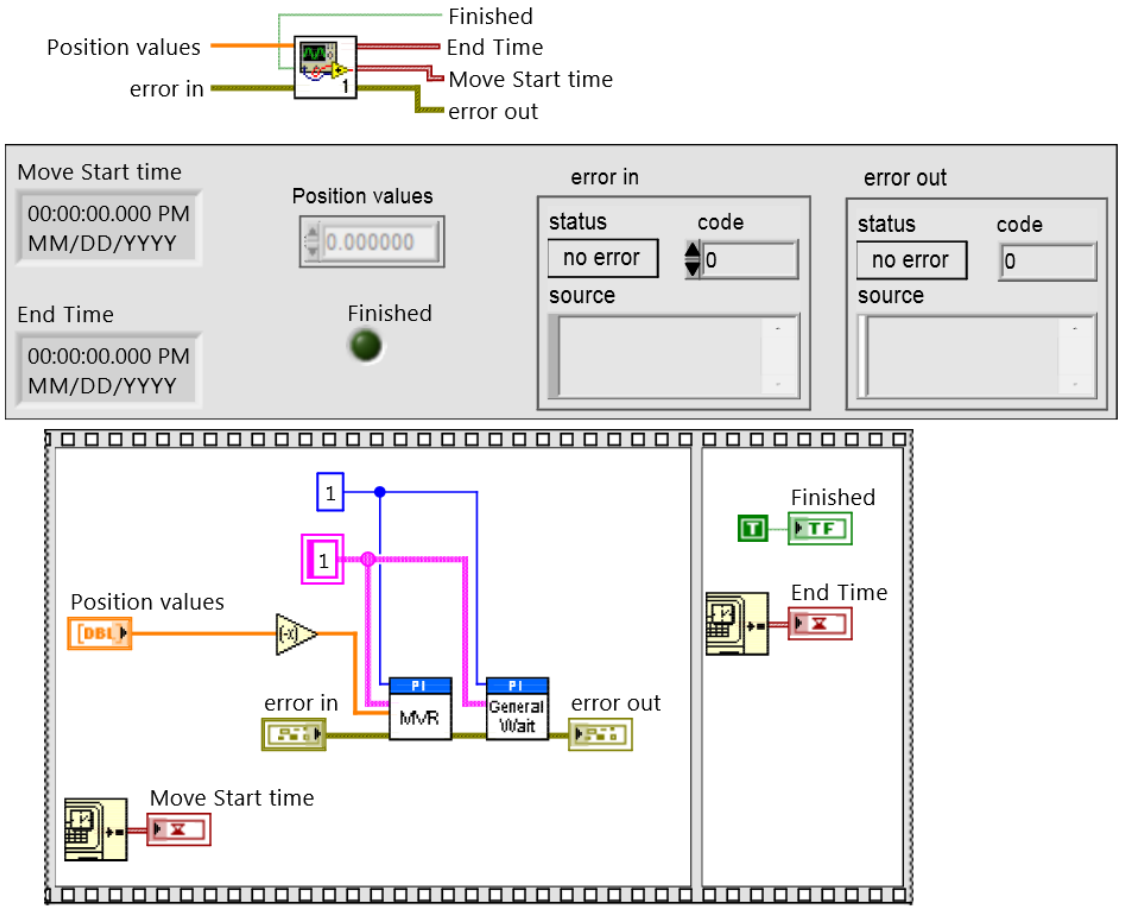

Figure D-5: Displacement control subVI of PedsTES. Icon, front panel, and block diagram. SubVI allows user to input desired displacement and sends command to actuator to move.

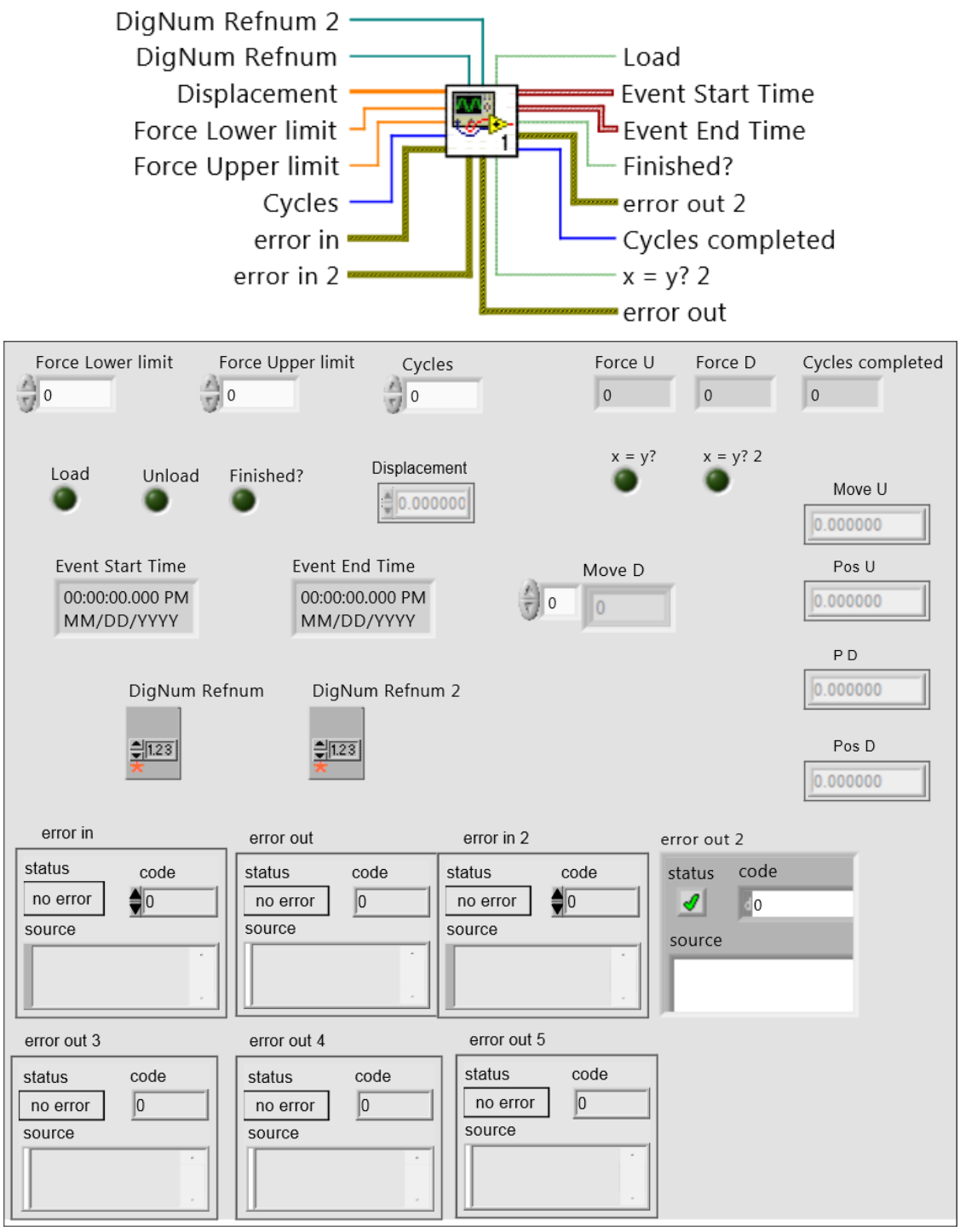

Figure D-6: Preconditioning subVI of PedsTES. Icon and front panel. SubVI uses force control to perform preconditioning. Force and number of cycles are user inputs.

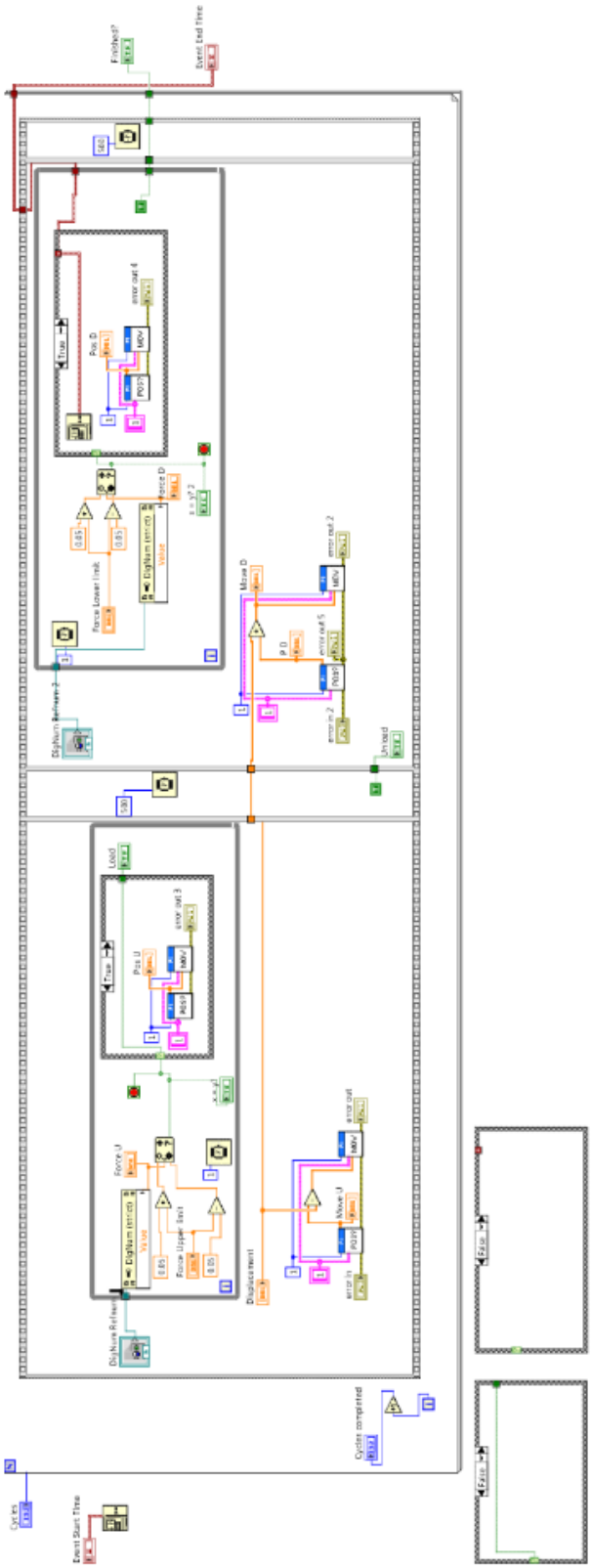

Figure D-7: Preconditioning subVI block diagram. Preconditioning subVI uses force control with a 500 ms delay between loading and unloading phases.

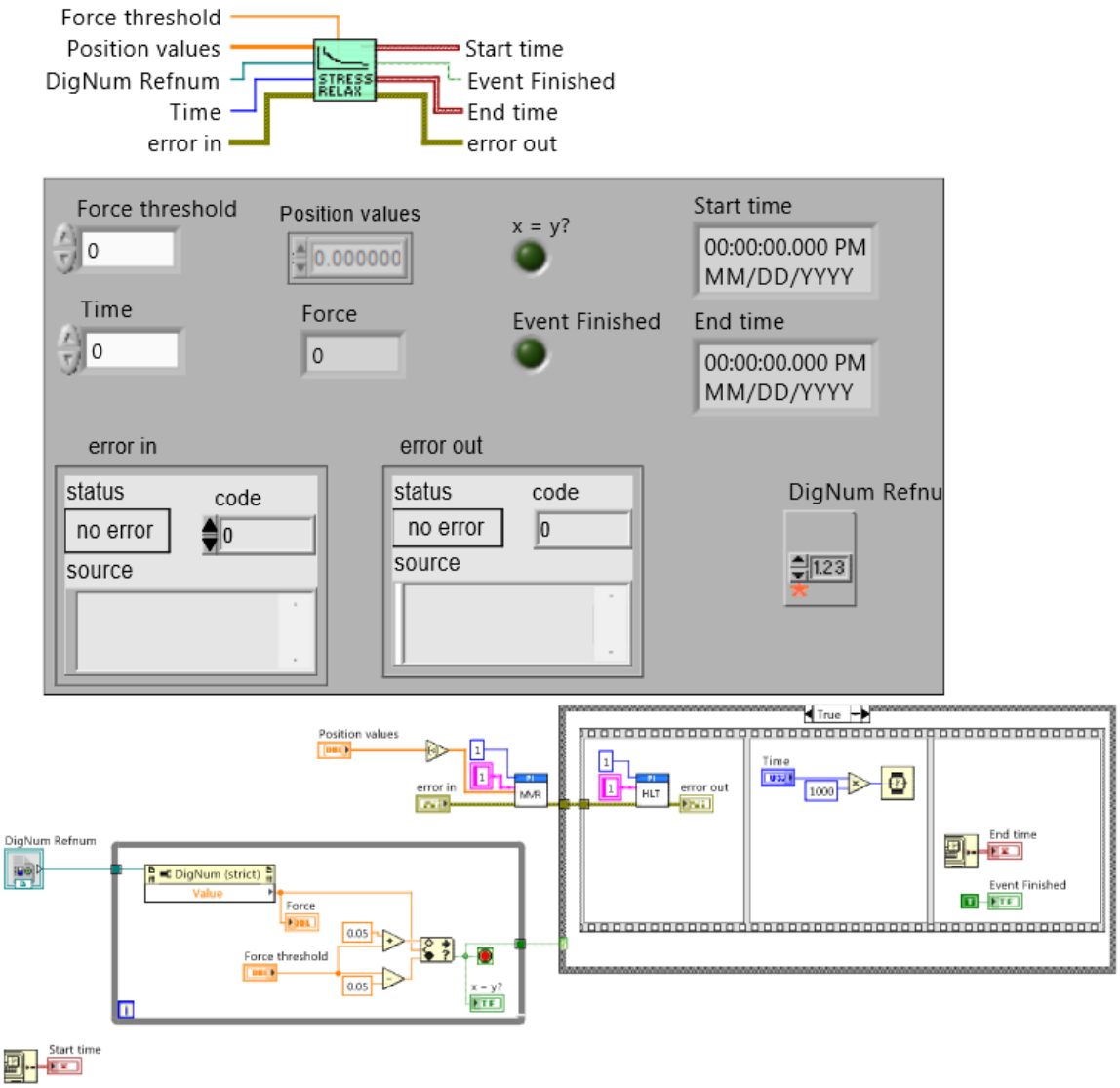

Figure D-8: Stress relaxation control subVI of PedsTES. Icon, front panel, and block diagram. SubVI sends signal to actuator to move until force threshold is reached, then held in position for desired time.

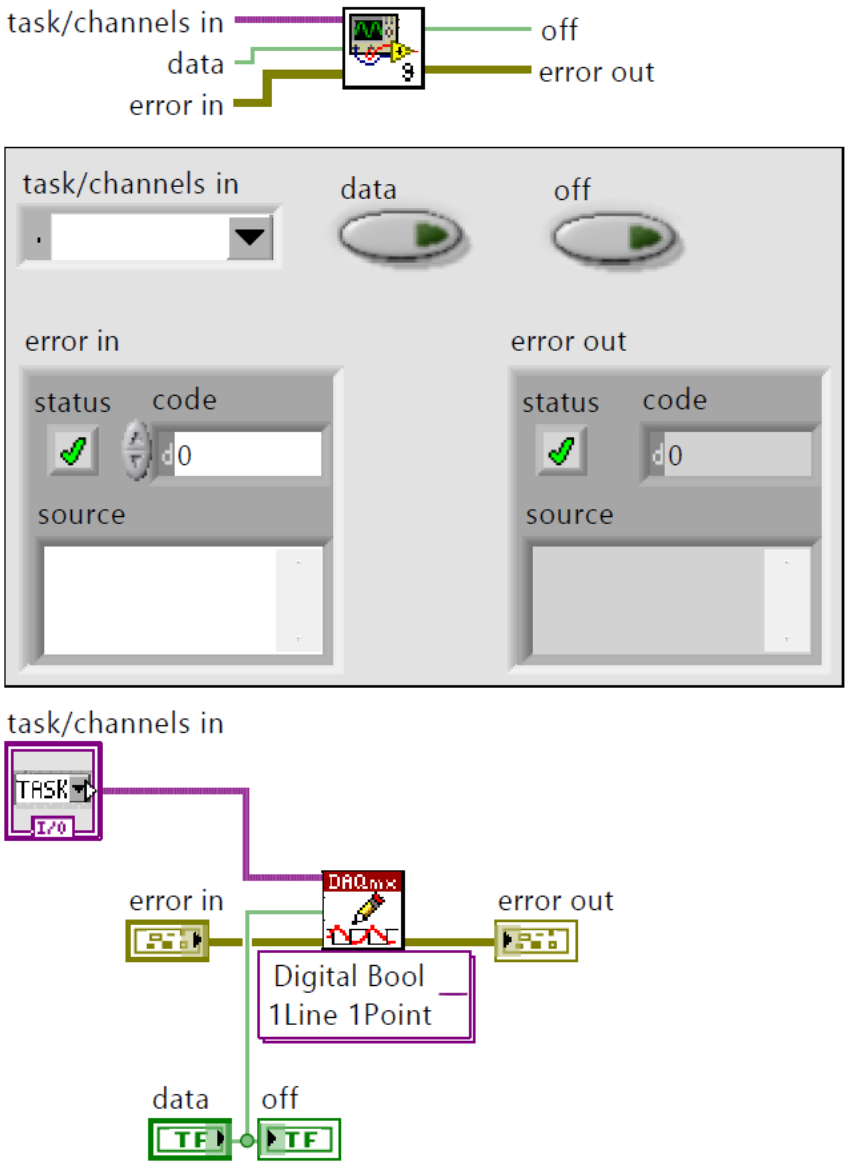

Figure D-9: LED control subVI of PedsTES. Icon, front panel, and block diagram. SubVI used to turn on and off LED to indicate when test is running.

APPENDIX G: CLUBFOOT RESEARCH: A POEM

Imagine your 1 of 200,000 newborns and your foot is in a cast,
because in utero your foot turned in and down as time passed.

Around your displaced bones in an abnormal fusion of tissue;
Restricting movement, so short and stiff, a major part of the issue.

An uncorrected clubfoot could lead to limits and pain in your future,
but which treatment to pick, conservative or with a suture.

Now stuck in a cast from week to week, your foot changes position.
Add a year or so with a brace, the Ponseti method has corrected your condition.

Cast materials are in abundance as either synthetic or plaster,
But which material will hold your foot in place; which will fix you faster.

A simulated clubfoot treatment was built to run the test.
Three types of cast materials were tested to see which performed the best.

They experienced minimal rotation; therefore each one could be used.
Longer time to weight-bearing, or some correction you will lose.

That abnormal soft tissue around your ankle could hinder your outcome.
Insight into its behavior could lead to improved strategies in years to come.

To find out how this tissue would respond to loads and time conditions,
A mechanical test machine was built to test clubfoot specimens removed by clinicians.

An actuator, load cell, and camera were all synchronized to record.
Fishing line and rabbit ligament validated this system that labs could afford.

The clubfoot tissue was harvested and testing with this machine.
Cyclic loading and stress relaxation data, now what does it mean?

Another piece of the puzzle lies within the organization of its structure.
Is it different from normal ligaments; do the fibers direct all over?

The tissue mechanics and structure vary from patient to patient.
We can use this knowledge to better identify a shorter precise treatment.